



Personal Neoantigen Vaccines Induce Persistent Neoantigen-Specific Memory T Cell Responses and Epitope Spreading in High-Risk Melanoma Patients

Citation

Leet, Donna. 2020. Personal Neoantigen Vaccines Induce Persistent Neoantigen-Specific Memory T Cell Responses and Epitope Spreading in High-Risk Melanoma Patients. Doctoral dissertation, Harvard Medical School.

Permanent link

<https://nrs.harvard.edu/URN-3:HUL.INSTREPOS:37365205>

Terms of Use

This article was downloaded from Harvard University's DASH repository, and is made available under the terms and conditions applicable to Other Posted Material, as set forth at <http://nrs.harvard.edu/urn-3:HUL.InstRepos:dash.current.terms-of-use#LAA>

Share Your Story

The Harvard community has made this article openly available. Please share how this access benefits you. [Submit a story](#).

[Accessibility](#)

Personal neoantigen vaccines induce persistent neoantigen-specific memory T cell responses and epitope spreading in high-risk melanoma patients

by

Donna Leet

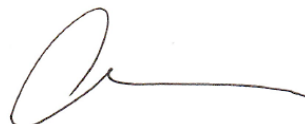
Harvard-MIT Division of Health Sciences and Technology

Submitted in Partial Fulfillment of the Requirements for the M.D. Degree
with Honors in a Special Field at Harvard Medical School

February 2020

Area of concentration: Cancer Immunology / Medical Oncology
Project Advisor: Catherine J. Wu, M.D.
Prior Degrees: B.A. Biology and French, Amherst College

I have reviewed this thesis. It represents work done by the author under my guidance/supervision.



Catherine J. Wu

Abstract

Cancer vaccines have long been envisioned as an effective approach to generate, amplify and diversify T cell responses against tumors. The recent availability of next-generation sequencing (NGS) has enabled the comprehensive identification of mutations within a patient's tumor, which represent an abundant source of tumor-specific potential antigens. Tumor neoantigens, altered peptides generated from somatic mutations in tumor cells, are promising therapeutic targets due to their exquisite tumor specificity and exemption from central tolerance mechanisms. Notably, highly effective antitumor responses have been associated with the presence of neoantigen-specific T cells. Recently, the Wu lab and others have demonstrated that personalized neoantigen-targeting vaccines are safe, feasible and highly immunogenic in phase I trial of stage III/IV resected high-risk melanoma^{1,2}. The Wu lab's neoantigen vaccine (NeoVax), consisting of up to 20 long peptides and poly-ICLC, induced strong polyfunctional neoantigen-specific T-cells that recognized patient tumors *in vitro*. In addition, two patients who were vaccinated and received anti-PD-1 checkpoint blockade (CPB) therapy upon relapse had durable complete responses (CRs).

To define the long-term effects of a therapeutic vaccine directed against personal tumor neoantigens, we evaluated the clinical outcomes and circulating immune responses of eight patients with high-risk melanoma, at a median of 50.5 and 46 months, respectively, after initiation of treatment with NeoVax. All patients remain alive, and 6 of 8 are currently without evidence of disease. In the current study, we report consistent long-term persistence of neoantigen-specific T cell responses following vaccination, *ex vivo* detection of neoantigen-specific T cells with a memory phenotype, expansion and diversification of neoantigen-specific T cell clones over time, and epitope spreading, indicating on-target vaccine-induced tumor destruction. These data

demonstrate that personalized neoantigen peptide vaccines durably induce T cell responses in melanoma patients over the course of years, broadening the spectrum of tumor-specific cytotoxicity and contributing to enduring immunoprotection.

Table of Contents

Abstract	1
Acknowledgments	5
List of Abbreviations	6
Introduction	8
Methods	29
Results	48
Discussion	60
Suggestions for Future Work	68
Conclusions	72
Lay Summary.....	73
References	75
Figures	95
Extended Data Figures	103
Supplementary Table Legends.....	112
Supplementary Tables	113

Acknowledgments

I would like to thank Dr. Catherine Wu, who has been a wonderful, kind, inspiring, and caring mentor throughout my time at HMS. I am deeply grateful for the many opportunities she has provided for me to learn and grow, and she truly exemplifies the model physician-scientist I aspire to become. She has not only taught me how to craft interesting and unanswered questions, write a convincing proposal, and design experiments for hypothesis-driven research, but she has exhibited an unmatched level of patience and kindness, and has been accepting and supportive of all my decisions. Given the challenging path ahead, I feel fortunate to have such a kind, compassionate mentor to guide me along the way.

I would also like to thank all of the members of the Wu Lab, who provided me with invaluable discussion and advice over the years, and made lab life fun! In particular, I would like to thank Zhuting Hu for her guidance, mentorship, and friendship – she has taught me incredible amounts about immunology and scientific scholarship, and I could not have done this without her instrumental contributions!

Finally, I would like to thank Dr. Patrick Ott, Ed Fritsch, and Giacomo Oliveira for their insights and discussion in the writing of this thesis.

The work described in this thesis represents the culmination of work by a number of investigators in the Wu Lab and our collaborators. I describe their contributions below:

- Personalized neoantigen vaccines were designed by Catherine Wu, Patrick Ott, Edward Fritsch, and Nir Hacohen (Fig. 1).
- Systemic vaccine-specific immune responses in clinical trial patients were monitored using ELISPOT, performed by Zhuting Hu (Fig. 1, Extended Data Fig. 1)
- Intracellular cytokine staining was performed by Jinyan Liu (Fig. 1d). Zhuting Hu and I analyzed the results.
- Somatic mutation calling of relapsed tumors was performed by Sachet Shukla and Juliet Forman (Fig. 2). Juliet Forman and I analyzed the results.
- Peptide predictions were performed by Sachet Shukla and Juliet Forman.
- Tetramer-staining experiments were performed by me and Zhuting Hu (Fig. 3, 5 and Extended Data Fig. 4).
- Single cell RNA sequencing analysis was performed by Rosa Allesoe. I analyzed the transcriptome data to interpret cluster signatures (Fig. 3).
- Shuqiang Li and Kenneth Livak performed single cell TCR sequencing. Adrienne Luoma helped to prepare T cells for TCR sequencing. I analyzed the TCR sequencing results and interpreted TCR evolutionary patterns. (Fig. 4, 5)
- Zhuting Hu and I selected epitope spreading peptides with the assistance of Ed Fritsch, then performed epitope spreading experiments (Fig. 6)
- Immunohistochemistry experiments were performed by Ana Lako and Scott Rodig (Extended Data Fig. 1)
- Adrienne Luoma and Kai Wucherpfennig designed and generated tetramers.
- Statistical analysis was performed with Donna Neuberg and Robert Redd; Robert Redd also helped to create the TCR clonotype tracking plots in Fig. 3.

List of Abbreviations

ACT – Adoptive cellular therapy
ACTB – Beta-actin
AICD – Activation-induced cell death
APC – Antigen-presenting cell
ASP – Assay peptides (15–16 amino acids, CD4 responses)
CAR – Chimeric antigen receptor
CCL – C-C chemokine ligand
CCR7 – C-C chemokine receptor 7
CD26L – L-selectin (a.k.a SELL)
CDR3 – Complementarity determining region 3
CPB – Immune checkpoint blockade
CR – Complete response
CTLA-4 – Cytotoxic T-lymphocyte associated protein 4
DC – Dendritic cell
ELISA – Enzyme-linked immunosorbent assay
ELISPOT – Enzyme-linked immunospot assay
EPT – Epitope peptides (9–10 amino acids, CD8 responses)
FACS – Fluorescence-activated cell sorting
FBS – Fetal bovine serum
FFPE – Formalin-fixed paraffin-embedded
GBM – Glioblastoma
GZMA – Granzyme A
GNLY – Granulysin
HLA – Human leukocyte antigen
HOPX – Homeodomain-only protein
IC50 – Half-maximum inhibitory concentration
IL – Interleukin
IDH1/2 – Isocitrate dehydrogenase 1/2
IFN γ – Interferon gamma
IL13Ra2 – Interleukin-13-receptor alpha 1
IMP – Immunizing peptide contained in vaccine
KPS – Karnofsky performance status
LAG3 – Lymphocyte-activation gene 3
LEF-1 – Lymphoid enhancer-binding factor 1
MGMT – Methylguanine methyltransferase
MHC – Major histocompatibility complex
NeoORF – Novel open reading frame
NFAT – Nuclear factor of activated T cells
OLIG2 – Oligodendrocyte transcription factor 2
OVA – Ovalbumin
OS – Overall survival
PBMC – Peripheral blood mononuclear cells
PCR – Polymerase chain reaction
PD-1 – Programmed cell death receptor 1

PD-L1 – Programmed cell death ligand
PFS – Progression-free survival
PHA – Phytohemagglutinin
poly-ICLC – Polyinosinic and polycytidylic acid, stabilized with poly-l-lysine and carboxymethylcellulose
pMHC – Peptide-MHC complex
PRF1 – Perforin 1
RANO – Response Assessment in Neuro-Oncology
RLU – Relative luminescence unit
RNA-Seq – RNA sequencing
SATB1 – Special AT-rich sequence binding protein 1
scRNA – Single-cell RNA
SFC – Spot-forming cell
SFU – Spot-forming units
SOX2 – SRY (sex determining region Y)-box 2
sSNV – Somatic single nucleotide variants
TAA – Tumor-associated antigen
TCR – T cell receptor
TIGIT – T cell immunoreceptor with Ig and ITIM domains
TIL – Tumor-infiltrating lymphocyte
TIM3 – T-cell immunoglobulin and mucin-domain containing-3
TLR – Toll-like receptor
TMB – Tumor mutation burden
TNF – Tumor necrosis factor
TNFAIP8 – TNF Alpha Induced Protein 8
TOX – Thymocyte selection-associated high mobility group box protein
TPM – Transcript-per-million
Treg – Regulatory T cell
tSNE – T-distributed stochastic neighbor embedding
TXK – Tyrosine-protein kinase
VEGF – Vascular endothelial growth factor
VISTA – V-domain Ig suppressor of T cell activation
WES – Whole exome sequencing
WT – Wildtype

Introduction

The Cancer-Immunity Cycle

Cancer is characterized by the accumulation of genetic mutations in oncogenes and tumor suppressors and the loss of normal cellular regulatory processes (Tian et al., 2011). These events result in the expression of tumor antigens, including tumor-associated antigens and tumor-specific antigens³ which can stimulate an immune response via the presentation of peptides bound to major histocompatibility class I and II (MHC I/II) molecules on the surface of cancer cells. These cancer-specific peptide-MHC (pMHC) complexes can then be recognized by T cells produced spontaneously in cancer patients⁴.

To generate an effective anticancer immune response, a stepwise series of events must ensue (**Figure 1**). First, tumor antigens are released and captured by dendritic cells (DCs) and other antigen-presenting cells (APCs) for processing, supported by stimulatory immunogenic signals from proinflammatory cytokines and factors released by dying tumor cells. The antigen-loaded APCs then travel through the lymphatics to the draining lymph nodes, which are the primary site of T cell priming. The next critical step involves recognition of tumor-antigens presented on APC MHC I and MHC II molecules by T cells through the T cell receptor (TCR)—CD3 complex and the binding of costimulatory molecules such as B7 and CD28, on APCs and T cells respectively (signal 2). Costimulation is augmented by IL-12 and type I interferons (IFNs) produced by APCs. This results in the priming and activation of effector T cell responses against the tumor antigens against which central tolerance has been incomplete. Finally, activated tumor-specific T cells must traffic to and infiltrate to tumor sites, recognize tumor antigens expressed on the surface of tumor cells, and mediate tumor cell lysis through cytotoxicity and the production of effector

cytokines, such as IFN γ and tumor necrosis factor (TNF). In turn, the lysed cancer cells can release additional tumor antigens, which can undergo the same process to induce polyclonal T cell responses, thereby increasing the antigenic breadth and depth of the antitumor immune response and leading to epitope spreading.⁵

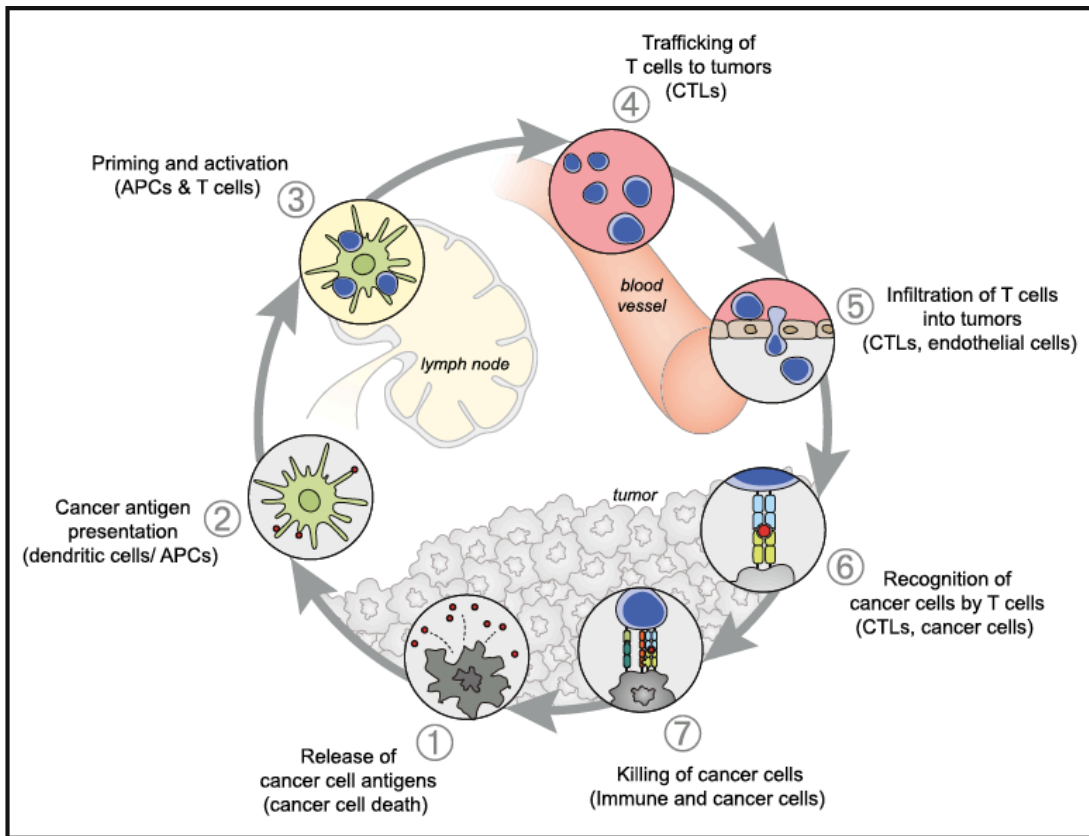


Figure 1. The Cancer-Immunity cycle. The generation of antitumor immunity is a cycle that can be divided into seven major steps, starting with the release of antigens from the cancer cell and ending with the killing of cancer cells.⁵ Taken from Chen et al. *Immunity* 2013.

In cancer patients, this cycle is rendered dysfunctional, and T cell responses rarely provide protective immunity. Deficiencies can include suboptimal or flawed tumor antigen recognition leading to an imbalance of T cell regulatory and effector cells, persistent antigen exposure leading to expression of programmed cell death protein 1 (PD-1) and other immune checkpoint molecules⁶, T cell homing issues, tumor microenvironment suppressive effects, and tumor immune editing^{5,7}.

T cell subsets in cancer immunity

CD8⁺ T lymphocytes play a central role in cancer immunity through their capacity to kill malignant cells upon T-cell receptor (TCR)-mediated recognition of specific antigenic peptides presented on the surface of target cells by human leukocyte antigen class I (HLA-I)/beta-2-microglobulin (β 2m) complexes (MHC class I)⁸. This leads to the clustering of TCR and associated signaling molecules at interface of the T cell and tumor cell, triggering cytotoxic T lymphocyte (CTL) effector functions. These functions are mediated either directly, through synaptic exocytosis of cytotoxic granules containing perforin and granzymes into the target cell resulting in cancer cell destruction, or indirectly, through secretion of cytokines, such as IFN γ and TNF.⁸

CD8⁺ T cells are thought to dominate the cellular immune response against tumors, as tumor cells express little, if any, MHC class II molecules that can bind to CD4.^{9,10} Even when MHC class II molecules are present, high expression of the invariant chain often results in the generation of class II-associated invariant chain peptides that prevent the presentation of endogenous peptides by tumor cells⁹. Consequently, T cell-based therapies have been primarily conceptualized to stimulate the CD8⁺ T cell response. In animals, tumor-specific CD8⁺ T cells are highly protective against tumor¹¹, and in humans, tumor-specific CD8⁺T cells have been isolated in the blood of patients with hematologic and solid malignancies and within the pool of tumor-infiltrating lymphocytes (TILs)⁸. However, they have also been found to express high levels of PD-1, indicating suppressed effector activity¹². Tumor associated antigen (TAA)-specific CD8⁺ T cells have also been detected in spontaneously regressing tumors.¹³ Moreover, a correlation between tumor progression control and the infiltration rate of CD8⁺ T cells in the tumor has been established¹⁴.

More recently, studies have suggested a vital role for CD4⁺ T cells in antitumor immunity. For one, they can influence antibody production and amplify the magnitude of antitumor B cell responses¹⁵. Furthermore, they can act as helper-T cells to activate tumor-specific cytotoxic CD8⁺ T cells and establish memory CD8⁺ T cells^{15,16}. T-cell help occurs when a CD4⁺ T cell and a CD8⁺ T cell both recognize their respective antigens on the same DC, enabling the DC to deliver specific cytokine and co-stimulatory signals to the CD8⁺ T cell, thereby inducing clonal expansion and specifying differentiation (**Figure 2**). They can also target tumor cells, either directly by eliminating them through cytotoxicity, or indirectly by modulating the tumor microenvironment^{12,15}. The importance of CD4⁺ T cells has been illustrated in cancer patients: CD4⁺ T cell responses against self-antigens have been detected in circulation and at tumor sites^{17,18,19}, and CD4⁺ T cells have also been reported to lyse tumor cells in a MHC class II–restricted manner by perforin- or granzyme-mediated killing^{20,21,22}.

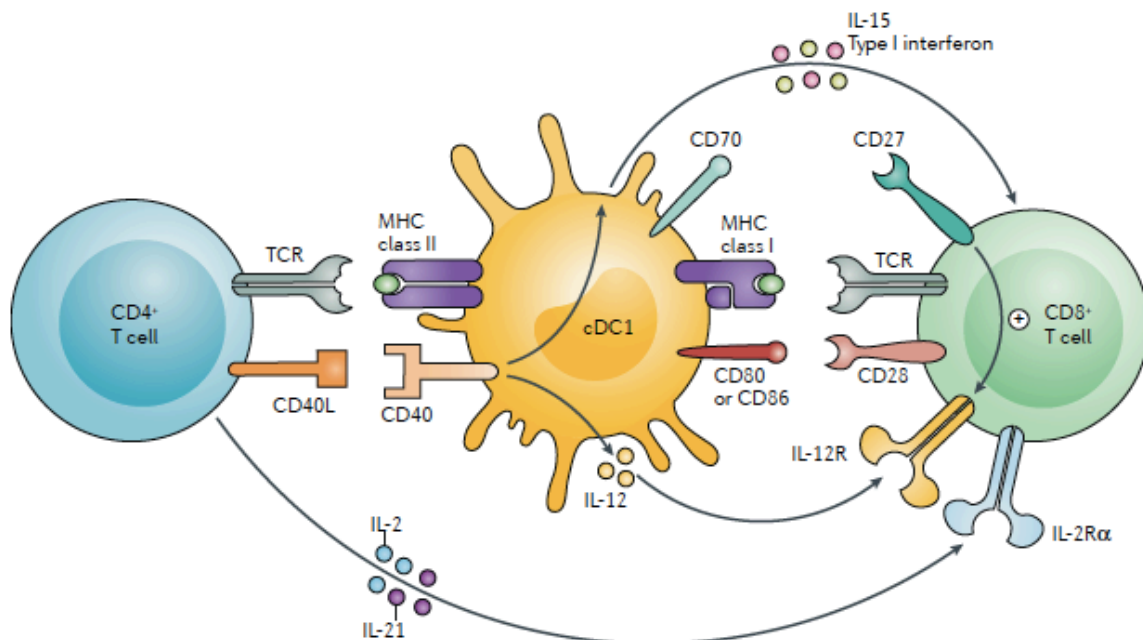


Figure 2. Receptor–ligand interactions during T cell priming. Antigen presentation by a lymph node-resident conventional type 1 dendritic cell (cDC1) to CD4⁺ T cells increases their expression of CD40 ligand (CD40L). Next, CD40L–CD40 binding leads to increased DC antigen presentation ability and expression of co-stimulatory ligands and cytokines. Type I interferon, IL-12 and IL-15 produced by DCs act directly on CD8⁺ T cells to influence their differentiation into effector cytotoxic T lymphocytes (CTLs). CD27 signaling drives differentiation, survival and metabolism in CTLs, and CD4⁺ T cell-derived IL-2 and IL-21 can also support the CTL response.¹⁵ Taken from Borst et al. *Nature Reviews Immunology* 2018.

The T cell receptor

The antigen specific of any T cell is dictated by the sequence and structure of the TCR. A TCR consists of two paired protein chains (TCR α and TCR β), which together recognize a specific peptide bound to MHC proteins on APCs. Each of the TCR α - and β -chains are made up of V and C regions. In the V region of each TCR chain, there are three hypervariable, or complementarity-determining, regions (CDR), each corresponding to a loop in the V domain. Of these, the greatest variability is in the CDR3, which is located at the junction of the V and C regions, and is the most important region for antigen recognition. Between the V and C genes are groups of several short coding sequences called diversity (D) and joining (J) gene segments. During lymphocyte development, a T cell's unique TCR is generated through V(D)J recombination, a somatic rearrangement of the germline TCR loci in T cells²³. During V(D)J recombination, various variable (V), diversity (D), and joining (J) gene segments are recombined (V-J recombination for the TCR α and V-D-J recombination for TCR β) (**Figure 3**). Further diversity can be introduced at the junctions between gene segments, via exonuclease-guided removal of nucleotides, terminal deoxyribonucleotidyl transferase (TdT)-guided random addition of nucleotides forming “N” regions, and through DNA break repair forming P-nucleotides. These junctional sequences and the D and J segments encode the amino acids of the CDR3 loop. In the process of creating junctional diversity, many genes may be produced with sequences that cannot code for proteins and are

therefore useless, necessitating checkpoints during lymphocytes maturation at which only cells with useful receptors are selected to survive. As a result of these mechanisms, the nucleotide sequence at the site of V(D)J recombination in one T cell clone differs from the sequence at the V(D)J site generated by every other clone, leading to the generation of a diverse TCR repertoire that is able to recognize countless foreign or mutant antigens.

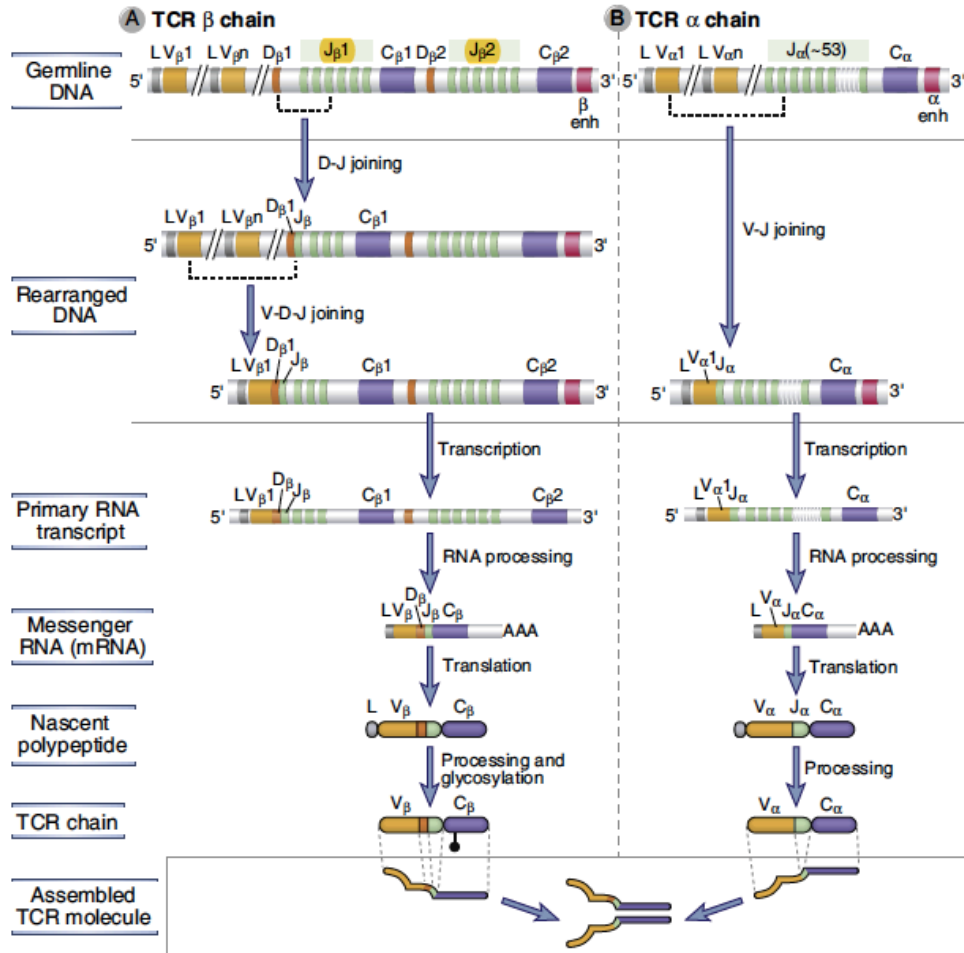


Figure 3. TCR α and β chain gene recombination. Examples of the recombination and gene expression events are shown for the TCR β chain (A) and the TCR α chain (B). In A, the variable (V) region of the rearranged TCR β chain includes the V β 1 and D β 1 gene segments and the third J segment in the J β 1 cluster. The constant (C) region in this example is encoded by the exons of the C β 1 gene. At the TCR β chain locus, D-to-J joining is followed by V-to-DJ joining. In B, the V region of the TCR α chain includes the V α 1 gene and the second J segment in the J α cluster.²⁴

There are three key properties that dictate the functionality of a T cell: affinity, avidity, and functional avidity. The TCR affinity refers to the physical strength of the monomeric interaction between the TCR and the pMHC complex, and is measured using the dissociation constant K_d ²⁵. Previous studies indicate that a lower K_d and thus a stronger interaction lead to a better T-cell response²⁶. TCR avidity refers to the strength of multimeric TCR-pMHC interactions, and thus can be measured by staining live T cells with pMHC-tetramers and measuring fluorescent intensity²⁷. Avidity is determined partially by TCR affinity, but also by other factors, such as TCR clustering and coreceptor interactions²⁸ which stabilize TCR/pMHC interactions and are critical for the functionality of low-affinity TCRs²⁹. Finally, functional avidity of a T cell is defined by its ability to biologically respond to titrated pMHC complexes, as measured by functional readouts such as cytotoxicity, cytokine release, proliferation, or antitumor responses^{25,30}. In this way, functional avidity is also influenced not only by the intrinsic TCR affinity, but also by the expression levels of the TCR and CD4⁺/CD8⁺ coreceptors and downstream signaling molecules^{31,32}. Though these three parameters typically correlate, they do not have to; for example, the presence of inhibitory molecules may decrease functional avidity even in the setting of a high affinity TCR. Characterizing these parameters in T cells is becoming increasingly critical given the recent advancements in cancer immunotherapy.

Furthermore, it is essential to improve our understanding of the interaction between TCR and antigen through analysis of antitumor TCR repertoires. Early TCR repertoire analysis methodologies included complementarity determining region 3 (CDR3) spectratyping, flow cytometry with monoclonal antibodies directed against different V α and V β segments, and bulk sequencing of the TCR β chain³³. More recently, single-cell sequencing technologies such as 10x

have enabled detailed analysis of the CDR3 region from paired TCR α and TCR β chains, enabling more granular reconstructions of TCR repertoires³⁴⁻³⁶. Moreover, our lab has honed a high-throughput and sensitive plate-based method to interrogate TCR repertoires involving single-cell and bulk sequencing that can be combined with single cell transcriptome data, allowing for correlation of T cell transcriptional states with TCR identity.

Harnessing T cells to fight cancer: Cancer Immunotherapy

Over the past decade, the treatment of both solid and hematologic cancers has been revolutionized by methods to harness and strengthen the antitumor immune response, and specifically, the antitumor T cell response. These strategies include immune checkpoint blockade, chimeric antigen receptor (CAR-T) therapies, and personalized cancer vaccination.

Immune checkpoint blockade (CPB) therapies are monoclonal antibodies directed against immune checkpoint molecules, such as cytotoxic T-lymphocyte protein 4 (CTLA-4) and programmed cell death protein 1 (PD-1). These agents act by reestablishing or augmenting pre-existing antitumor responses in patients through the inhibition of checkpoint signaling, a suppressive mechanism which normally dampens immune responses and protects against autoimmunity. These agents have demonstrated striking clinical efficacy, beginning with ipilimumab (anti-CTLA-4) for advanced melanoma in 2011³⁷. Drugs targeting PD-1 and PD-L1 have also been successful in melanoma, non-small-cell lung cancer (NSCLC), and renal-cell carcinoma^{38,39}, as have combinations of the two classes of checkpoint inhibitors in melanoma^{40,41}. However, currently, a minority of tumors and patients respond to checkpoint blockade, suggesting that a pre-existing tumor-specific immune response is insufficient or absent in the majority of patients⁴²⁻⁴⁴.

In adoptive cellular therapy (ACT), patients are treated with autologous T cells derived from tumor-infiltrating lymphocytes (TILs) or genetically modified to express highly avid and tumor-specific TCRs. There are currently three types of ACT: T cell receptor-engineered T cells, chimeric antigen receptor (CAR)-T cells, and TIL-therapy. TILs are generally isolated from surgically resected tumor, selected for on the basis of *in vitro* tumor-specificity, and expanded *in vitro* before reinfusing into the patient⁴⁵. T cell receptor-engineered T cells are generated by expressing tumor-reactive and highly avid TCRs on normal T cells. Together, TIL therapy and T cell receptor-engineered T cells have shown clinical efficacy in the treatment of various cancers⁴⁶⁻⁴⁸, achieving up to 72% objective response rates (ORR) in metastatic melanoma⁴⁹⁻⁵³. CAR-T cells are genetically engineered to express a chimeric receptor consisting of the antigen-binding domain of an antibody fused to the signaling components of a T cell receptor⁵⁴. CAR-T cells are theoretically applicable to a wider range of patients in whom suitable TILs cannot be isolated⁵⁵. Notably, they have shown clinical efficacy in CD19-expressing B cell malignancies such as childhood acute lymphoblastic leukemia (ALL)⁵⁶⁻⁵⁸, but efforts in solid tumors have achieved limited success.

These strategies illustrate the effectiveness of stimulating T cells to recognize cognate tumor antigens, but they are not without limitations. By design, CAR-T cell therapy is limited by its restriction to a single antigen target, which is a feasible approach for tumors that are mostly uniform and express a common dominant antigen (such as CD19), but is suboptimal for solid tumors, which typically lack a common surface antigen target. Similarly, the ORR of single-agent CPB is limited to 30% in most tumor types for which activity has been shown^{38,59,60}, and ORRs have been negligible to minimal in several cancers, including microsatellite-stable colorectal cancer and pancreatic cancer³⁹. Notable exceptions include microsatellite-unstable tumors⁶¹,

Merkel cell carcinoma⁶² and Hodgkin lymphoma⁶³, for which ORRs of CPB are 50–80%. Biomarkers to predict therapeutic benefit are clearly needed, as are better approaches to achieve maximal tumor specificity while minimizing toxicity. Combining CPB with a therapy that can pre-sensitize the host immune system to the tumor may be a rational strategy to achieve this goal.

Cancer Vaccines

Many believe that cancer vaccines could offer a combinatorial solution by steering the immune response to more specifically target tumor both through the generation of new tumor-specific T cell responses and the amplification of existing responses (**Figure 4**). Until recently, however, cancer vaccine efforts have been limited by a general lack of understanding of how to stimulate potent cytotoxic T cell responses in human patients. Specifically, uncertainties have abounded regarding the identities of antigens to use, optimal delivery vehicles, the types of adjuvants required, and ideal vaccine formulations^{3,64}. Two of these elements, vaccine formulations and tumor antigens, are discussed below.

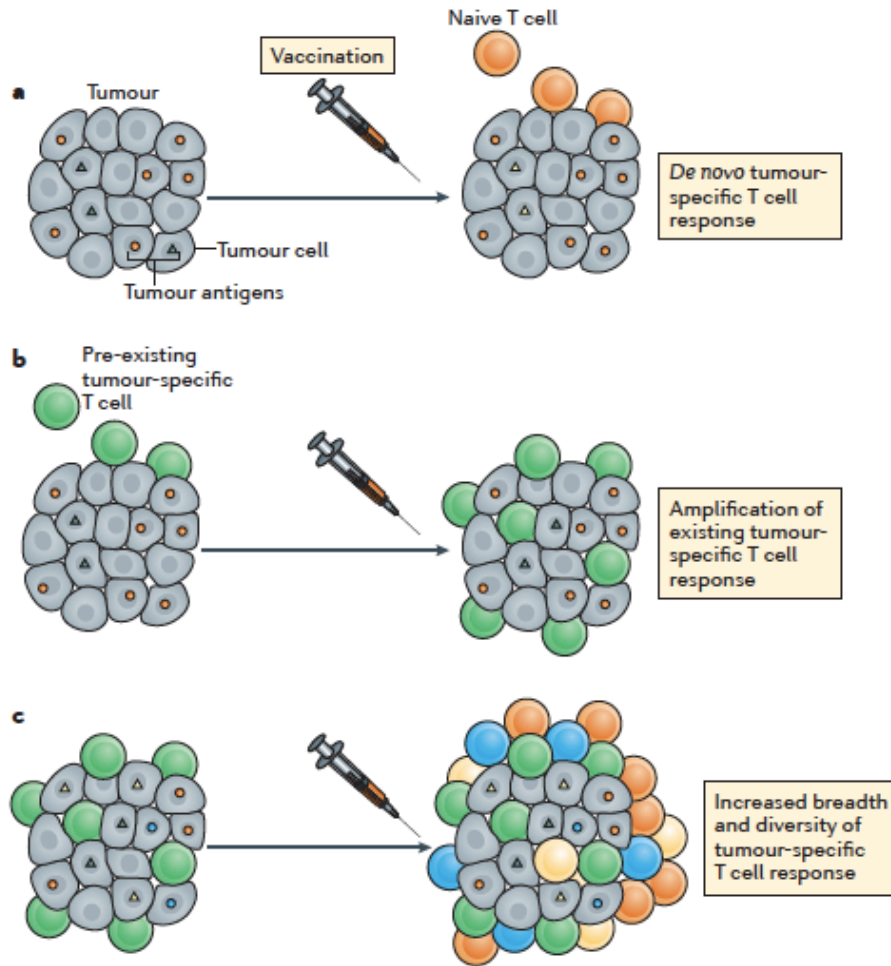


Figure 4. Mechanisms of action by cancer vaccines. a) Cancer vaccines can generate *de novo* tumor-specific T cell responses. b) Cancer vaccines can amplify pre-existing tumor-specific T cell responses. c) Finally, cancer vaccines can increase the breadth and diversity of tumor-specific T cell responses.³ Taken from Hu et al. *Nature Reviews Immunology* 2018.

Vaccine Formulations

Two general classes of vaccine formulations exist: 1) those that broadly target all antigens within a tumor, and 2) those that target one or multiple specific tumor antigens. The most common vaccine type within the first class is the whole tumor cell-based vaccine. These vaccines can be generated from irradiated intact tumor cells or tumor cell lysates, autologous tumor tissues, or established tumor cell lines^{65,66}. Variations of these have shown clinical efficacy in pancreatic cancer, chronic lymphocytic leukemia, and in the post-transplant setting following HSCT for acute myeloid

leukemia (AML)⁶⁷⁻⁶⁹. In addition, DC-tumor cell hybrid vaccines have been created through the fusion of DCs with tumor cells, and have shown promising clinical activity in patients with AML and renal cell carcinoma^{70,71}. However, the effectiveness of whole tumor cell-based vaccines may be theoretically compromised by the dilution of the most immunogenic tumor antigens with all other self-antigens that are also present in normal cells.

By contrast, tumor antigen-specific vaccines only contain the parts of tumor cells that are necessary to elicit an immune response. Subtypes of this vaccine class include protein vaccines, which are typically composed of purified peptides, nucleic acid-based vaccines, including DNA and mRNA, viral vectors, and DC vaccines. Peptide vaccines have shown optimal success when composed of multiple long peptides (defined as 20-30mers) that require processing by APCs and have the potential to stimulate both CD4⁺ and CD8⁺ T cells through antigen presentation on MHC class II and I, respectively⁷²⁻⁷⁴. DNA-based vaccines have shown only modest immunogenicity and clinical success in various cancers, thus few have progressed beyond phase I clinical trials. mRNA-based vaccines have proven more promising, as demonstrated by the generation of potent antitumor immunity by a recent personalized mRNA mutanome vaccine for melanoma². However, RNA vaccines are hindered by the fact that they cannot be flexibly combined with certain potent immune adjuvants. A prostate cancer viral vector vaccine containing transgenes encoding PSA and three costimulatory molecules induced a modest immune response in patients with metastatic prostate cancer, and is now being evaluated in a phase III clinical trial⁷⁵. Finally, clinical trials assessing *ex-vivo*-generated DCs loaded with tumor antigens in various forms have been executed in multiple cancers, including prostate, melanoma, and colon cancer⁷⁶.

Tumor Antigens

Tumor antigens can be broken down into two main categories: 1) tumor-associated antigens (TAAs) and 2) tumor-specific antigens. TAAs include antigens that are overexpressed, involved in differentiation, or preferentially expressed by cancer cells. Well-established TAAs include HER2 (breast cancer), PSA (prostate cancer), and MART1 (melanoma). Cancer-testis antigens (CTAs) are a subset of TAAs that are thought to harbor greater tumor specificity, as they are highly expressed in tumors, and minimally expressed in normal tissues (they are only found in adult germline and trophoblastic cells). Notable examples of these include MAGE and NY-ESO-1^{77,78}. In general, as TAAs are also expressed in normal tissues, there is often a substantial degree of central immune tolerance against them, necessitating high levels of expression in tumor cells to reach the threshold of T cell recognition. Furthermore, even when these antigens are targeted, there is an inherent and substantial risk of inducing autoimmunity.

Tumor-specific antigens include oncogenic viral antigens and tumor neoantigens. Oncogenic viral antigens are commonly found in virally-induced cancers such as human papillomavirus (HPV)-associated cervical cancer, hepatitis B-associated hepatocellular carcinoma, and human herpesvirus 8-associated Kaposi sarcoma. Tumor neoantigens are altered peptides generated from somatic mutations in tumor cells. Whether a somatic mutation can form a neoantigen depends on several factors: 1) the capacity for the mutated sequence to be translated into protein, 2) the ability to process and present the mutated protein as peptides on APCs, 3) the affinity between the mutated peptide and patient MHC molecules, and 4) affinity of T cell receptor (TCR) for the mutant pMHC complex^{79,80}. As neoantigens are not only highly tumor specific but

also highly immunogenic given the lack of pre-existing central tolerance, they are regarded as ideal cancer vaccine targets (**Figure 5**).

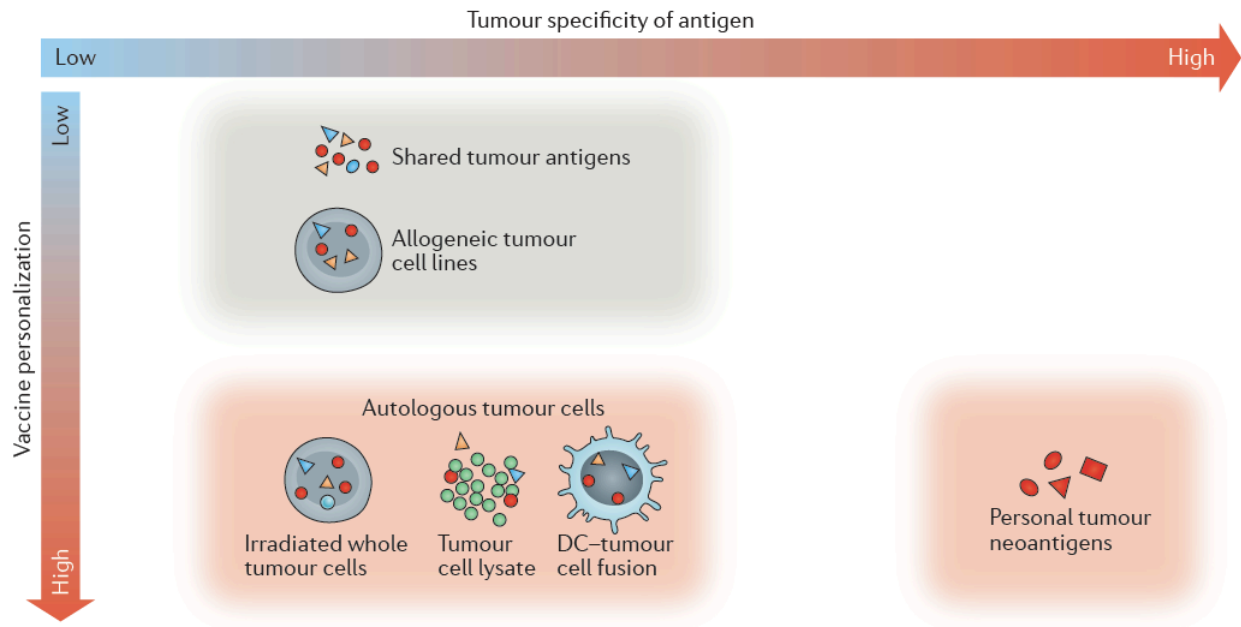


Figure 5. The range of tumor antigens. Potential antigens for use in cancer vaccines differ in terms of tumor specificity and viability for vaccine personalization. Neoantigens are ideal targets for personalized, highly tumor-specific cancer vaccines.³ Taken from Hu et al. *Nature Reviews Immunology* 2018.

Recent evidence supports a robust role for neoantigen-specific antitumor immune responses (**Figure 6**). For one, neoantigen load has been associated with responses to CPB and improved survival in cancer patients, especially in tumors with a high mutational burden such as melanoma, NSCLC, and colorectal cancer^{81–85} (**Figure 7**), indicating that overall mutational burden is associated with neoantigen load⁸⁶. Second, neoantigen-specific T cell populations are expanded in multiple settings of effective antitumor immunity, including following CPB and ACT^{87–90} and after HSCT⁹¹. Finally, animal and human studies have confirmed the presence neoantigen-specific cytotoxic T cell-mediated antitumor activity^{92–98}. However, personalized discovery of candidate neoantigens was not feasible until the advent of tools such as whole-exome sequencing (WES) and

RNAseq, which have enabled the comprehensive identification of mutated, expressed genes within a patient’s tumor, in addition to novel bioinformatics tools to predict corresponding MHC-binding neoepitopes. Because of this, the field is now experiencing a paradigm shift, in which it is possible to envision the generation of on-target effective tumor immunity without collateral damage to other tissues through the administration of personalized neoantigen vaccines.

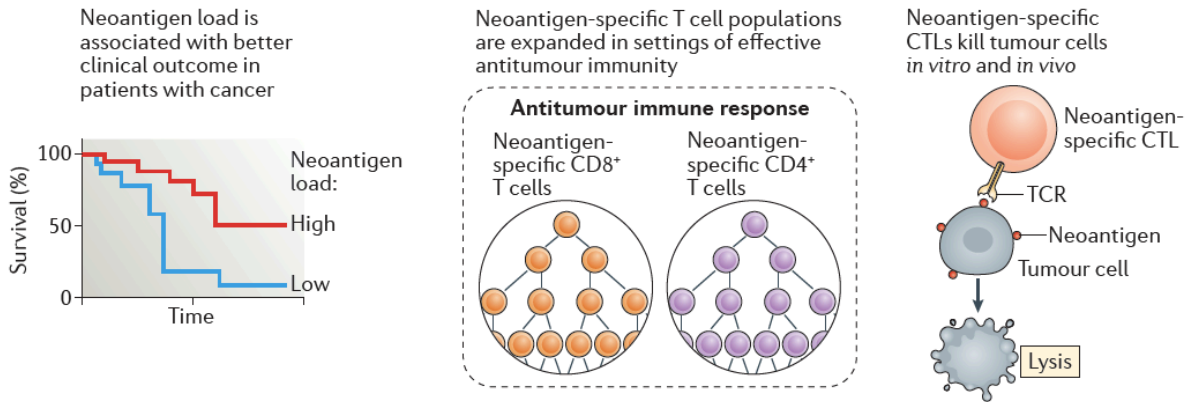


Figure 6. Evidence supporting neoantigens as targets of antitumor immunity.³ Taken from Hu et al. *Nature Reviews Immunology* 2018.

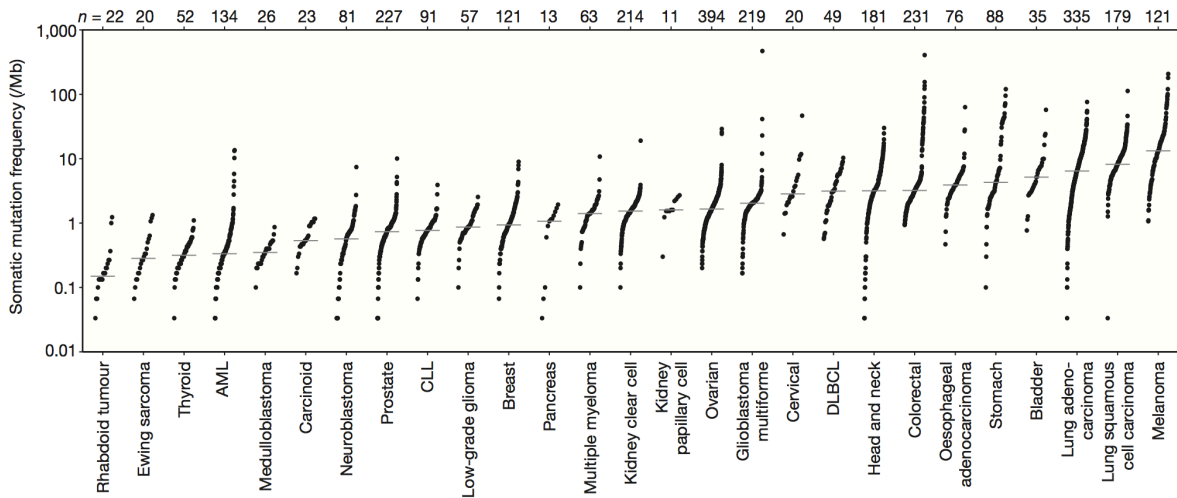


Figure 7. Mutational burden by tumor type. Each dot corresponds to a tumor-normal exome pair, with vertical position indicating the total frequency of somatic mutations in the exome. Tumor types are ordered by their median somatic mutation frequency, with the lowest frequencies on the left. A high somatic mutation burden is found in tumors induced by carcinogens such as tobacco smoke and UV light.⁹⁹ Taken from Lawrence et al. *Nature* 2013.

Personalized Neoantigen Vaccines

Our lab and others have established high-throughput pipelines to identify neoantigens, predict MHC-binding peptides, and select neoantigen epitopes (neoepitopes) for the generation of personalized neoantigen vaccines. Briefly, the pipeline proceeds as follows:

1) Identification of tumor-specific mutations

Tumor-specific mutations are identified through WES of matched resected tumor and normal tissue samples, and expression of mutated proteins is confirmed through RNAseq.

2) Prediction of MHC-binding peptides derived from mutations

Peptide regions encoding non-synonymous expressed mutations (including both missense mutations and frameshift mutations productive of novel open reading frames (neoORFs) are inputted into neural-network based algorithms such as NetMHCpan^{100,101} and/or mass-spectrometry-based methods^{95,102} to predict peptide binding affinity to MHC class I or MHC class II. Given the variability in MHC class II molecules and the complexity of the peptide-MHC binding process, most algorithms are optimized to predict MHC class I-binding peptides⁷⁹. Peptides with high predicted binding affinity (half-maximum inhibitory concentration (IC₅₀) < 500nM) are selected as candidate neoantigens.

3) Epitope selection

Predicted neoepitopes are prioritized for inclusion in vaccination based on predicted immunogenicity. Typically, neoepitopes arising from mutations generating neoORFs are given highest priority due to high sequence divergence from their normal counterparts. Neoantigens arising from single nucleotide variants (SNVs) are subsequently ranked on the basis of predicted HLA binding affinity and location of mutation (anchor residue vs. non-anchor residue). SNVs and neoORFs in oncogenes are given high priority. Finally,

peptide synthesizability and solubility factors are also taken into account (e.g. hydrophobicity, presence of multiple cysteines).¹

Several recent studies have demonstrated the safety, feasibility and immunogenicity of personalized neoantigen vaccines in patients with melanoma, which has a high mutational burden, and glioblastoma (GBM), which carries a low mutational burden^{1,2,103–105}. The first neoantigen-based vaccine consisted of dendritic cells pulsed with HLA-A2-restricted neoantigens¹⁰³. The vaccine targeted 7 neoantigens and was administered intravenously to three patients with melanoma who were previously treated with the CPB agent ipilimumab, a CTLA-4 inhibitor. Researchers found that the cellular diversity of the antitumor response was increased after vaccination, but specific vaccine effects were difficult to parse from those of ipilimumab. In another study, a neoantigen-based mRNA vaccine was tested in patients with high-risk melanoma following surgical resection². Vaccines consisted of mRNA encoding up to 10 neoantigens for each patient predicted to bind to HLA class I and class II, and were administered intranodally. Prior to personalized vaccine administration, patients with NY-ESO-1-positive and/or tyrosinase-positive melanoma also received a single dose of an mRNA vaccine encoding these TAAs. Out of the 13 patients, eight who had no detectable disease at the time of vaccination remained tumor-free throughout a follow-up of 12–23 months. Of the five patients who had metastatic disease at the time of vaccination, two experienced a vaccine-related objective response, and one had a complete response in combination with anti-PD-1 therapy. Moreover, the vaccine induced *de novo* CD4⁺ and CD8⁺ T cell responses in all vaccinated patients.

In a third study, fifteen patients with GBMs positive for HLA-A*02:01 or HLA-A*24:02 were treated with 2 vaccines in series: the first was composed of a premanufactured library of 33 peptides derived from shared unmutated antigens, and the second vaccine was composed of 7 personalized neoepitope peptides derived from neoantigens and predicted to bind strongly to HLA class I and II¹⁰⁵. Promisingly, this vaccine strategy elicited continuous CD8⁺ and CD4⁺ T cell responses in the majority of patients. Furthermore, the median overall survival (OS) was 29.0 months, which compares favorably to the median OS of 20.0 months observed in the ACT IV trial, which tested rindopepimut with temozolomide for patients with newly diagnosed, EGFRvIII-expressing GBM, and could cautiously be considered as a reference cohort, acknowledging the limitations of comparing small early phase trials to phase III trials.

In a fourth study, one patient with methylguanine methyltransferase (MGMT)-unmethylated GBM was treated with a heterologous personalized vaccine, including an autologous tumor lysate-dendritic cell vaccine (“DCVax”) followed by a neoantigen-based vaccine (“GBM.PVax”)¹⁰⁶ composed of 8 long peptides encompassing 7 neoantigens. Analysis of post-treatment peripheral blood demonstrated detectable neoantigen-specific CD8⁺ (1 neoantigen) and CD4⁺ T cell (2 neoantigens) responses after peptide vaccination. A similar pattern of reactivity was seen in post-treatment TILs. Finally, genomic and transcriptomic characterization of the mutational landscape and tumor microenvironment pre- and post-treatment revealed tumor clonal evolution and evidence of potential immune evasion.

Our lab has recently studied personalized neoantigen vaccines (coined “NeoVax”) in two phase I clinical trials for 1) patients with previously untreated high-risk (stage IIIB/C and IVM1a/b)

melanoma after surgical resection with curative intent¹, and 2) patients with newly diagnosed methylguanine methyltransferase (MGMT)-unmethylated glioblastoma after surgical resection and conventional radiotherapy¹⁰⁴. In the melanoma study, immunizing long peptides (IMP; 15-30mers) targeting up to 20 neoantigens per patient were admixed with the Toll-like receptor 3 (TLR3) and melanoma differentiation-associated protein 5 (MDA-5) agonist poly-ICLC, and administered subcutaneously in pools to 6 patients in a prime-boost schedule.¹ Of the six patients, four with stage III disease at the time of vaccination showed no signs of tumor recurrence for up to 32 months after vaccination. Two patients with stage IV melanoma at the time of vaccination experienced disease recurrence shortly after vaccination, but had complete tumor regression after treatment with anti-PD-1 therapy. Immunological assays on peripheral blood demonstrated that NeoVax induced robust, polyfunctional T cell responses in all patients. Overall, a T cell response was generated against 60-70% of predicted immunizing neoantigens, and in most cases, neoantigen-specific T cells could discriminate between mutant and wild-type antigens. Of note, more neoantigen-specific CD4⁺ responses were generated than CD8⁺ T cells responses (which was also true of the aforementioned mRNA vaccine), despite the use of HLA class I binding algorithms to select immunizing peptides. This phenomenon may be explained by differences in the physical structure of the HLA class I and HLA class II binding grooves: while HLA class I-binding epitopes fit precisely within a close-ended binding pocket, HLA class II-binding epitopes are typically longer and extend out of the core-binding site, allowing for promiscuous binding properties and

¹ Initially, ten patients were enrolled. However, only eight demonstrated the high mutation rate expected for melanoma, carried expected melanoma-associated mutations (that is, in *BRAF*, *NRAS*, and others) and predominantly C→T transitions (consistent with ultraviolet exposure), and expressed multiple melanoma markers. For these 8 patients, 13–20 immunizing long peptides (IMP) per patient (with lengths of 15–30 amino acids) were synthesized and grouped into 4 separate immunizing pools. Only 6 patients ultimately initiated vaccination.

thus a larger number of peptides to function as epitopes for multiple HLA class II molecules^{107,108}. Furthermore, the finding may be related to the relative paucity of cross-presenting C-type lectin domain family 9 member A (CLEC9A)⁺ DCs, a DC subtype that is especially efficient at processing extracellular antigens and cross-presenting them on major histocompatibility complex (MHC) class I¹⁰⁹. Therefore, many more APCs are likely to be available for MHC class II-restricted antigen presentation to CD4⁺ T cells¹¹⁰. Finally, in mice, DCs that present to CD8⁺ T cells are mostly found in the deep paracortex of lymph nodes where antigen quantities are reduced, whereas those that activate CD4⁺ T cells typically reside in the periphery of the lymph node, resulting in greater activation of CD4⁺ T cells¹¹¹.

In the glioblastoma NeoVax trial, a median of 12 (range 7-20) IMPs per patient were admixed with poly-ICLC and administered subcutaneously in pools to 8 patients in a prime-boost schedule. Patients who did not receive dexamethasone for cerebral edema generated circulating polyfunctional neoantigen-specific CD4⁺ and CD8⁺ T cell responses that were primarily of a memory phenotype, and exhibited an increase in the number of tumor-infiltrating T cells. Single-cell T cell receptor analysis also revealed evidence of trafficking of neoantigen-specific T cells from the peripheral blood into an intracranial tumor. Despite these immune responses, all patients ultimately experienced tumor recurrence and died of progressive disease (median OS 16.8 months), indicating that the induced T cell responses were not robust enough to produce clinically relevant antitumor activity. This could be in part due to the expression of multiple co-inhibitory receptors in neoantigen-specific T cells, consistent with a profound exhaustion phenotype¹¹².

Collectively, these initial clinical trials testing personal neoantigen vaccines are encouraging. However, only relatively short-term immune responses have been reported to date. Furthermore, recent studies have demonstrated that proper T-cell priming is critical for the clinical efficacy of PD-1 blockade, and that PD-1 blockade can induce exhaustion of tumor-directed T cell responses¹¹³, emphasizing the importance of elucidating the functionality of tumor-specific T cell responses in the context of immune checkpoint inhibition.

Thesis Aims

This thesis aims to delineate the clinical courses and vaccine-induced neoantigen-specific T cell responses, including their phenotype and functionality, of the 6 patients with high-risk melanoma who received NeoVax¹, and of 2 additional high-risk melanoma patients who received NeoVax after the original report was published. First, we set out to characterize the neoantigen-reactive T cell response in the 2 new patients (Pts. 11 and 12) following vaccination (at 16 weeks) and in all patients several years (median 46 months) following vaccination. In 5 patients who experienced a cancer recurrence during long-term follow-up, we investigated genomic and transcriptomic differences between the original resected tumors and relapsed tumors, and assessed for loss of neoantigens targeted by the vaccines. We next explored phenotypic trajectories and TCR repertoires of neoantigen-specific CD4⁺ T cells in a subset of patients to determine the clonal evolution of neoantigen-specific T cell populations over time. Finally, to determine if vaccination in combination with anti-PD-1 therapy elicited the expansion of T cell responses to new antigens not included in the vaccine, an indication of direct tumor killing, we evaluated epitope spreading.

Methods

Study design

Patients with high-risk melanoma were consented and enrolled between April 2014 and October 2015 to a single center, phase I clinical trial approved by the Dana-Farber/Harvard Cancer Center Institutional Review Board (IRB) (NCT01970358). This study was conducted in accordance with the Declaration of Helsinki. Key eligibility criteria were clinically or radiographically evident, pathologically confirmed stage IIIB/C or IVM1a/b melanoma deemed amenable to complete surgical resection and an ECOG performance status of 0 or 1. More details about eligibility criteria have been described previously¹. The primary endpoints of the study were safety and feasibility; secondary endpoints were induction of tumor- and neoantigen-specific cellular immune responses and the number of patients alive at 2 years after melanoma resection.

Each personalized neoantigen-targeting vaccine was generated as previously described¹. In brief, each vaccine consisted of long peptides combined into 4 distinct immunizing peptide pools with 0.3 mg of each peptide admixed with 0.5 mg poly-ICLC per pool in a volume of 1 ml; these were administered subcutaneously (SC) on days 1, 4, 8, 15 and 22 (priming phase) and weeks 12 and 20 (booster phase). Each of the 4 neoantigen vaccine pools per patient was assigned to one of four “non-rotating” extremities (or the left or right midriff as an alternate anatomical location) for each injection.

The safety of study treatment was assessed based on the occurrence of adverse events, which were categorized and graded according to National Cancer Institute Common Terminology Criteria for Adverse Events (CTCAE, version 4.0). During the treatment phase, safety assessments were

performed on the day of vaccination and one week after each vaccination. During the initial follow up phase, safety assessments were conducted every 3 months. Surveillance scans (computer tomography or combined position emission tomography/computer tomography) were performed every 6 months; standard RECIST 1.1 criteria were used for assessment of disease recurrence.

Patient samples

Heparinized blood samples were obtained from study subjects on IRB-approved protocols at the DFCI. Patient peripheral blood mononuclear cells (PBMCs) were isolated by Ficoll/Hypaque density-gradient centrifugation (GE healthcare) and cryopreserved with 10% dimethylsulfoxide in FBS (Sigma-Aldrich). Cells from patients were stored in vapor-phase liquid nitrogen until the time of analysis. HLA class I and class II molecular typings were determined by PCR-rSSO (reverse sequence specific oligonucleotide probe), with ambiguities resolved by PCR-SSP (sequence specific primer) techniques (One Lambda Inc., BWH Tissue Typing Laboratory).

Patient tumor samples were obtained immediately following surgery. A portion of the sample was removed for formalin fixation and paraffin embedding (FFPE). The remainder of the tissue was carefully minced manually, suspended in a solution of collagenase D (200 unit/mL) and DNase I (20 unit/ml) (Roche Life Sciences), transferred to a sealable plastic bag and incubated with regular agitation in a Seward Stomacher Lab Blender for 30-60 min. After digestion, any remaining clumps were removed and the single cell suspension was recovered, washed and immediately frozen in aliquots and stored in vapor-phase liquid nitrogen. For patients 1, 2, 3, 5, 7, 11, and 12, the frozen tumor cell suspensions were used for WES and RNA-seq. For patients 4 and 6, WES and RNA-seq were performed on scrolls from the FFPE tissue. (**Supplementary Table 1**).

Whole-Exome Sequencing (WES)

CLIA-certified WES was conducted by the Clinical Research Sequencing Platform, Broad Institute (CLIA #:22D2055652). Library construction from surgical melanoma specimens and matched germline DNA of all 8 patients was performed as previously described¹¹⁴. Pts. 1-6 have been previously described¹ and Pts. 11 and 12 in addition to the relapsed tumors of Pts. 1, 2, 3, 5 and 6 were processed in the same way. Briefly, cell suspensions were used for WES, and whole-exome capture was performed using the Illumina Nextera Rapid Capture Exome v1.2 bait set. Resulting libraries were then qPCR quantified, pooled, and sequenced with 76 base paired-end reads using HiSeq 2500 sequencers (Illumina). Data were analyzed using the Broad Picard Pipeline which includes de-multiplexing, duplicate marking, and data aggregation.

RNA sequencing (RNA-Seq)

RNA was extracted from fresh frozen sections (Patient 1 relapsed tumor), or FFPE samples (patients 2, 3, 5, 6 relapsed tumors) using the Qiagen AllPrep DNA/RNA/miRNA Universal Kit or the Qiagen AllPrep DNA/RNA FFPE Kit, respectively. RNA-seq libraries were prepared using Illumina TruSeq Stranded mRNA Library Prep Kit (for cell suspensions) or Illumina's TruSeq RNA Access Library Prep Kit (for FFPE samples). Flowcell cluster amplification and sequencing were performed according to the manufacturer's protocols using the HiSeq 2500. Each run was a 101 bp paired-end with an eight-base index barcode read. Data was analyzed using the Broad Picard Pipeline which includes de-multiplexing and data aggregation.

DNA quality control

Standard Broad Institute protocols as previously described^{115,116} were used for DNA quality control. The identities of all tumor and normal DNA samples were confirmed by mass spectrometric fingerprint genotyping of 95 common SNPs by Fluidigm Genotyping (Fluidigm). Sample contamination from foreign DNA was assessed using ContEst¹¹⁷ (**Supplementary Table 2**).

RNA quality control

All RNA was quantified using the Quant-It RiboGreen RNA reagent, an ultrasensitive fluorescent nucleic acid stain used for quantitating RNA in solution, and a dual standard curve. The assay generates a quantity metric which can be 2-1000ng/uL. The dilution plate generated with 3uL of sample was used for entire QC process. The RNA was then qualified using the LabChip GX Touch. The assay generated a quality metric – the RNA Quality Score – which was used to establish acceptance criteria for further analysis of the samples. The RQS ranges from 0 to 10, with 10 representing the highest quality. This metric correlates closely with Agilent's RIN score. The LabChip GX instrument primed the chip and automatically initiated the electrophoretic analysis of the samples. The samples were aspirated one-by-one into the chip through the sipper capillary. Once samples were in the chip, it was stained, separated, and detected in microfluidic channels. For poor quality samples, such as FFPE, a DV200 score was used which was originally developed by Illumina. A score of 35% or greater was considered likely to perform well in sequencing.

Modified explanation of RQS from the LabChip GX user guide: RQS stands for Relative Quality Score. The software determines the quality of the RNA sample by measuring the amounts of known RNA fragments relative to the total RNA present in the sample. The raw data was filtered and the resulting electropherograms of all wells were plotted. A curve spline fit to the data was performed to generate a baseline above which RNA fragment peaks are detected. This baseline was displayed as a blue line on the electropherogram and was adjusted as needed. A sizing ladder, which is a mixture of RNA fragments of different known sizes, was run first from the ladder vial. The ladder was analyzed and a standard curve of migration time versus RNA size was plotted from the RNA ladder by interpolation between individual RNA fragment size/migration points. A dye matching the lowest peak in the ladder was run with each of the samples. This is called the lower marker (LM), which is used to align the ladder data with data from the sample wells. The standard curve and the markers were used to calculate RNA fragment sizes for each well from the migration times measured. The Total RNA present was computed by finding the area under the electropherogram trace. The baseline for this integration is a straight line starting at the end of the lower marker and ending at the baseline end time. The height of the baseline endpoints was computed from an average of a five second window around the baseline Start Time and End Time. These values were used to create a Relative Quality Score which allowed us to evaluate the quality of RNA before it moves forward for sequencing (**Supplementary Table 2**).

Somatic mutation calling

Mutation analysis

Analyses of whole-exome sequencing data of tumor and matched PBMCs (as source of normal germline DNA) from the patients were used to identify coding-sequence specific mutations and

small insertions/deletions. We utilized GAT4 pipelines in Terra for somatic mutation detection (<https://terra.bio/>). Paired-end Illumina reads were aligned to the hg19 human genome reference using the Picard pipeline to yield BAM files containing aligned reads (bwa version 0.5.9) with well-calibrated quality scores. Cross-sample contamination was assessed with the GATK's CalculateContamination tool with a 5% threshold. Point mutations and indels were identified using the M2 tool (v2.7.0). Possible artifacts due to orientation bias and alignment errors were removed through a series of filters (github.com/gatk-workflows/gatk4-somatic-snvs-indels/Mutect2). A random subset of alterations were manually reviewed in integrated genome viewer (IGV)¹¹⁸. The final list of filtered mutations, insertions and deletions were annotated using Funcotator. **(Supplementary Table 3).**

Copy number analysis

Copy number events were called and filtered using GATK4 ModelSegments¹¹⁹ [<https://gatkforums.broadinstitute.org/dsde/discussion/11682/>; <https://gatkforums.broadinstitute.org/dsde/discussion/11683/>]. In order to minimize false positives, we utilized a copy number panel-of-normals created based on germline samples processed using the same platform. We applied a custom conversion script to format the outputs of ModelSegments (both copy ratio and allelic fraction) to be compatible with ABSOLUTE¹²⁰, the tool used to estimate sample purity and ploidy as well as cancer cell fractions (CCFs). ABSOLUTE solutions were picked by manual inspection. The final chosen purity and ploidy solutions were used to estimate CCFs for detected somatic alterations in each sample. Mutations were considered clonal if the expected CCF of the mutation as estimated by ABSOLUTE was 1, or if the estimated probability of the mutation being clonal was greater than 0.5.

Transcriptomic analysis

RNA-seq data from the CheckMate 010 and 025 cohorts were aligned using STAR¹²¹, quantified using RSEM¹²², and evaluated for quality using RNA-seqQC2¹²³. Samples were excluded if they had an interquartile range of $\log_2(\text{TPM}+1) < 0.5$ (indicating low dynamic range), had less than 15,000 genes detected (indicating low library complexity), had an End 2 Sense Rate < 0.90 , or End 1 Sense Rate > 0.10 (as defined by RNA-seqQC2, indicating strand bias).

Identification of target epitopes for peptide design

For Pt. 11, NetMHCpan v2.4¹⁰⁰ was used to identify mutation-containing epitopes that are predicted to bind to the individual patients' MHC class I molecules, as previously described¹. For Pt. 12, 30 peptides were initially designed using netMHCpan v2.4 as above. The bottom 6 were then replaced with distinct epitopes based on binding predictions from a preliminary version of HLAthena¹²⁴, a machine-learning algorithm trained on mass spectrometry-identified peptides¹⁰², using all other criteria as previously described¹. Thirty peptides of 17-26 amino acids length ("long peptides") from up to 30 independent mutations were selected and prioritized for each patient (**Supplementary Table 4, 5, 6**).

Identification of target epitopes for epitope spreading peptide design:

For Pts. 2 and 6, NetMHCpan v2.4 was used to identify non-vaccine mutation-containing epitopes (neoepitopes) predicted to bind to the individual patients' MHC class I molecules. Non-vaccine neoepitope assay peptides (including EPT and ASP) were then selected and prioritized for peptide preparation. NetMHCpan-predicted neoepitopes not included in the original vaccines were chosen for epitope spreading experiments on the basis of a pre-defined set of criteria in the following rank

order: (1) neoORFs which included predicted binding epitopes; (2) high predicted affinity (<150 nM) somatic single nucleotide variations due to anchor residue changes; (3) high-affinity (<150 nM) somatic single nucleotide variations due to mutations in positions other than anchor residues; (4) neoORFs with no predicted binding epitopes; (5) lower affinity (<150–500 nM) versions of (2) and (3) (**Supplementary Table 7a**).

For Pt. 3, ASP peptides were selected based on NetMHCpan v2.4-predicted binding affinities of non-vaccine neoepitopes using the same criteria as above. For Pt. 3 EPT peptides, we selected peptides based on NetMHCpan v4.0 and a preliminary version of HLATHENA. We used the following criteria for initial peptide selection: (1) TPM>1; (2) T_alt_count>5; (3) No cysteine. From the peptides that met the above criteria, for NetMHCpan prediction, we ordered peptides from the lowest ell_rank_m that had Ell_rank_mut <0.5. For HLATHENA-based prediction, we ordered peptides from the highest MSEC (a binding affinity metric that is calculated based on sequencing of HLA-bound peptides by mass spectrometry, expression (TPM), and cleavability) that had a MSEC>0.85. For HLA-C*06:02, we selected 9-mers only, as this HLA mostly presents 9-mers¹²⁵. After we listed the peptides predicted by NetMHCpan and HLATHENA by the above criteria, we selected peptides in the following manner: (4) selected the top 38 overlapping peptides among NetMHCpan and HLATHENA predicted peptides; (5) selected 10 additional peptides that had the lowest Ell_rank_mut by netMHCpan prediction; (6) selected 10 additional peptides that had highest MSEC by MS-based prediction (**Supplementary Table 7a**).

For Pt. 2 and 5, TAA EPT peptides originating from a chosen set of common melanoma TAAs (**Supplementary Table 7b**) expressed in patient tumors and predicted by a preliminary version of

HLAthena were chosen. The 20 peptides with the highest MSEC score were chosen for inclusion (**Supplementary Table 7c**). The MAGEEF1 and MAGED2 peptides were selected by accident.

For Pt. 3, TAA EPT peptides were predicted by a preliminary version of HLAthena and chosen for inclusion on the basis of a pre-defined set of criteria in the following rank order: (1) high predicted binding affinity peptides MSEC > 0.9; (2) high expression in the patient's tumor (TPM > 100); (3) T_alt_count>5; (4) peptides not containing cysteine residues; (5) only 9- and 10-mer peptides; (6) for HLA-C*06:02-binding peptides, only 9-mers. For those peptides that met these criteria, we listed the peptides from the highest MSEC. We then selected the top 5 peptides for each gene. (**Supplementary Information Table 7c**).

Synthesis of long peptides, pooling and final vaccine preparation:

As previously described¹, GMP peptides for all 8 subjects were synthesized and purified (CS Bio) using standard solid-phase synthetic peptide chemistry and Reverse Phase High Performance Liquid Chromatography (RP-HPLC). Up to twenty peptides were formulated in an aqueous solution containing $\leq 4\%$ DMSO in isotonic dextrose and mixed into up to 4 pools (for Pts. 11 and 12, 3-4 peptides per pool), with a final dose of 0.3 mg of each peptide per vaccine. On the day of vaccine administration, each peptide pool was admixed with 0.5 mg poly-ICLC (Hiltonol®; Oncovir Inc.) by syringe-to-syringe transfer at the DFCI Clinical Pharmacy.

Immunohistochemical evaluation of primary melanoma cells:

Dual immunohistochemical staining of the antigen presentation components: HLA class I (Abcam, EMR8-5, 1:6000) and HLA class II (Dako, CR3/43 M0775, 1:750) with the melanoma marker

SOX10 (EP 268, Cell Marque, 1:1500) was performed using an automated staining system (Bond III, Leica Biosystems) according to the manufacturer's protocol, as previously described¹²⁶. Semi-quantitative scoring was performed for the intensity of positive staining of melanoma cell membranes for the marker of interest (0, negative; 1, weak; 2, moderate; 3, strong) and for the percentage of positive staining malignant cells (0-100%). A cumulative “H score” was obtained by multiplying intensity score (0-3) by the percentage of malignant cells with positive staining (0%-100%; with any intensity of positive staining). Stained slides were first reviewed and scored independently by two individuals and subsequently reviewed together with a final, consensus score tabulated as previously described¹²⁶.

Generation and detection of patient neoantigen-specific T cells

PBMCs were cultured in RPMI-1640 medium supplemented with L-glutamine, nonessential amino acids, HEPES, β -mercaptoethanol, sodium pyruvate, penicillin/streptomycin (Gibco), and 10% AB-positive heat-inactivated human serum (Gemini Bioproduct). For *in vitro* expansion (‘pre-stimulation’) of antigen-specific T cells, PBMCs were stimulated in 24-well cell culture plates at 5×10^6 cells per well with individual (1.5-2 $\mu\text{g/ml}$) or pooled peptides (each at 1.5-2 $\mu\text{g/ml}$) in the presence of IL-7 (20 ng/ml; R&D Systems). On day 3, low-dose IL-2 (20 U/ml; Amgen) was added. Half-medium change and supplementation of cytokines were performed every 3 days, as described previously¹²⁷. After 10-21 days, T cell (referred to as ‘T cell lines’) specificity was tested against peptide by interferon (IFN)- γ ELISPOT in RPMI-1640 medium supplemented with penicillin/streptomycin and 10% FBS (complete RPMI). For deconvolution of CD4⁺ and CD8⁺ T cell responses, T cells were enriched with CD4⁺ or CD8⁺ T cell Isolation Kit beads (Miltenyi Biotec) prior to plating for ELISPOT.

Antigen formats for immune monitoring

Assay (ASP) and predicted class I epitope peptides (EPT) were synthesized and lyophilized (from either JPT Peptide Technologies or RS Synthesis or Automated Flow Synthesis¹²⁸ (>80% purity). ASP were 15-16 aa and overlapped by at least 11 aa, covering the IMP sequence. EPT were 9-10 aa. Peptides for generation of class II tetramers were synthesized to >90% purity (21st Century Biochemicals).

IFN- γ enzyme-linked immunospot (ELISPOT) assay

IFN- γ ELISPOT assays were performed as described previously¹. Briefly, for pre-stimulated T cells, 5×10^3 T cells and $1-3 \times 10^4$ CD8⁺ T cells for detection of CD4⁺ and CD8⁺ T cell responses, respectively, were co-cultured with 1×10^4 autologous CD4⁺ and CD8⁺ T cell-depleted PBMC (APCs). Peptides (10 $\mu\text{g/ml}$) were directly added to the ELISPOT wells with APCs and incubated with T cells overnight in complete RPMI at 37°C. For *ex vivo* ELISPOT, 2×10^5 PBMC were plated with 5 $\mu\text{g/ml}$ peptide and incubated overnight. For the experiments in **Extended Data Fig. 4a**, non-nucleofected B cells or B cells nucleofected with minigenes encoding mutated or WT peptides were used as APCs, and APCs were cultured on the ELISPOT plate with HLA blocking antibodies (10 $\mu\text{g/ml}$, pan anti-DR [clone: L243]) as previously described¹. Responses were scored positive if spot forming cells (SFC) were at least 2.5 standard deviations (SD) over the DMSO control. For **Extended Data Fig. 1b**, for each patient, the numbers of SFC were regressed on assay, time, and the interaction of assay and time using repeated measures models with an unstructured covariance. P-values (t-test) for the comparisons of each pool against the mock were adjusted using the Benjamini-Hochberg procedure to maintain an overall alpha of 0.05 at each time within patient.

Flow cytometry staining

Patient PBMCs were rested in RPMI containing 10% FBS and 50 U/ml Pen/Strep in 50 ml conical tube overnight. The next day, intracellular cytokine staining (ICS) was performed. ICS assays were performed as described previously¹²⁹ with $1-5 \times 10^6$ PBMC that were incubated for 9 hours at 37°C with media, 10 pg/ml phorbol myristate acetate (PMA) and 1 µg/ml ionomycin, or pooled ASP peptides (5 or 10 µg/ml each) that elicited ex vivo CD4⁺ T cell responses at week 16 post-vaccination. Cultures contained monensin, brefeldin A. BD Cytofix/Cytoperm Kit was used. Cells were then stained with predetermined titers of mAbs against Aqua L/D, CD3 (clone UCHT1; APC-R700), CD4 (clone L200; BV711), CD8 (clone RPA-T8; BV570), PD-1 (clone EH12.1; BB700), CD27 (clone O323; BV786), CD45RA (clone 5H9; APC-H7), CD69 (clone TP1.55.3, ECD), IFN-γ (clone B27; BUV395), IL-2 (clone MQ1-17H12; BUV737), TNF-α (clone Mab11; BV650) (**Supplementary Table 8**).

Generation of HLA-DR tetramers loaded with defined neoantigen peptides

DR1/CLIP or and DR4/CLIP were expressed in stably transfected CHO cells as previously described¹³⁰. The DRα and β chain extracellular domains carried Jun and Fos dimerization domains; a C-terminal BirA site was attached to the DRα chain to enable site-specific biotinylation. The peptide binding site was occupied by a CLIP peptide that was linked through a thrombin-cleavable linker to the N-terminus of the mature DRβ chain. DR/CLIP complexes were purified from CHO cell supernatants by affinity chromatography using mAb L243 (American Type Culture Collection). Purified DR molecules were biotinylated with a 1:20 molar ratio of BirA:DR as described¹³⁰. Prior to peptide loading, DR complexes were treated with thrombin for 2 h to release the CLIP peptide. Peptide-exchange reactions were carried out with a 15-fold molar excess of

dansyl-labeled peptides (21st Century Biochemicals) in a buffer containing 50 mM sodium citrate, 1% octylglucoside, 100 mM NaCl, and 1x protease inhibitor cocktail overnight at 30 °C. DR/peptide complexes were separated from unbound peptide using a Superose 12 HPLC gel filtration column (Amersham). DR molecules loaded with defined neoantigen peptides (**Table 1**) were then isolated using an anti-dansyl affinity column. Complexes were eluted from the column using 50 mM CAPS, pH 11.5 and neutralized with 1 M phosphate, pH 6.0. Biotinylated DR/peptide monomers were buffer exchanged with PBS, concentrated to >1 mg/mL, and frozen in aliquots at -80°C. Fluorophore-labeled streptavidin (either PE or APC) was added to biotinylated DR/peptide monomers at a 1:4 molar ratio in four separate additions over 40 min at room temperature.

DR3/CLIP and DR7/CLIP complexes were expressed in Sf9 insect cells as previously described¹³¹. DR α and β chain constructs were cloned into the pAcDB3 vector for dual p10 promotor-driven expression. Recombinant Baculoviruses was prepared, amplified, and used for protein expression in Sf9 cells cultured in SF900 II medium (Life Technologies). Cells were harvested 72 hours after infection and DR/CLIP complexes were purified from concentrated supernatants by affinity chromatography using mAb L243. Subsequent purification and peptide loading was performed as described above for DR1 and DR4 molecules.

Tetramer Reagents

Streptavidin-R-Phycoerythrin (PE), Prozyme

Streptavidin-Allophycocyanin (APC), Invitrogen

Peptides (21st Century Biochemicals)

Name	Sequence
P1-RUSC2	SVGDFSQEFSPIQEAQQD(K-dansyl)-amide
P4-ARHGAP29	PGKIHLEAEFTQVAKKE(K-dansyl)-amide
P2-ADM2	RTQLLWTPAAPTAMAE(K-dansyl)-amide
P3-FAM190A	SSHYKFSKPALQSQS(K-dansyl)-amide
P3-GTF3C2	HHYLLFQNTDLGSFHDLRL(K-dansyl)-amide
P3-ADAMTS7	RGRELRFNLIANQHLLAPGF(K-dansyl)-amide
P4-PATL1	SPSQFARVPGYVGSPLA(K-dansyl)-amide
P5-ZNF281	SQRTSWEFLQSLVSIKQEK(K-dansyl)-amide
P5-MAP4K4	LASLKNNVSPVLRSHSF(K-dansyl)-amide
P6-MLL	SRLQTRKNKKLALSSTPSN(K-dansyl)-amide

Table 1. Neoantigen Peptides

Tetramer labeling of CD4⁺ T cells

Patient PBMCs that were CD4-enriched using CD4⁺ T cell Isolation Kit (Miltenyi Biotec) were stained with both APC- and PE-labeled tetramers (**Supplementary Table 13**) at 20 µg/mL in RPMI containing 10% FBS, 10 mM HEPES, 2mM glutamine and 50 U/mL Pen/Strep for 1 h at room temperature. DR/CLIP tetramers were used as negative controls. The cell density during staining was 10-20x10⁶ cells/mL. Unbound tetramer was removed using two washes with flow staining buffer (PBS +2%FBS). Cells were then stained with Live/Dead Aqua (Invitrogen) for 15 min at room temperature, following by staining with anti-CD4 (Alexa Fluor700, OKT4,

Biolegend), anti-CD3 (BV421, UCHT1, Biolegend), and anti-CD14/CD19 (BV510) for 20 min at 4°C (**Table 2**). Cells were washed once with PBS and analyzed on a BD Aria cell sorter.

Specificity	Clone	Fluorophore	Supplier
αCD4	OKT4	Alexa Fluor700	Biolegend
αCD3	UCHT1	BV421	Biolegend
αCD14	M5E2	BV510	Biolegend
αCD19	6D5	BV510	Biolegend

Table 2. Tetramer staining antibodies

Single cell RNAseq data generation and analysis

Tetramer-specific CD4⁺ T cells were dry sorted into 96 well plates for Patients 3, 4 and 5 for whole transcriptome sequencing and TCR sequencing. Whole transcriptome sequencing in plates was performed by Smart-seq2 based on the protocols previously described¹³². The FASTQ files were initially trimmed and adaptors were removed using Flexbar¹³³ before aligned to NCBI Human Reference Genome Build GRCh38 (hg38) using the STAR aligner¹²¹. The Transcript Per Million (TPM) counts were quantified from the alignment using RSEM¹²². Further QC was performed excluding cells from the analysis based on four criteria. (1) cells with no CD45 and CD3 expression (either as CD3D, CD3E or CD3G), (2) cells with less than 500 genes expressed, (3) cells expressing housekeeping genes (**Table 3**) with $\log_2(\text{TPM}+1) < 2.5$ and (4) percent mitochondrial genes $< 10\%$. For the downstream analysis we only used genes expressed with $\log_2(\text{TPM}+1) > 1$ in at least 5 cells or $\log_2(\text{TPM}+1) > 8$ in at least one cell. For each patient cells from all time points passing the QC were combined before clustering cells from all patients using the integration

method in Seurat v3¹³⁴. The clustering was performed using the standard workflow with a resolution of 0,6 and a lower number of principal components (15) in the principal component analysis (PCA) to account for the low variance between the T cells. To account for unwanted variation caused by differences in ribosomal gene content between samples we excluded ribosomal genes from the variable gene set used in the PCA. Differential expressed genes were identified both between time-points, patients and clusters as wells as combinations of these using the default Wilcoxon Rank Sum test implementation in Seurat (**Supplementary Table 9**).

ACTB	RPL13	RPL27A	RPL39L	RPS12	RPS27	RPS6KB1
B2M	RPL13A- PS1	RPL28	RPL3L	RPS13	RPS27A	RPS6KB2
HNRPLL	RPL14	RPL29	RPL4	RPS14	RPS27L	RPS6KC1
HPRT	RPL15	RPL3	RPL41	RPS15	RPS28	RPS6KL1
PPIA	RPL17	RPL30	RPL5	RPS15A	RPS29	RPS7
PRPS1	RPL18	RPL32	RPL6	RPS16	RPS3	RPS8
PRPS1L1	RPL18A	RPL34	RPL7	RPS17	RPS3A	RPS9
PRPS1L3	RPL19	RPL35	RPL7A	RPS18	RPS4X	RPSA
PRPS2	RPL21	RPL35A	RPL7L1	RPS19	RPS5	TRPS1
PRPSAP1	RPL22	RPL36	RPL8	RPS19- PS3	RPS6	UBB
PRPSAP2	RPL22L1	RPL36A	RPL9	RPS19BP1	RPS6KA1	
RPL10	RPL23	RPL36AL	RPLP0	RPS20	RPS6KA2	
RPL10A	RPL23A	RPL37	RPLP1	RPS21	RPS6KA3	

RPL10L	RPL24	RPL37A	RPLP2	RPS24	RPS6KA4	
RPL11	RPL26	RPL38	RPS10	RPS25	RPS6KA5	
RPL12	RPL27	RPL39	RPS11	RPS26	RPS6KA6	

Table 3. Housekeeping genes

Targeted TCR Sequencing and Analysis

For single-cell TCR sequencing for Pt. 2, FACS-sorted tetramer-stained cells were loaded onto a 10X Genomics Chromium Chip A and completed single-cell 5' barcoding (V1) according to the manufacturer's protocol. TCR sequences were directly amplified from the cDNA and prepared Illumina-compatible libraries, also according to manufacturer's protocol. Library quality was assessed using a BioAnalyzer and traces were as expected. Paired end sequencing was performed using the manufacturer's recommended parameters for Chromium Single Cell 5' chemistry for TCR sequencing, generating >3000 read pairs per cell (**Supplementary Table 12**).

For single-cell TCR sequencing for Pts. 3, 4, and 5, targeted TCR amplification (Step 1A(xxix–xxxv)) was performed by first transferring an aliquot of each normalized single-cell cDNA library to a 96- or 384-well plate. Then, a pair of barcode rhPCR primers with the structures P5.IDTxxx.Rd1x.x1 and P7.IDTyyy.Rd2x.x1 were added to each well (**Supplementary Table 10**). P5 and P7 refer to the Illumina sequences required for attachment to the flow cell; IDTxxx and IDTyyy refer to 8-nt index sequences; and Rd1x and Rd2x refer to the 5' portions of the Illumina TruSeq Read1 and Read 2 primers, respectively. The designations IDTxxx and IDTyyy indicate that the two index sequences added to any particular well are not the same sequence. Using the pipetting scheme outlined in **Table 4** enabled transferring of barcode primers stored in 96-well

plates to a 384 well plate such that each well was assigned a unique dual index. Next, a PCR mix containing rhPCR primers specific for TCR was added to each well. The structures of these primers are Rd1.AVxx, Rd1.BVxx, Rd2.AC, and Rd2.BC. Rd1 and Rd2 refer to the sequences corresponding to the Illumina TruSeq Read1 and Read 2 primers, respectively; AVxx refers to sequences specific for all functional TRAV genes; BVxx refers to sequences specific for all functional TRBV genes; and AC and BC refer to TRAC- and TRBC-specific sequences, respectively. In the PCR, the concentrations of the TCR-specific primers were low (50 nM) and those of the barcode primers are high (2 μ M). This was done to favor the formation of full-length P5/P7-containing amplicons, but this strategy is not 100% effective. Therefore, after pooling and purification (Steps 2–16) of the 96 or 384 reactions from the TCR-specific amplification, a second PCR was performed using the generic primers P5 and P7 (Steps 17–18). The products of this second PCR were purified and qualified for sequencing by Bioanalyzer analysis (Steps 19–29). Standard paired-end MiSeq sequencing was performed using the 300-cycle kit and reads of 248-nt read 1, 48-nt read 2, 8-nt index 1, and 8-nt index 2 (Steps 30–35) (**Supplementary Table 11**).

	1	2	3	4	5	6	7	8	9	10	11	12	13	14	15	16	17	18	19	20	21	22	23	24
A	A	B	A	B	A	B	A	B	A	B	A	B	A	B	A	B	A	B	A	B	A	B	A	B
B	C	D	C	D	C	D	C	D	C	D	C	D	C	D	C	D	C	D	C	D	C	D	C	D
C	A	B	A	B	A	B	A	B	A	B	A	B	A	B	A	B	A	B	A	B	A	B	A	B
D	C	D	C	D	C	D	C	D	C	D	C	D	C	D	C	D	C	D	C	D	C	D	C	D
E	A	B	A	B	A	B	A	B	A	B	A	B	A	B	A	B	A	B	A	B	A	B	A	B
F	C	D	C	D	C	D	C	D	C	D	C	D	C	D	C	D	C	D	C	D	C	D	C	D
G	A	B	A	B	A	B	A	B	A	B	A	B	A	B	A	B	A	B	A	B	A	B	A	B
H	C	D	C	D	C	D	C	D	C	D	C	D	C	D	C	D	C	D	C	D	C	D	C	D
I	A	B	A	B	A	B	A	B	A	B	A	B	A	B	A	B	A	B	A	B	A	B	A	B
J	C	D	C	D	C	D	C	D	C	D	C	D	C	D	C	D	C	D	C	D	C	D	C	D
K	A	B	A	B	A	B	A	B	A	B	A	B	A	B	A	B	A	B	A	B	A	B	A	B
L	C	D	C	D	C	D	C	D	C	D	C	D	C	D	C	D	C	D	C	D	C	D	C	D
M	A	B	A	B	A	B	A	B	A	B	A	B	A	B	A	B	A	B	A	B	A	B	A	B
N	C	D	C	D	C	D	C	D	C	D	C	D	C	D	C	D	C	D	C	D	C	D	C	D
O	A	B	A	B	A	B	A	B	A	B	A	B	A	B	A	B	A	B	A	B	A	B	A	B
P	C	D	C	D	C	D	C	D	C	D	C	D	C	D	C	D	C	D	C	D	C	D	C	D

The numbers in the column headings and the letters in the leftmost column indicate the coordinates of a 384-well plate. The remaining letters A, B, C, and D refer to four 96-well plates. Using an 8-channel pipette, primers in each column of the 96-well plate A are pipetted into a column with wells marked A in this diagram of a 384-well plate. This requires 12 transfers. The process is repeated for 96-well plates B, C, and D. The overall operation requires 48 transfers, with eight wells being pipetted per transfer.

Table 4. Scheme for pipetting from 4 96-well plates into one 384-well plate. Taken from Li et al. *Nature Protocols* 2019¹³⁵.

TCR Clonotype Analysis

To define the rank order of tetramer-specific TCR clonotypes for each patient, we applied this set of criteria in the following rank order: (1) the highest number of timepoints the clonotype appeared in, (2) the highest rank (ordered by number of cells per clonotype) of the clonotype in any timepoint, and (3) the average rank of the clonotype across all observed timepoints.

Results

Personal neoantigen vaccines yield promising long-term clinical and immunologic outcomes in high-risk melanoma patients

On NCT01970358, a total of 8 patients received vaccines, 6 of whom were previously reported¹. In total, the enrolled patients had either stage IIIB/C disease (n=6), or stage IVM1b (n=2) disease by AJCC v.8 (**Supplementary Table 1**). At a median follow-up of 55 months (range 38-64) after surgery, all patients are alive, and 6 of 8 remain without evidence of active disease (**Fig. 1a**). In our extended analysis, no further vaccine-related toxicities were detected beyond the transient, mild flu-like symptoms, injection site reactions, rash and fatigue previously reported. Three of 6 patients with initial stage IIIB/C disease remain without disease recurrence. The other three have since experienced disease recurrences: Patient 3 had local recurrence of a soft tissue metastasis at 26 months after study surgery, which was treated with surgical resection followed by adjuvant radiation, and has subsequently remained without evidence of disease to 57 months. Patient 5 experienced a recurrence of an isolated lung metastasis at 40 months, which was treated with surgical resection and adjuvant anti-PD-1 blockade therapy (nivolumab); at 53 months, several new metastases in both lungs were evident on surveillance scans, and the patient is planned to receive therapy with nivolumab in combination with ipilimumab. Patient 1 developed multiple brain metastases at 40 months and underwent surgical resection of the dominant lesion. This was followed by multiple lines of therapy including radiation, dabrafenib and trametinib, ipilimumab plus nivolumab, and nivolumab alone, ultimately resulting in clinical stability of the multiple brain metastases and a continued lack of extracranial disease progression at 64 months. As previously reported, the two patients who entered the study with stage IVM1b disease (resected lung metastases, patients 2 and 6) experienced disease recurrence shortly following vaccination.

Treatment with the anti-PD-1 antibody pembrolizumab resulted in complete radiographic responses after 4 doses in both patients. After being treated with pembrolizumab for 11 and 24 months, respectively, disease responses in patients 2 and 6 are ongoing to 47 and 38 months after the start of PD-1 inhibition.

To assess for neoantigen-specific T cell responses in Pts. 11 and 12, overlapping 15- to 16-mer assay peptides (ASP) spanning the entirety of each IMP and 9- to 10-mer peptides corresponding to each predicted class I epitope (EPT) were prepared and pooled to match the corresponding IMP pool (**Extended Data Fig. 1a**). Robust neoantigen-specific *ex vivo* CD4⁺ responses against ASP pools were detected immediately following vaccination in patients 11 and 12, similar to the previously reported 6 patients (**Extended Data Fig. 1b-c**). The vaccines for these 2 additional patients consisted of 16 and 11 long peptides (lengths 17-26 aa), encompassing 15 and 11 mutated epitopes (**Supplementary Table 3, 4, 6**). By *ex vivo* ELISPOT (**Methods**), peripheral blood monocytes (PBMC) obtained at week 16 exhibited reactivity against ASP pool A and ASP pools A/C in Pts. 11 and 12, respectively (**Extended Data Fig. 1b**).

Deconvolution of the reactive pools (**Methods**) after one round of *in vitro* stimulation revealed CD4⁺ T cell reactivity against 16 of 71 ASP peptides (corresponding to 11 of 27 immunizing peptides) tested across these 2 patients (**Extended Data Fig. 1c-d, Extended Data Fig. 2**). No CD8⁺ responses were detected following both *ex vivo* and *in vitro* stimulation against 42 EPT peptides (corresponding to 27 immunizing peptides). Altogether, we detected *ex vivo* or *in vitro* stimulated CD8⁺ T cell responses against 14% and CD4⁺ T cell responses against 56%, respectively, of the immunizing peptides that were tested across the 8 patients. *Ex vivo* responses

to pooled peptides for patients 11 and 12 were only detectable for CD4⁺ T cells, consistent with our previous observations¹. Of note, immunohistochemical evaluation of HLA class I and II expression of the originally surgically resected metastatic tumors demonstrated detectable class I expression in Pt. 12 but not in Pt. 11 tumors (**Extended Data Fig. 1e-f**).

Personalized neoantigen vaccines generate memory T cell responses that persist for years

To test the persistence of vaccine-induced, neoantigen-specific memory T cells, we measured T cell responses using PBMC samples collected 28 to 55 months following initiation of vaccination. For each of 8 patients, we stimulated PBMC *in vitro* for one round using pools of ASP and EPT peptides that had previously induced IFN- γ responses 16 weeks after vaccine initiation, and in the cases of Pt. 2 and 6, several weeks after pembrolizumab initiation as well. Remarkably, the magnitude of responses measured by IFN- γ ELISPOT assay was largely sustained across the majority of immunizing peptides. In the example of Pt. 3 (**Fig. 1b**), we observed strong T cell responses both at week 16 (frozen PBMC) and 3 years (46 months) post-vaccination (fresh PBMC) to ASP peptides, recognizing potential differences between the testing of frozen versus fresh PBMC. In Patients 3 and 6, all peptides which had previously generated CD4⁺ and CD8⁺ T cell responses at week 16 still generated detectable responses several years later (47 and 44 months, respectively). For the other 6 patients, between 13 and 85% of peptides stimulating CD4⁺ and 0-100 % of peptides stimulating CD8⁺ T cell responses observed at week 16 remained detectable 28 to 56 months post-vaccination initiation (**Fig. 1c**). In Pt. 2, who received anti-PD-1 therapy after vaccination, none of the peptides stimulating CD4⁺ T cell responses observed after anti-PD-1 therapy remained detectable 54 after vaccination. In Pt. 6, who also received anti-PD-1 therapy, 2 out of 2 peptides stimulating CD4⁺ responses and 1 out of 2 peptides stimulating CD8⁺ responses

observed after anti-PD-1 therapy remained detectable 44 months after vaccination. In Pts. 3 and 5, we could also detect persistent CD4⁺ T cell responses directly *ex vivo* against 53% and 5% of the tested ASP peptides, respectively. Overall, we detected memory CD4⁺ and CD8⁺ T cell responses to an average of 61.5% and 44.4%, respectively, of vaccine-targeted neoantigen responses found at 16 weeks and after pembrolizumab.

To determine the functional status of circulating T cells early (week 16) and later (3 years) following vaccination, we performed multi-parameter flow cytometry on Patient 3 PBMC samples stimulated *ex vivo* with pooled ASP peptides that had previously generated *ex vivo* CD4⁺ responses against a panel of 11 markers (**Methods, Extended Data Fig. 3a, Supplementary Table 8**). These markers were selected to evaluate cytokine secretion, activation (PD-1), and naïve (CD27⁺/CD45RA⁺), effector (CD27⁻/CD45RA⁺), central memory (CD27⁺/CD45RA⁻), and effector memory (CD27⁻/CD45RA⁻) T cell phenotypes (**Fig. 1d**). Consistent with the ELISPOT results, we detected evidence of cytokine production after stimulation with the immunogenic peptides (**Extended Data Fig. 3b**). We detected IFN- γ , TNF- α , and IL-2 production by CD4⁺ T cells at week 16 post-vaccination, and these cells were primarily PD-1-expressing central memory T cells, in contrast to the total peptide-responsive CD4⁺ T cell population (**Extended Data Fig. 3c-d**). At 3 years post-vaccination, we detected a persistence of IFN- γ , TNF- α , and IL-2 production and polyfunctional cytokine-producing cells. The majority of cytokine-producing T cells remained of central memory phenotype, but there was a 39% average decrease in the expression of PD-1, suggesting a correlation between active vaccination and T cell activation. At both timepoints, the majority of CD4⁺ T cells were TNF- α -producing, with polyfunctional TNF- α /IL-2-coexpressing cells representing the next most dominant subpopulation.

Relapsed tumors exhibit shifts in immunizing neoantigen expression

Five of 8 patients experienced tumor relapse at a median of 26 months after surgery (range: 8 to 40 months). For these patients, we performed whole-exome sequencing of relapsed tumors. This analysis revealed that the majority (median 89.7%, range 69.2% to 93.7%) of somatic mutations persisted in the relapsed tumors. Only a fraction of the mutations were lost over time (median 10.3%, range 6.2% to 30.8%); in all cases, new somatic mutations (median 93, range 52 to 260) were also gained in the relapsed tumors (**Fig. 2a**). WES revealed that in 3 of 5 patients, the relapsed tumors no longer harbored at least one somatic mutation (median: 2 mutations, range 1-4) that had been targeted by neoantigen peptide vaccination (**Fig. 2b**). Of the 7 total lost mutations, neoantigen-specific CD4⁺ or CD8⁺ T cell responses had been detected against 4 of them at 16 weeks and/or 3-4 years (**Fig. 2c**). In Pt. 3, since the pretreatment and relapsed tumors originated from the same site (left posterior calf), our data point to the possibility of vaccine-induced selection pressure given the presence of a detectable persistent T cell response against one of the lost neoantigens.

Neoantigen-specific CD4⁺ T cells following vaccination exhibit memory and cytotoxic signatures

To determine whether the fraction and functional state of circulating vaccine-induced neoantigen-specific T cells evolve over time, we evaluated neoantigen-reactive T cells identifiable by tetramer staining across serial timepoints. We focused on the isolation and characterization of neoantigen-reactive CD4⁺ T cells, since our previous studies had revealed their robust *ex vivo* detection by week 16 after vaccination. Furthermore, we focused on HLA-DR restricted responses, as class II tetramers against peptide-HLA-DR complexes could be reliably generated (**Methods, Extended**

Data Fig. 4a, Supplementary Table 13). In total, we generated tetramers for 6 patients: mut-*RUSC2* (Pt 1), mut-*ADM2* (Pt 2), mut-*ADAMT27* (Pt 3), mut-*ARHGAP29* (Pt 4), mut-*ZNF281* (Pt. 5), and mut-*MLL* (Pt 6), all neoantigens which remained present in the relapsed tumors of Pts 1, 2, 3, 5 and 6 (**Supplementary Table 3**). We could detect tetramer-specific CD4⁺ T cells in serially collected PBMC from 4 of 6 patients (Pts 1, 3, 4, and 5) directly *ex vivo* following vaccination, and persisting over the course of treatment (**Fig. 3a-b, Extended Data Fig. 4b**).

For 3 of these 4 patients, we utilized a plate-based approach to isolate the small subpopulations of tetramer-reactive circulating CD4⁺ T-cells, and characterized the transcriptional states of the individual neoantigen-specific CD4⁺ T cells from these patients over time (**Methods**). Across the 3 patients, neoantigen-specific CD4⁺ T cells from a median of 6 post-vaccination timepoints (range 5-6) were collected, totaling a median of 310 cells (range 297 to 378) per patient, with a median of 189 cells per timepoint (range 80 to 228) (**Fig. 3c**). For comparison, we also collected 91 and 73 non-tetramer specific CD4⁺ T cells from Pts. 4 and 5 from prior to vaccination, respectively. On average, we collected a total of 1,149 CD4⁺ T cells.

Cumulatively, for all 3 patients, we observed an increase in cytotoxicity markers following priming, primarily *GZMA* and *GZMB* (**Extended Data Fig. 5a**). Furthermore, while there was a paucity of exhausted cells before vaccination, various exhaustion genes were upregulated following vaccination, including *PD-1*, *TOX*, and *TIGIT*. Finally, there was a generalized upregulation of naïve/memory markers such as *CD62L*, *CCR7*, and *IL7R* in all patients and timepoints; these are notably enriched in the specific clusters and timepoints described below.

By pooling all cells and performing tSNE joint-clustering and integration using Seurat v3, we observed five distinct clusters, each composed of cells from all three patients (**Methods, Fig. 3d, Extended Data Fig. 5b, Supplementary Table 9**). Evaluation of the differentially expressed genes per cluster (average log fold change >0.4 or <-0.4) revealed each to represent distinct T cell states defined by specific gene signatures (**Fig. 3e**). Cluster 0 ('memory-like') was characterized by *CD62L* upregulation and *HOPX* downregulation, indicative of a memory/naïve phenotype. Cluster 1 ('cytotoxic-like') was distinctly defined by cytotoxicity markers (i.e. *GZMA*, *GNLY*, *GZMK*). This cluster was also characterized by markers of exhaustion and a non-naïve effector state (i.e. presence of *HOPX*, *CCL4*, *CCL5*, and downregulation of *CCR7* and *CD62L*). We observed a clear shift in the transcriptional profile of the cells that dominated Cluster 2 ('AICD-like') to a state consistent with activation-induced cell death (AICD) and the contraction phase of an immune response. This cluster was characterized by a pan-downregulation of numerous genes, including markers of naïve T cells (*LEF-1*), memory/naïve T cells (*CD62L*), T cell activation (*CD69*), TNF- α induced apoptosis (*TNFAIP8*)¹³⁶, and cytotoxicity (*GZMB*). Cluster 3 ('naïve-like') was characterized by differential upregulation of a set of naïve T cell markers (i.e. *CCR7*, *LEF1*), in addition to markers of Th1 subtypes (*TXK*) and repression of exhaustion (*SATB1*). A small cluster of cells (Cluster 4) had high expression of housekeeping genes such as *ACTB*, few immune-related genes, and had the highest gene count despite being the smallest cluster, suggesting the presence of doublets (**Extended Data Fig. 5b**). Furthermore, we observed significant *MALAT* downregulation, which has been previously associated with poor quality cells in previous studies¹³⁷. For these reason, we chose not to further evaluate Cluster 4.

To determine if particular transcriptional states were associated with distinct phases of vaccination, we evaluated cluster membership by timepoint (**Fig. 3f**). Non-tetramer sorted CD4⁺ T cells isolated before vaccination are primarily found in Cluster 3, consistent with its “naïve-like” T cell phenotype. Neoantigen-specific T cells from post-priming and early post-boosting timepoints (weeks 8 – 20) compose the majority of Clusters 1 and 2, indicating a transition in the state of the cells towards cytotoxicity and AICD with continued vaccination. Finally, neoantigen-specific T cells from the last timepoint, during the boosting phase of vaccination, make up most of Cluster 0, aligning with its “memory-like” phenotype. Overall, from pre-vaccination to priming to boosting, there is an overall trajectory from naïve cells, to effector and apoptosing cells, and finally, to memory CD4⁺ T cells.

Neoantigen-specific TCR clonotypes persist and diversify following vaccination

For Pts. 3, 4 and 5, we also assessed the TCR repertoires of the tetramer-isolated CD4⁺ T cells. Across a median of 6 timepoints (range 5-6), there were 183, 89 and 107 distinct clonotypes identified from 266, 329 and 210 single cells, respectively (**Extended Data Fig. 6a-b, Supplementary Table 11, Methods**). We also performed reference single-cell TCR sequencing of 73 and 66 non-tetramer-isolated CD4⁺ T cells from a pre-vaccination timepoint for Pts. 4 and 5, respectively. Across the 3 patients, none of the pre-vaccination TCRs were observed at post-vaccination timepoints, suggesting a substantial shift in the composition of TCR repertoires after vaccination (**Fig. 4a**). Conversely, with vaccination, we observed persistence of numerous tetramer-specific clones from priming through boosting, as well as the emergence of new tetramer-specific clones with both priming and boosting, indicating diversification.

For each patient, we ranked distinct tetramer-specific TCR clonotypes based on (from highest to lowest priority): the number of post-vaccination timepoints the clonotype appeared in, the highest rank of the clonotype in any timepoint (as determined by numbers of T cells per clonotype), and the average rank of the clonotype across all observed timepoints. Based on these criteria, we identified the top ten dominant TCR clones from each patient, and evaluated if there were common trajectories through vaccination among the clones. Acknowledging the existence of potential sampling bias and the limitations associated with small numbers of neoantigen-specific cells, we observed 3 primary patterns of clonal dynamics: (i) Pattern A: relative persistence of the clonotype from priming through boosting (14 paired TCRs across 3 patients); (ii) Pattern B: emergence of the clonotype with priming followed by gradual extinction, even with boosting (8 TCRs across 3 patients), and (iii) Pattern C: emergence of the clonotype with boosting (4 TCRs across 2 patients) (**Fig. 4b, Extended Data Fig. 6c-d**).

Neoantigen-specific TCR clonotypes shift following vaccination and anti-PD-1 therapy

For Patients 2 and 6, we further had the opportunity to evaluate the TCR clonotypic shifts following exposure to not only vaccine but also subsequent anti-PD-1 therapy (pembrolizumab). For both of these patients, tetramer-positive populations could be detected following one round of *in vitro* stimulation (**Methods**). For Patient 2, we observed a robust population of tetramer-specific T cells 16 weeks (4 months) after vaccination initiation, and a subsequent contraction of tetramer-specific T cells to a much smaller population after pembrolizumab at 20 months (89 weeks) (**Fig. 5a**). In contrast, for Patient 6, we observed a four-fold increase in tetramer-specific T cells (from 0.88 at week 16 to 0.398% at 16 months (71 weeks) following pembrolizumab (**Fig. 5a**)). However, these shifts are difficult to interpret in the setting of *in vitro* stimulation. Tetramer-specific TCR

sequencing for Pt. 2 revealed that the majority of TCR clonotypes present at week 16 were absent after pembrolizumab (**Fig. 5b-c, Supplementary Table 12**). There was, however, a small proportion of novel clones after pembrolizumab. Of the 25 clones that persisted from week 16 to after pembrolizumab, most clonotypes expanded between week 16 and after PD-1 blockade, and several clones that were infrequent at week 16 became dominant, illustrating increased clonality of the TCR repertoire. All together, these population dynamics indicate a shift in the TCR repertoire and selection for certain TCR clones following anti-PD-1 therapy.

Personalized neoantigen vaccines induce epitope spreading of T cell responses, indicative of tumor cytotoxicity

As patients in this study did not have measurable disease at the time of vaccine initiation, we were unable to directly detect *in situ* vaccine-mediated anti-tumor activity. Therefore, as an indication of on-target tumor killing *in vivo*, we tested for epitope spreading against additional antigens, as tumor destruction would be expected to result in the release of new tumor neoantigens or tumor-associated antigens (TAAs) into the immune microenvironment, and subsequently, trigger additional tumor-directed immune responses. To this end, we assessed T cell reactivity via IFN- γ ELISPOT assays in Patients 2, 3, and 6 to neoantigens and TAAs that were not targeted by the vaccines. To this end, we selected and synthesized EPT (9-10mer) and overlapping ASP (15-16mer) peptides corresponding to a selected neoantigens that had the highest rank of predicted binding affinity (IC₅₀ of <500 nM using NetMHCpan) to autologous HLA alleles with confirmed transcript expression in the tumor, but were not included in the vaccines (“non-vaccine neoantigens”) (**Fig. 6a, Methods, Extended Data Fig. 7a, Supplementary Table 7**). We also synthesized EPT and overlapping ASP peptides corresponding to common melanoma TAAs that

had the highest rank of predicted binding affinity (MSEC>0.85 using a preliminary version of HLAthena¹²⁴), were found to be highly expressed in the patient tumors (TPM>100), and met an additional set of criteria detailed in **Methods (Extended Data Fig. 7b, Supplementary Table 7)**.

We first evaluated Patient 3, one of the patients who did not receive subsequent anti-PD-1 therapy. For Pt 3, week 16 (post-vaccination) PBMC were stimulated with pools of peptides encompassing 58 an 38 non-vaccine EPT and ASP neoantigen peptides, respectively and 39 TAA peptides for a single round of *in vitro* expansion, then tested for T cell reactivity. Upon peptide deconvolution, we observed CD4⁺ T cell responses against 3 of 38 ASP peptides corresponding to 2 non-vaccine neoantigens (mut-*EYA3*^a and mut-*EYA3*^b, mut-*P2RY4*) following vaccination, which were not detected prior to vaccination (**Fig. 6b, Extended Data Fig. 8**). These results indicate the presence of epitope spreading following vaccination against the limited set of targets that we interrogated.

For Pts. 2 and 6, we could evaluate the impact of vaccination and subsequent anti-PD-1 therapy (pembrolizumab). For Pt. 2, week 16 (post-vaccination) PBMCs and post-pembrolizumab PBMCs were stimulated with pools of peptides encompassing 13 and 24 non-vaccine EPT and ASP neoantigen peptides respectively, and 22 non-vaccine TAA EPT peptides, for a single round of *in vitro* expansion. For Pt. 2, both following vaccination and after pembrolizumab, we detected a CD4⁺ T cell response against 1 of 24 non-vaccine neoantigen ASP peptides (mut-*AGAP3*^c) and a CD8⁺ T cell response against 1 of 30 non-vaccine TAA EPT peptides (*MAGEF*) (**Fig. 6c, Extended Data Fig. 8**). Moreover, after pembrolizumab (89 weeks), we detected an additional CD4⁺ T cell response against a non-vaccine neoantigen 15-mer peptide (mut-*AGAP3*^b), and an additional CD8⁺ T cell response against a TAA 10-mer peptide (*MAGED*). No CD8⁺ T cell

responses were observed against any of the 13 and 58 non-vaccine neoantigen peptides in Pt. 2 and 3, respectively, and no post-vaccination CD4⁺ or CD8⁺ T cell responses were observed against non-vaccine neoantigen nor non-vaccine TAA peptides in Pt. 6.

We also tested functional avidity of non-vaccine neoantigen-specific CD4⁺ T cells and TAA-specific CD8⁺ T cells by stimulating with APCs pulsed with mutated and wildtype (WT) non-vaccine neoantigen peptides across a range of concentrations (from 10pM to 10μM; **(Fig. 6b and c inset)**). T cells demonstrated similar avidities for all mutant neoantigen and TAA epitopes. All of the non-vaccine neoantigen-specific CD4⁺ T cell lines were able to discriminate between mutated from wildtype antigens (**Fig. 6b and c inset**). Finally, we observed a persistence and amplification of CD4⁺ T cell responses to the identified non-vaccine neoantigens, but not to TAA peptides, out to 4 and 3 years after vaccination in Pts. 2 and 3, respectively (**Fig. 6d**).

Discussion

Specificity, memory, functionality, and adaptability are key attributes that render the immune system uniquely able to mediate long-term control of tumor growth and evolution. We report here a long-term update on the clinical course of 8 patients treated with NeoVax, a personal neoantigen vaccine, at a median follow-up of 4 years, and investigate important questions including long-term persistence of vaccine-induced neoantigen-specific T cell responses, phenotypes and T cell receptor repertoire evolution of single neoantigen-specific T cells over time, and the on-target tumor cell killing ability of neoantigen-specific T cells as measured through epitope spreading.

Clinically, at a median follow-up time of 48.5 months (range 27 – 59 months), all 8 patients on trial (who had stage IIIB or higher disease) remained alive. The combined rate of relapse (for stage 3 patients and progression (for stage 4 patients) was 37.5%. It is difficult to interpret these clinical outcomes given the small sample size and the fact that several patients received other cancer therapies after neoantigen vaccination. However, for reference, it is worth reviewing survival outcomes of stage III and IV melanoma patients treated with immunotherapies and targeted agents, as PD-1 inhibition with either nivolumab or pembrolizumab, or BRAF/MEK inhibition with dabrafenib and trametinib for BRAF mutant melanoma have become standard adjuvant therapy for high risk melanoma patients since the initiation of this trial in 2014. In the KEYNOTE-001 trial, patients with stage IV melanoma were treated with pembrolizumab, and at 5 years (55 months), median OS was 23.8 months, and PFS was 8.3 months¹³⁸. In the KEYNOTE-006 trial, patients with stage IV melanoma were treated with pembrolizumab or ipilimumab. The 5-year (57.7 months) median OS for pembrolizumab was 32.7 months, and that of ipilimumab was 15.9 months¹³⁹. Median PFS was 8.4 months for pembrolizumab, and 3.4 months in the ipilimumab

group. While the PFS for the two stage IV NeoVax patients was only 2.5 months, both patients have remained disease-free for a median of 41.5 months since initiation of pembrolizumab following disease recurrence, suggesting that combining NeoVax with pembrolizumab may lead to favorable survival outcomes. In regards to targeted therapies, dabrafenib plus trametinib was found to have a 4-year (48 months) PFS rate of 21% and OS rate of 37%¹⁴⁰ in a trial of patients with stage IV melanoma.

Several of these treatment strategies have also been investigated in patients with stage III melanoma in the adjuvant setting (following surgical resection). In a clinical trial of adjuvant pembrolizumab, the 1-year RFS rate was 75.4%¹⁴¹, and in a trial of adjuvant nivolumab versus ipilimumab, the 1-year RFS rate was 70.5% for nivolumab and 60.8% for ipilimumab¹⁴². Dabrafenib plus trametinib was found to have a 3-year RFS rate of 58% and OS rate of 86%¹⁴³. In the NeoVax trial, 3 of 6 stage III patients were treated with checkpoint blockade (anti-PD-1) and/or dabrafenib plus trametinib following tumor recurrence. These recurrences indicate that neoantigen vaccination alone was not have been sufficient to generate lasting clinically relevant antitumor immunity in these patients.

Given that a hallmark of productive vaccination is the generation of durable immunity, we are encouraged by the long-term persistence of the majority of CD4⁺ and CD8⁺ T cell responses against the majority of immunizing epitopes in all 8 patients. It is important to note that in a minority of cases, positive T cell responses from week 16 post-vaccination reported originally in 2017 were not detected when we measured the response again, side-by-side with year 3-4 post-vaccination PBMC, as positive controls. Therefore, we cannot conclusively interpret negative 3

year responses in those cases. The fact that we were not able to reproduce some week 16 responses could be due cryopreservation-related T cell defects¹⁴⁴ and peptide degradation secondary to sequence-dictated instability or suboptimal storage conditions¹⁴⁵, as it has been over 4 years since we measured them for the original 2017 report. In addition, the pools of peptides used for our original report contained positive and negative peptides, whereas for this recent experiment, we pooled all the positive peptides in one pool due to limited PBMC availability. Therefore, competition effects of the positive peptides may have prohibited the generation of some previously observed T cell responses. Despite these experimental limitations, the ability to induce neoantigen-specific T cell responses lasting several years at largely sustained frequencies underscores the ability of cancer vaccines to induce long-term immunity similar to vaccination against infectious organisms, that is, by utilizing targets that are “foreign” to the immune system and therefore not subject to central tolerance mechanisms in the thymus. Our flow cytometry-based phenotypic characterization of neoantigen-specific T cells 3-4 years after vaccination underlines that, as might be expected, these cells mostly likely harbor mostly a central memory phenotype, as evidenced by CD27⁺ CD45RA⁺ neoantigen-specific CD4⁺ T cells.

Nevertheless, despite the persistent presence of neoantigen-reactive T cells in the circulation out to 4 years after vaccination, five patients did have recurrences of their melanoma. This disconnect could theoretically be attributable to factors such as poor tumor infiltration or low frequencies of neoantigen-specific T cells, limited presentation of immunogenic neoantigens by the tumor, tumor microenvironment immunosuppressive effects, insufficient tumor-directed cytolytic activity, and tumor immune editing. Our whole exome sequencing analysis of the five relapsed tumors revealed that the majority of mutations were persistent over time and across tumor sites, including the brain,

suggesting that tumor immune editing may not contribute substantially to the tumor recurrences. This finding also supports the notion that a single-site tumor biopsy may be sufficient to detect driver mutations that can be targeted by personalized therapy. Importantly, previous studies in other solid tumors have suggested that despite high levels of tumor heterogeneity, recurrent driver mutations are present in every tumor clone and tumor region¹⁴⁶, and thus represent potentially robust and relevant therapeutic targets^{147,148}. It is possible that the accumulation of small numbers of new mutations and the loss of others in the relapsed tumors may be a reflection of immune escape; however, the small sample size and the lack of a control cohort precludes meaningful assessment of this hypothesis in our study.

Notably, to our knowledge, we have successfully performed the first single-cell transcriptome analysis of human neoantigen-reactive CD4⁺ T cells through the course of cancer vaccination. Although our clustering analysis yielded one cluster with low-quality cells, we were able to identify a sequential progression of gene signatures through vaccination, from naïve T cells, to effector T cells, to memory T cells, consistent with the canonical progression of a T cell in response to infection¹⁴⁹. Single cell RNA sequencing of virus vaccine-specific T cells post-vaccination¹⁵⁰ has previously been performed in mice and humans. Transcriptional analysis in a single patient vaccinated against dengue virus revealed that following vaccination, acutely activated CD8⁺ T cells assume distinct transcriptional profiles, including effector, naïve, and proliferative phenotypes. Furthermore, dengue virus-reactive TCR clonotypes isolated from virus-specific CD8⁺ memory T cells were identified within the population of activated CD8⁺ T cells. Finally, clonally expanded virus-specific TCRs (defined as TCRs expressed in >2 cells) were preferentially enriched in the effector/cytotoxic cluster. Similarly, a portion of neoantigen-reactive CD4⁺ T cells

in our study were found to exhibit a transcriptional signature associated with cytotoxicity (*GZMA*, *GZMB*, *GNLY*) that was most pronounced during the boosting phase, suggesting that these vaccine specific CD4⁺ T cells may be able to kill tumor targets directly. We also identified memory and naïve populations, underlining the phenotypic diversity of cancer and viral antigen-specific T cells induced by vaccination. Another study of B cells from 6 patients collected seven days after influenza vaccination found that vaccine-induced plasmablasts were transcriptionally distinct from the vaccine-negative population¹⁵¹. Finally, in a study of 14 patients with non-small cell lung cancer (NSCLC) after checkpoint blockade therapy with the anti-PD-L1 antibody atezolizumab, neoantigen-specific CD8⁺ T cells were more often detected in responding patients, and phenotypic analysis revealed that they were primarily differentiated effector cells similar to CMV-specific T cells, whereas more memory-like profiles were observed for patients with progressive disease¹⁵². Both these studies and ours demonstrate the ability to identify correlates of antitumor and antiviral T cell-mediated immunity by longitudinally tracking single T cell clones; efforts which will inevitably be improved through further innovations in single cell sequencing technologies and access to larger cell populations in the future.

T cell receptor repertoire diversity is believed to be critical to immune protection, as epitope-specific cells exhibiting greater clonotypic diversity have been found to be more enriched for high-avidity T cells¹⁵³, provide heterologous immune protection¹⁵⁴, and limit immune escape¹⁵⁵. To study TCR repertoire diversity, we successfully identified and tracked the dynamics of unique paired TCR α/β sequences specific to a single tumor neoantigen in four patients at serial timepoints spaced weeks to months apart throughout vaccination. In spite of the relatively small numbers of T cells isolated at each timepoint, we uncovered several notable features of the neoantigen-specific

TCR repertoire. First, we observed persistence of several individual TCR clonotypes throughout vaccination, suggesting that these clones may be most relevant for the vaccine-induced antitumor immune response, perhaps due to increased TCR affinity or avidity¹⁵⁶. We also observed an apparent diversification of the TCR repertoire with vaccination as illustrated through the continual addition of novel TCR clonotypes through time in combination with the aforementioned persistence of certain clones. Biologically, these kinetics could reflect the coexistence of naïve and memory neoantigen-specific T cells at later timepoints. Interestingly, we did not observe a clear pattern of increasing numbers of TCR clonotypes present at each timepoint through vaccination, nor did we note a clear time-related change in the clonality, or evenness, of the TCR repertoire. However, in a study in mice comparing TCR repertoires after primary and secondary immunization, a narrowing of the TCR repertoire was observed with secondary immunization, so perhaps an increase in the number of circulation TCR clonotypes with time would not be biologically expected¹⁵⁶.

The TCR repertoire analysis in Patient 2 revealed fewer unique neoantigen-specific TCRs identified after pembrolizumab administration compared to the 16-week post-vaccination timepoint. This is likely a reflection of the smaller number of neoantigen-specific T cells isolated after pembrolizumab. As these cells were stimulated *in vitro* for several weeks prior to tetramer staining and thus likely underwent significant expansion in culture, we cannot interpret or compare the absolute percentages of tetramer-positive T cells at the two timepoints. However, if *ex vivo* experiments were to replicate this contraction in tetramer-positive T cells, this may be indicative of selection for and proliferation of T cells harboring higher affinity TCRs¹⁵⁷; alternatively, it could simply be a manifestation of the fact that the chosen neoepitope for the Patient 2 tetramer-staining

experiment was not highly processed and presented by MHC molecular on tumor cells, and thus could indicate that the abundance of neoantigen-specific T cells identified at week 16 of vaccination was primarily stimulated by the vaccine itself, whereas those seen after pembrolizumab were actually stimulated by tumor cells. Perhaps more interestingly, Pt. 6 neoantigen-specific CD4⁺ T cells from after pembrolizumab exhibited an increased intensity of tetramer staining, perhaps a more reliable indicator of selection for T cells with increased functional avidity after anti-PD-1 therapy.

Building on our previously reported observations¹ that NeoVax-induced T cells can recognize autologous melanoma cells in a subset of patients, we demonstrated that T-cells may be able to recognize and kill tumor targets *in vivo*, leading to tumor cytolysis and release of novel antigens into the tumor microenvironment. We provide evidence of NeoVax-induced *in vivo* tumor cytolysis by demonstrating T cell recognition of tumor associated antigens and neoantigen targets that were expressed by the tumors, but not contained in vaccines, of 2 of 3 patients with available PBMC samples. Patient 2 developed recurrent melanoma metastases during vaccination and therefore may have had radiographically evident tumors at the time of vaccine priming, whereas patient 3 remained without evidence of disease while CD4⁺ T cell responses against 3 non-vaccine neoepitopes emerged, suggesting that determinant spreading can occur in patients with clinical evident metastases, but also in the presence of only micrometastatic disease. In both patients, non-vaccine antigen directed responses (against neoepitopes in both patients, in addition to a TAA peptide in Patient 2) were detected after treatment with NeoVax alone, and patient 2 subsequently developed two additional responses against a neoepitope and a TAA after anti-PD-1 therapy.

Notably, these responses were not observed before vaccination, suggesting that at least some degree of tumor cytolysis can be attributed to NeoVax.

Evidence of epitope spreading following cancer therapy has previously been demonstrated in both mouse models and in humans. In mice, T-cell mediated epitope spreading was observed following PD-1 blockade in the form of an increased number of functional subdominant CD8⁺ T cell clones¹⁵⁸, and another study of mice bearing carcinoembryonic antigen (CEA)-expressing tumors vaccinated with a CEA-based vaccine showed effective antitumor CD8⁺ T cell responses to both CEA and other TAAs not included in the vaccine¹⁵⁹. In humans, epitope spreading has been observed after trastuzumab plus a HER2/neu-based vaccine for breast cancer (both intra and intermolecular epitope spreading)¹⁶⁰, after a MAGE-based vaccine for melanoma, and after CTLA-4 blockade for melanoma¹⁶¹. In the case of the MAGE-based vaccine for melanoma, epitope spreading was associated with tumor regression¹⁶². A clinical trial for the combination of anti-PD-1 therapy (nivolumab) plus another personal neoantigen vaccine, NEO-PV-01, for patients with unresectable or metastatic melanoma, lung cancer, and bladder cancer, is ongoing. Results thus far suggest that the combination induces both neoantigen-specific immune responses similar to NeoVax and epitope spreading, which in turn appears to be associated with a longer PFS¹⁶³. Although sample size does not allow for this type of analysis in our study, we anticipate that future studies with more patients will yield similar results.

Suggestions for Future Work

We have established the persistence of persistent neoantigen-specific T cell responses out to 4 years following vaccination with a personalized neoantigen vaccine. In ongoing analyses, we intend to characterize the transcriptional profiles of the neoantigen-reactive T cells at 3-4 years to determine whether or not they represent memory T cells. It will also be important to characterize the TCR repertoires of these cells and compare the diversity and composition of the repertoires to the earlier timepoints. Ideally, we would also isolate larger numbers of neoantigen-specific T cells in order to enhance our ability to make more definitive conclusions about patterns or trends we observe.

By performing whole-exome sequencing on the relapsed tumors of several patients, we showed that most mutations persisted, and the majority of neoantigens targeted by the vaccines were not lost. Future studies will further examine the genomics and transcriptional profiles of these relapsed tumor samples. Using computation tools such as PhylogicNDT, we hope to infer the order of clonal driver events, subclonal populations of cells and their phylogenetic relationships, and overall clonal dynamics of the melanomas of the patients who relapsed after NeoVax. Additionally, future NeoVax studies will be performed in patients with metastatic disease and incorporate prospective tumor sampling to allow for optimal tracking of clonal trajectories. Furthermore, RNA sequencing will be performed on the relapsed tumors to identify changes in expression of antigen presentation machinery, checkpoint inhibitory receptors, and other gene-sets. Findings will be confirmed by immunohistochemistry and immunofluorescence. Finally, it would be informative to isolate tumor-infiltrating lymphocytes from the relapsed tumor samples and compare their phenotypic and TCR identities to those isolated from the peripheral circulation described in this thesis.

We also plan to optimize the joint-clustering analysis of our existing single cell RNAseq data from the neoantigen-specific CD4⁺ T cells of Pts. 3, 4, and 5. As described in **Results**, one of the clusters (Cluster 4) had a high average gene count per cell and was characterized by upregulation of various housekeeping genes, overall suspicious for a cluster of unhealthy cells. Therefore, I chose not to analyze it further in this thesis. To address this cluster, we plan to perform re-clustering after setting a gene count threshold, thereby eliminating cells with high gene counts which may represent doublets. We will also try re-clustering after removal of cells collected from week 3, which comprises the majority of Cluster 4, as these cells may be low-quality. We would also like to further investigate Cluster 2, the ‘AICD-like’ cluster, as the expression pattern of its top three differentially expressed genes (CH507.513H4.3, CH507.513H4.6, and CH507.513H4.4) is very distinctive across all clusters (**Fig. 3e**): these genes are very upregulated in some cells, and very downregulated in others. It is possible that cells from a single patient or timepoint are driving this result, a question which warrants further investigation. Beyond these technical inquiries, future studies could also focus on refining and providing more robust evidence to support our interpretations of the phenotypes represented in each cluster. Gene-set enrichment analysis tools could be applied in this vein.

Using tetramer-staining, we successfully elucidated TCR repertoires of neoantigen-specific CD4⁺ T cells, and qualitatively showed increases in TCR clonotype diversity and patterns of expansion and contraction with vaccination. We also highlighted differing proportions of neoantigen-specific T cells before and after anti-PD-1 therapy. Our analysis was certainly limited by small numbers of neoantigen-specific T cells and thus an inherent inability to capture all circulating neoantigen-

specific TCRs. Our sample sizes restricted our ability to calculate reliable indices of species diversity. Various ecological indices and tools have previously been utilized to measure TCR repertoire diversity, ranging from simply the number of unique TCR species in the population¹⁵⁴ to the Shannon-Weaver and Simpson indices¹⁶⁴, to a Poisson-based parametric computational estimator of unseen species¹⁶⁵. Studying these metrics in future studies will enable quantitative analysis of TCR repertoire diversity. Comparing bulk TCR sequencing data to the neoantigen-specific TCR data could also enable us to confirm the evolutionary patterns we observed, although such an analysis would be limited by the ability to detect low-frequency TCRs. Future studies could also confirm antigen specificity and examine functional avidity of individual TCRs through cloning and expression in T cell lines followed by *in vitro* functional analyses as in other studies^{104,166}. Moreover, we are actively working to sequence the neoantigen-specific TCRs of Patient 6, and because the neoantigen-specific T cells were index sorted, we will be able to link each TCR identity with its intensity of tetramer staining, a measure of functional avidity. Linking TCR specificity with information about T-cell function in this way will serve to further our understanding of how neoantigen vaccines drive an effective anti-tumor immune response, and will provide insight into how to amplify the strongest and most relevant neoantigen-specific T cell responses.

Finally, the favorable long-term outcomes of the two stage IV patients who received pembrolizumab following relapse suggests that combining personal neoantigen vaccination with checkpoint blockade may prove to be a more effective clinical therapy than either therapy alone. Subsequent trials of personal neoantigen vaccines are planned to include combination with immune checkpoint blockade. It will be critical to determine the optimal timing of administration

of these complementary agents by using experimental models to assess how the timing of administration of checkpoint blockade prior, concurrently, or following neoantigen vaccine affects priming of de novo immune responses, and establishment of T cell memory. Future studies of personal neoantigen vaccines in other non-adjuvant settings are planned, and immunologic analyses of patient T cells and tumors from these trials will further our understanding of the roles of various tumor cell-intrinsic (i.e., degree of MHC expression, peptide processing and presentation, PD-1 expression) and T-cell intrinsic factors (i.e., TCR repertoire diversity, TCR binding avidity, specificity, phenotype, tumor infiltration) in influencing the effectiveness of a vaccine-induced T cell response.

Conclusions

- Multi-epitope personalized neoantigen vaccines can induce lasting favorable clinical responses in high-risk melanoma patients.
- Personalized neoantigen vaccines generate functional neoantigen-specific effector and memory CD4⁺ and CD8⁺ T cell responses that persist for years after vaccination.
- Most neoantigens targeted by the vaccines are present in relapsed tumors, underscoring the biological significance of long-lasting circulating neoantigen-specific T cells, and suggesting that designing personalized therapies based on information provided from single tumor biopsies is rational.
- Neoantigen-specific CD4⁺ T cells appear only after vaccination and exhibit cytotoxic, naïve, and memory phenotypic signatures.
- The neoantigen-specific TCR repertoire expands and shifts throughout vaccination and after anti-PD-1 therapy.
- Neoantigen vaccines provoke spreading of novel T cell responses to tumor epitopes not-targeted by vaccines, indicative of vaccine-induced tumor cytolysis.

Lay Summary

Over the past decade, the treatment of both solid and hematologic cancers has been revolutionized by methods to harness and strengthen the anti-tumor immune response, such as immune checkpoint blockade, chimeric antigen receptor (CAR-T) therapies, and personalized cancer vaccination. Especially important to the generation of an effective anti-tumor response is the activation of T cells directed against tumor antigens. The recent availability of next-generation sequencing (NGS) has enabled the comprehensive identification of mutations within a patient's tumor, which represent an abundant source of tumor-specific potential antigens. Termed neoantigens, these antigens are promising therapeutic targets due to their exquisite tumor specificity. Notably, highly effective antitumor responses have been associated with the presence of neoantigen-specific T cells. Recently, the Wu lab harnessed NGS and computational MHC class I epitope prediction algorithms to develop NeoVax, a personalized neoantigen-based cancer vaccine. In the Phase I NeoVax trial in Stage IIIB/C melanoma patients after surgical resection (and hence patients lacking clinically evident tumor burden), vaccines were found to generate potent circulating anti-tumor immune responses. Here, we show that these neoantigen-specific T cells persist out to 4 years after vaccination. We also show that during vaccination, these T cells transition from naïve, to effector, to memory cells, and harbor diverse T-cell receptor repertoires that change and expand through vaccination and after checkpoint blockade therapy. We also investigate the somatic mutation burden within relapsed tumors of five patients who experienced disease recurrence following vaccination, and show that most of the neoantigens targeted by vaccines remain. Finally, we reveal that personalized neoantigen vaccines induce T-cell responses to tumor antigens that were not originally targeted by vaccines, suggesting that these vaccines can cause release of new tumor antigens into the environment through T cell-mediated tumor killing.

These results underline that neoantigen-based vaccines can mount long-lasting and functional immune response against tumors, and provides a foundation for further exploration into using neoantigen-based personalized approaches alone and in combination with other immunotherapies in future studies.

References

1. Ott PA, Hu Z, Keskin DB, Shukla SA, Sun J, Bozym DJ, Zhang W, Luoma A, Giobbie-Hurder A, Peter L, Chen C, Olive O, Carter TA, Li S, Lieb DJ, Eisenhaure T, Gjini E, Stevens J, Lane WJ, Javeri I, Nellaiappan K, Salazar AM, Daley H, Seaman M, Buchbinder EI, Yoon CH, Harden M, Lennon N, Gabriel S, Rodig SJ, Barouch DH, Aster JC, Getz G, Wucherpfennig K, Neuberg D, Ritz J, Lander ES, Fritsch EF, Hacohen N, Wu CJ. An immunogenic personal neoantigen vaccine for patients with melanoma. *Nature*. Nature Publishing Group; 2017 Jul 13;547(7662):217–221. PMID: 28678778
2. Sahin U, Derhovanessian E, Miller M, Kloke BP, Simon P, Löwer M, Bukur V, Tadmor AD, Luxemburger U, Schrörs B, Omokoko T, Vormehr M, Albrecht C, Paruzynski A, Kuhn AN, Buck J, Heesch S, Schreeb KH, Müller F, Ortseifer I, Vogler I, Godehardt E, Attig S, Rae R, Breitkreuz A, Tolliver C, Suchan M, Martic G, Hohberger A, Sorn P, Diekmann J, Ciesla J, Waksman O, Brück AK, Witt M, Zillgen M, Rothermel A, Kasemann B, Langer D, Bolte S, Diken M, Kreiter S, Nemecek R, Gebhardt C, Grabbe S, Höller C, Utikal J, Huber C, Loquai C, Türeci Ö. Personalized RNA mutanome vaccines mobilize poly-specific therapeutic immunity against cancer. *Nature*. Nature Publishing Group; 2017 Jul 13;547(7662):222–226. PMID: 28678784
3. Hu Z, Ott PA, Wu CJ. Towards personalized, tumour-specific, therapeutic vaccines for cancer. *Nat Rev Immunol* [Internet]. Nature Publishing Group; 2018;18(3):168–182. Available from: <http://dx.doi.org/10.1038/nri.2017.131>
4. Boon T, Cerottini J-C, Van den Eynde B, van der Bruggen P, Van Pel A. Tumor Antigens Recognized by T Lymphocytes. *Annu Rev Immunol* [Internet]. 1994 Apr [cited 2020 Jan 13];12(1):337–365. Available from: <http://www.annualreviews.org/doi/10.1146/annurev.iy.12.040194.002005>
5. Chen DS, Mellman I. Oncology meets immunology: The cancer-immunity cycle. *Immunity*. 2013;39(1):1–10. PMID: 23890059
6. Xia A, Zhang Y, Xu J, Yin T, Lu XJ. T Cell Dysfunction in Cancer Immunity and Immunotherapy. *Front Immunol*. 2019;10(July):1719.
7. Motz GT, Coukos G. Immunity Review Deciphering and Reversing Tumor Immune Suppression. [cited 2020 Jan 13]; Available from: <http://dx>.
8. Durgeau A, Virk Y, Corgnac S, Mami-Chouaib F. Recent advances in targeting CD8 T-cell immunity for more effective cancer immunotherapy. *Front Immunol*. 2018;9(JAN).
9. Koretz K, Moldenhauer G, Majdic O, Möller P. Correlation of HLA-D/II antigen expression in breast carcinoma with local lymphohistiocytic infiltration reveals considerable dysregulation in a subset of tumors. *Int J Cancer* [Internet]. 1989 Nov 15 [cited 2020 Jan 13];44(5):816–822. Available from: <http://doi.wiley.com/10.1002/ijc.2910440512>
10. Marincola FM, Jaffee EM, Hickljin DJ, Ferrone S. Escape of human solid tumors from t-

- cell recognition: molecular mechanisms and functional significance. *Adv Immunol.* 2000;(74):181–273. PMID: 10605607
11. Offringa R, Van Der Burg SH, Ossendorp F, Toes RE, Melief CJ. Design and evaluation of antigen-specific vaccination strategies against cancer. *Current Opinion in Immunology.* Current Biology Ltd; 2000. p. 576–582.
 12. Zanetti M. Tapping CD4 T Cells for Cancer Immunotherapy: The Choice of Personalized Genomics. *J Immunol.* 2015;194(5):2049–2056.
 13. Boon T, Coulie PG, Van Den Eynde B. Tumor antigens recognized by T cells. *Immunology Today.* Elsevier Ltd; 1997. p. 267–268.
 14. Pagès F, Berger A, Camus M, Sanchez-Cabo F, Costes A, Molitor R, Mlecnik B, Kirilovsky A, Nilsson M, Damotte D, Meatchi T, Bruneval P, Cugnenc P-H, Trajanoski Z, Fridman W-H, Galon J. Effector Memory T Cells, Early Metastasis, and Survival in Colorectal Cancer. *N Engl J Med [Internet].* 2005 Dec 22 [cited 2020 Jan 13];353(25):2654–2666. Available from: <http://www.nejm.org/doi/abs/10.1056/NEJMoa051424>
 15. Borst J, Ahrends T, Bąbała N, Melief CJM, Kastenmüller W. CD4+ T cell help in cancer immunology and immunotherapy. *Nat Rev Immunol.* 2018;18(10):635–647.
 16. Kennedy R. Multiple roles for CD4 T cells in anti-tumor immune responses. 2008;222:129–144.
 17. Zeng G, Wang X, Robbins PF, Rosenberg SA, Wang RF. Cd4+ T cell recognition of MHC class II-restricted epitopes from NY-ESO-1 presented by a prevalent HLA DP4 allele: Association with NY-ESO-1 antibody production. *Proc Natl Acad Sci U S A.* 2001 Mar 27;98(7):3964–3969.
 18. Kudela P, Sun Z, Fourcade J, Janjic B, Kirkwood JM, Maillere B, Zarour HM. Epitope Hierarchy of Spontaneous CD4 + T Cell Responses to LAGE-1 . *J Immunol.* The American Association of Immunologists; 2011 Jan 1;186(1):312–322.
 19. Tsuji T, Matsuzaki J, Ritter E, Miliotto A, Ritter G, Odunsi K, Old LJ, Gnjatich S. Split T Cell Tolerance against a Self/Tumor Antigen: Spontaneous CD4+ but Not CD8+ T Cell Responses against p53 in Cancer Patients and Healthy Donors. Rodrigues MM, editor. *PLoS One [Internet].* 2011 Aug 12 [cited 2020 Jan 13];6(8):e23651. Available from: <https://dx.plos.org/10.1371/journal.pone.0023651>
 20. Thomas WD, Hersey P. CD4 T cells kill melanoma cells by mechanisms that are independent of Fas (CD95). *Int J Cancer [Internet].* 1998 Jan 30 [cited 2020 Jan 13];75(3):384–390. Available from: <http://doi.wiley.com/10.1002/%28SICI%291097-0215%2819980130%2975%3A3%3C384%3A%3AAID-IJC10%3E3.0.CO%3B2-9>
 21. Hombach A, Köhler H, Rappl G, Abken H. Human CD4 + T Cells Lyse Target Cells via Granzyme/Perforin upon Circumvention of MHC Class II Restriction by an Antibody-Like Immunoreceptor . *J Immunol.* The American Association of Immunologists; 2006

Oct 15;177(8):5668–5675. PMID: 17015756

22. Manici S, Sturniolo T, Imro MA, Hammer J, Sinigaglia F, Noppen C, Spagnoli G, Mazzi B, Bellone M, Dellabona P, Protti MP. Melanoma cells present a MAGE-3 epitope to CD4⁺ cytotoxic T cells in association with histocompatibility leukocyte antigen DR11. *J Exp Med*. 1999 Mar 1;189(5):871–876.
23. Alt FW, Oltz EM, Young F, Gorman J, Taccioli G, Chen J. VDJ recombination. *Immunology Today*. 1992. p. 306–314.
24. Abul K, Abbas AHL and SP. Cellular and Molecular Immunology, Ninth Edition. Cellular and Molecular Immunology. 2018.
25. Viganò S, Utschneider DT, Perreau M, Pantaleo G, Zehn D, Harari A. Functional avidity: A measure to predict the efficacy of effector T cells? *Clin Dev Immunol*. 2012;2012.
26. Tian S, Maile R, Collins EJ, Frelinger JA. CD8 + T Cell Activation Is Governed by TCR-Peptide/MHC Affinity, Not Dissociation Rate . *J Immunol*. The American Association of Immunologists; 2007 Sep 1;179(5):2952–2960.
27. Holmberg K, Mariathasan S, Ohteki T, Ohashi PS, Gascoigne NRJ. TCR Binding Kinetics Measured with MHC Class I Tetramers Reveal a Positive Selecting Peptide with Relatively High Affinity for TCR. *J Immunol*. The American Association of Immunologists; 2003 Sep 1;171(5):2427–2434.
28. Stone JD, Chervin AS, Kranz DM. T-cell receptor binding affinities and kinetics: impact on T-cell activity and specificity. *Immunology* [Internet]. 2009 Feb [cited 2020 Jan 13];126(2):165–176. Available from: <http://doi.wiley.com/10.1111/j.1365-2567.2008.03015.x>
29. Laugel B, Van Den Berg HA, Gostick E, Cole DK, Wooldridge L, Boulter J, Milicic A, Price DA, Sewell AK. Different T cell receptor affinity thresholds and CD8 coreceptor dependence govern cytotoxic T lymphocyte activation and tetramer binding properties. *J Biol Chem*. 2007 Aug 17;282(33):23799–23810.
30. Zhong S, Malecek K, Johnson LA, Yu Z, De Miera EVS, Darvishian F, McGary K, Huang K, Boyer J, Corse E, Shao Y, Rosenberg SA, Restifo NP, Osman I, Krogsgaard M. T-cell receptor affinity and avidity defines antitumor response and autoimmunity in T-cell immunotherapy. *Proc Natl Acad Sci U S A*. 2013;110(17):6973–6978.
31. Valitutti S, Müller S, Dessing M, Lanzavecchia A. Different responses are elicited in cytotoxic T lymphocytes by different levels of T cell receptor occupancy. *J Exp Med*. 1996 Apr 1;183(4):1917–1921. PMID: 8666949
32. Hofmann M, Radsak M, Rechtsteiner G, Wiemann K, Günder M, Bien-Gräter U, Offringa R, Toes REM, Rammensee H-G, Schild H. T cell avidity determines the level of CTL activation. *Eur J Immunol* [Internet]. 2004 Jul [cited 2020 Jan 13];34(7):1798–1806. Available from: <http://doi.wiley.com/10.1002/eji.200425088>

33. Six A, Mariotti-Ferrandiz ME, Chaara W, Magadan S, Pham HP, Lefranc MP, Mora T, Thomas-Vaslin V, Walczak AM, Boudinot P. The past, present, and future of immune repertoire biology - the rise of next-generation repertoire analysis. *Front Immunol.* 2013;4(NOV).
34. Dash P, McClaren JL, Oguin TH, Rothwell W, Todd B, Morris MY, Becksfort J, Reynolds C, Brown SA, Doherty PC, Thomas PG. Paired analysis of TCR α and TCR β chains at the single-cell level in mice. *J Clin Invest.* 2011 Jan 4;121(1):288–295.
35. Han A, Glanville J, Hansmann L, Davis MM. Linking T-cell receptor sequence to functional phenotype at the single-cell level. *Nat Biotechnol.* Nature Publishing Group; 2014;32(7):684–692.
36. Kobayashi E, Mizukoshi E, Kishi H, Ozawa T, Hamana H, Nagai T, Nakagawa H, Jin A, Kaneko S, Muraguchi A. A new cloning and expression system yields and validates TCRs from blood lymphocytes of patients with cancer within 10 days. *Nat Med.* 2013 Nov;19(11):1542–1546.
37. Hodi FS, O’Day SJ, McDermott DF, Weber RW, Sosman JA, Haanen JB, Gonzalez R, Robert C, Schadendorf D, Hassel JC, Akerley W, van den Eertwegh AJM, Lutzky J, Lorigan P, Vaubel JM, Linette GP, Hogg D, Ottensmeier CH, Lebbé C, Peschel C, Quirt I, Clark JI, Wolchok JD, Weber JS, Tian J, Yellin MJ, Nichol GM, Hoos A, Urba WJ. Improved Survival with Ipilimumab in Patients with Metastatic Melanoma. *N Engl J Med* [Internet]. 2010 Aug 19 [cited 2020 Jan 14];363(8):711–723. Available from: <http://www.nejm.org/doi/abs/10.1056/NEJMoa1003466>
38. Topalian SL, Hodi FS, Brahmer JR, Gettinger SN, Smith DC, McDermott DF, Powderly JD, Carvajal RD, Sosman JA, Atkins MB, Leming PD, Spigel DR, Antonia SJ, Horn L, Drake CG, Pardoll DM, Chen L, Sharfman WH, Anders RA, Taube JM, McMiller TL, Xu H, Korman AJ, Jure-Kunkel M, Agrawal S, McDonald D, Kollia GD, Gupta A, Wigginton JM, Sznol M. Safety, Activity, and Immune Correlates of Anti-PD-1 Antibody in Cancer. *N Engl J Med* [Internet]. 2012 Jun 28 [cited 2020 Jan 14];366(26):2443–2454. Available from: <http://www.nejm.org/doi/10.1056/NEJMoa1200690>
39. Brahmer JR, Tykodi SS, Chow LQM, Hwu WJ, Topalian SL, Hwu P, Drake CG, Camacho LH, Kauh J, Odunsi K, Pitot HC, Hamid O, Bhatia S, Martins R, Eaton K, Chen S, Salay TM, Alaparthi S, Grosso JF, Korman AJ, Parker SM, Agrawal S, Goldberg SM, Pardoll DM, Gupta A, Wigginton JM. Safety and activity of anti-PD-L1 antibody in patients with advanced cancer. *N Engl J Med.* 2012;366(26):2455–2465. PMID: 22658128
40. Wolchok JD, Chiarion-Sileni V, Gonzalez R, Rutkowski P, Grob J-J, Cowey CL, Lao CD, Wagstaff J, Schadendorf D, Ferrucci PF, Smylie M, Dummer R, Hill A, Hogg D, Haanen J, Carlino MS, Bechter O, Maio M, Marquez-Rodas I, Guidoboni M, McArthur G, Lebbé C, Ascierto PA, Long G V., Cebon J, Sosman J, Postow MA, Callahan MK, Walker D, Rollin L, Bhore R, Hodi FS, Larkin J. Overall Survival with Combined Nivolumab and Ipilimumab in Advanced Melanoma. *N Engl J Med* [Internet]. 2017 Oct 5 [cited 2020 Jan 14];377(14):1345–1356. Available from:

<http://www.nejm.org/doi/10.1056/NEJMoa1709684>

41. Larkin J, Chiarion-Sileni V, Gonzalez R, Grob JJ, Cowey CL, Lao CD, Schadendorf D, Dummer R, Smylie M, Rutkowski P, Ferrucci PF, Hill A, Wagstaff J, Carlino MS, Haanen JB, Maio M, Marquez-Rodas I, McArthur GA, Ascierto PA, Long G V., Callahan MK, Postow MA, Grossmann K, Sznol M, Dreno B, Bastholt L, Yang A, Rollin LM, Horak C, Hodi FS, Wolchok JD. Combined Nivolumab and Ipilimumab or Monotherapy in Untreated Melanoma. *N Engl J Med* [Internet]. 2015 Jul 2 [cited 2020 Jan 14];373(1):23–34. Available from: <http://www.nejm.org/doi/10.1056/NEJMoa1504030>
42. Delamarre L, Mellman I, Yadav M. Neo approaches to cancer vaccines. *Science*. American Association for the Advancement of Science; 2015. p. 760–761.
43. Sharma P, Allison JP. Immune checkpoint targeting in cancer therapy: Toward combination strategies with curative potential. *Cell*. Cell Press; 2015. p. 205–214.
44. Whiteside TL, Demaria S, Rodriguez-Ruiz ME, Zarour HM, Melero I. Emerging opportunities and challenges in cancer immunotherapy. *Clin Cancer Res*. 2016;22(8):1845–1855.
45. Rosenberg SA, Restifo NP. Adoptive cell transfer as personalized immunotherapy for human cancer. *Science*. American Association for the Advancement of Science; 2015. p. 62–68. PMID: 25838374
46. Weber J, Atkins M, Hwu P, Radvanyi L, Sznol M, Yee C. White paper on adoptive cell therapy for cancer with tumor-infiltrating lymphocytes: A report of the CTEP subcommittee on adoptive cell therapy. *Clin Cancer Res*. 2011 Apr 1;17(7):1664–1673.
47. Rosenberg SA, Restifo NP, Yang JC, Morgan RA, Dudley ME. Adoptive cell transfer: A clinical path to effective cancer immunotherapy. *Nature Reviews Cancer*. 2008. p. 299–308.
48. June CH, Blazar BR, Riley JL. Engineering lymphocyte subsets: Tools, trials and tribulations. *Nature Reviews Immunology*. 2009. p. 704–716.
49. Morgan RA, Dudley ME, Rosenberg SA. Adoptive Cell Therapy: Genetic Modification to Redirect Effector Cell Specificity.
50. Rosenberg SA, Dudley ME, Gov M. Adoptive Cell Therapy for the Treatment of Patients with Metastatic Melanoma.
51. Dudley ME, Yang JC, Sherry R, Hughes MS, Royal R, Kammula U, Robbins PF, Huang J, Citrin DE, Leitman SF, Wunderlich J, Restifo NP, Thomasian A, Downey SG, Smith FO, Klapper J, Morton K, Laurencot C, White DE, Rosenberg SA. Adoptive cell therapy for patients with metastatic melanoma: evaluation of intensive myeloablative chemoradiation preparative regimens. *J Clin Oncol* [Internet]. 2008 Nov 10 [cited 2020 Jan 14];26(32):5233–9. Available from: <http://www.ncbi.nlm.nih.gov/pubmed/18809613> PMID: 18809613
52. Dudley ME, Wunderlich JR, Robbins PF, Yang JC, Hwu P, Schwartzentruber DJ,

- Topalian SL, Sherry R, Restifo NP, Hubicki AM, Robinson MR, Raffeld M, Duray P, Seipp CA, Rogers-Freezer L, Morton KE, Mavroukakis SA, White DE, Rosenberg SA. Cancer regression and autoimmunity in patients after clonal repopulation with antitumor lymphocytes. *Science* (80-). 2002 Oct 25;298(5594):850–854.
53. Johnson LA, Morgan RA, Dudley ME, Cassard L, Yang JC, Hughes MS, Kammula US, Royal RE, Sherry RM, Wunderlich JR, Lee CCR, Restifo NP, Schwarz SL, Cogdill AP, Bishop RJ, Kim H, Brewer CC, Rudy SF, VanWaes C, Davis JL, Mathur A, Ripley RT, Nathan DA, Laurencot CM, Rosenberg SA. Gene therapy with human and mouse T-cell receptors mediates cancer regression and targets normal tissues expressing cognate antigen. *Blood*. 2009;114(3):535–546.
 54. June CH, O'Connor RS, Kawalekar OU, Ghassemi S, Milone MC. CAR T cell immunotherapy for human cancer. *Science*. American Association for the Advancement of Science; 2018. p. 1361–1365. PMID: 29567707
 55. Morgan RA, Dudley ME, Wunderlich JR, Hughes MS, Yang JC, Sherry RM, Royal RE, Topalian SL, Kammula US, Restifo NP, Zheng Z, Nahvi A, De Vries CR, Rogers-Freezer LJ, Mavroukakis SA, Rosenberg SA. Cancer regression in patients after transfer of genetically engineered lymphocytes. *Science* (80-). 2006 Oct 6;314(5796):126–129. PMID: 16946036
 56. Grupp SA, Kalos M, Barrett D, Aplenc R, Porter DL, Rheingold SR, Teachey DT, Chew A, Hauck B, Wright JF, Milone MC, Levine BL, June CH. Chimeric antigen receptor-modified T cells for acute lymphoid leukemia. *N Engl J Med*. Massachusetts Medical Society; 2013 Apr 18;368(16):1509–1518.
 57. Garfall AL, Maus MV, Hwang WT, Lacey SF, Mahnke YD, Melenhorst JJ, Zheng Z, Vogl DT, Cohen AD, Weiss BM, Dengel K, Kerr NDS, Bagg A, Levine BL, June CH, Stadtmauer EA. Chimeric antigen receptor T cells against CD19 for multiple myeloma. *N Engl J Med*. Massachusetts Medical Society; 2015 Sep 10;373(11):1040–1047.
 58. Porter DL, Levine BL, Kalos M, Bagg A, June CH. Chimeric antigen receptor-modified T cells in chronic lymphoid leukemia. *N Engl J Med*. Massachusetts Medical Society; 2011 Aug 25;365(8):725–733. PMID: 21830940
 59. Topalian SL, Sznol M, McDermott DF, Kluger HM, Carvajal RD, Sharfman WH, Brahmer JR, Lawrence DP, Atkins MB, Powderly JD, Leming PD, Lipson EJ, Puzanov I, Smith DC, Taube JM, Wigginton JM, Kollia GD, Gupta A, Pardoll DM, Sosman JA, Hodi FS. Survival, durable tumor remission, and long-term safety in patients with advanced melanoma receiving nivolumab. *J Clin Oncol* [Internet]. 2014 Apr 1 [cited 2020 Jan 14];32(10):1020–30. Available from: <http://www.ncbi.nlm.nih.gov/pubmed/24590637> PMID: 24590637
 60. McDermott DF, Drake CG, Sznol M, Choueiri TK, Powderly JD, Smith DC, Brahmer JR, Carvajal RD, Hammers HJ, Puzanov I, Hodi FS, Kluger HM, Topalian SL, Pardoll DM, Wigginton JM, Kollia GD, Gupta A, McDonald D, Sankar V, Sosman JA, Atkins MB. Survival, Durable Response, and Long-Term Safety in Patients With Previously Treated Advanced Renal Cell Carcinoma Receiving Nivolumab. *J Clin Oncol* [Internet]. 2015 Jun

- 20 [cited 2020 Jan 14];33(18):2013–20. Available from:
<http://www.ncbi.nlm.nih.gov/pubmed/25800770> PMID: 25800770
61. Le DT, Durham JN, Smith KN, Wang H, Bartlett BR, Aulakh LK, Lu S, Kemberling H, Wilt C, Luber BS, Wong F, Azad NS, Rucki AA, Laheru D, Donehower R, Zaheer A, Fisher GA, Crocenzi TS, Lee JJ, Greten TF, Duffy AG, Ciombor KK, Eyring AD, Lam BH, Joe A, Kang SP, Holdhoff M, Danilova L, Cope L, Meyer C, Zhou S, Goldberg RM, Armstrong DK, Bever KM, Fader AN, Taube J, Housseau F, Spetzler D, Xiao N, Pardoll DM, Papadopoulos N, Kinzler KW, Eshleman JR, Vogelstein B, Anders RA, Diaz LA. Mismatch repair deficiency predicts response of solid tumors to PD-1 blockade. *Science* (80-). American Association for the Advancement of Science; 2017 Jul 28;357(6349):409–413. PMID: 28596308
 62. Nghiem PT, Bhatia S, Lipson EJ, Kudchadkar RR, Miller NJ, Annamalai L, Berry S, Chartash EK, Daud A, Fling SP, Friedlander PA, Kluger HM, Kohrt HE, Lundgren L, Margolin K, Mitchell A, Olencki T, Pardoll DM, Reddy SA, Shantha EM, Sharfman WH, Sharon E, Shemanski LR, Shinohara MM, Sunshine JC, Taube JM, Thompson JA, Townson SM, Yearley JH, Topalian SL, Cheever MA. PD-1 Blockade with Pembrolizumab in Advanced Merkel-Cell Carcinoma. *N Engl J Med* [Internet]. 2016 Jun 30 [cited 2020 Jan 14];374(26):2542–2552. Available from:
<http://www.nejm.org/doi/10.1056/NEJMoa1603702>
 63. Ansell SM, Lesokhin AM, Borrello I, Halwani A, Scott EC, Gutierrez M, Schuster SJ, Millenson MM, Cattray D, Freeman GJ, Rodig SJ, Chapuy B, Ligon AH, Zhu L, Grosso JF, Kim SY, Timmerman JM, Shipp MA, Armand P. PD-1 Blockade with Nivolumab in Relapsed or Refractory Hodgkin's Lymphoma. *N Engl J Med* [Internet]. 2015 Jan 22 [cited 2020 Jan 14];372(4):311–319. Available from:
<http://www.nejm.org/doi/10.1056/NEJMoa1411087>
 64. Palucka K, Banchereau J. Dendritic-Cell-Based Therapeutic Cancer Vaccines. *Immunity*. 2013. p. 38–48. PMID: 23890062
 65. Dranoff G, Jaffee E, Lazenby A, Golumbek P, Levitsky H, Brose K, Jackson V, Hamada H, Pardoll D, Mulligan RC. Vaccination with irradiated tumor cells engineered to secrete murine granulocyte-macrophage colony-stimulating factor stimulates potent, specific, and long-lasting anti-tumor immunity. *Proc Natl Acad Sci U S A*. National Academy of Sciences; 1993 Apr 15;90(8):3539–3543. PMID: 8097319
 66. Jaffee EM, Hruban RH, Biedrzycki B, Laheru D, Schepers K, Sauter PR, Goemann M, Coleman J, Grochow L, Donehower RC, Lillemoe KD, O'Reilly S, Abrams RA, Pardoll DM, Cameron JL, Yeo CJ. Novel allogeneic granulocyte-macrophage colony-stimulating factor-secreting tumor vaccine for pancreatic cancer: a phase I trial of safety and immune activation. *J Clin Oncol* [Internet]. 2001 Jan 1 [cited 2020 Jan 14];19(1):145–56. Available from: <http://www.ncbi.nlm.nih.gov/pubmed/11134207> PMID: 11134207
 67. Le DT, Wang-Gillam A, Picozzi V, Greten TF, Crocenzi T, Springett G, Morse M, Zeh H, Cohen D, Fine RL, Onners B, Uram JN, Laheru DA, Lutz ER, Solt S, Murphy AL, Skoble J, Lemmens E, Grous J, Dubensky T, Brockstedt DG, Jaffee EM. Safety and survival with

- GVAX pancreas prime and *Listeria Monocytogenes*-expressing mesothelin (CRS-207) boost vaccines for metastatic pancreatic cancer. *J Clin Oncol* [Internet]. 2015 Apr 20 [cited 2020 Jan 14];33(12):1325–33. Available from: <http://www.ncbi.nlm.nih.gov/pubmed/25584002> PMID: 25584002
68. Ho VT, Vanneman M, Kim H, Sasada T, Yoon JK, Pasek M, Cutler C, Koreth J, Alyea E, Sarantopoulos S, Antin JH, Ritz J, Canning C, Kutok J, Mihm MC, Dranoff G, Soiffer R. Biologic activity of irradiated, autologous, GM-CSF-secreting leukemia cell vaccines early after allogeneic stem cell transplantation. *Proc Natl Acad Sci U S A*. 2009 Sep 15;106(37):15825–15830.
 69. Burkhardt UE, Hainz U, Stevenson K, Goldstein NR, Pasek M, Naito M, Wu D, Ho VT, Alonso A, Hammond NN, Wong J, Sievers QL, Brusica A, McDonough SM, Zeng W, Perrin A, Brown JR, Canning CM, Koreth J, Cutler C, Armand P, Neuberg D, Lee JS, Antin JH, Mulligan RC, Sasada T, Ritz J, Soiffer RJ, Dranoff G, Alyea EP, Wu CJ. Autologous CLL cell vaccination early after transplant induces leukemia-specific T cells. *J Clin Invest*. American Society for Clinical Investigation; 2013 Sep 3;123(9):3756–3765.
 70. Phan V, Errington F, Cheong SC, Kottke T, Gough M, Altmann S, Brandenburger A, Emery S, Strome S, Bateman A, Bonnotte B, Melcher A, Vile R. A new genetic method to generate and isolate small, short-lived but highly potent dendritic cell-tumor cell hybrid vaccines. *Nat Med*. 2003 Sep 1;9(9):1215–1219.
 71. Avigan D, Figlin R, Childs R, Yang J. Dendritic cell-tumor fusion vaccines for renal cell carcinoma. *Clin Cancer Res*. 2004;10(18 II):6347–6353.
 72. Kenter GG, Welters MJ, Valentijn ARPM, Lowik MJG, Berends-van der Meer DMA, Vloon APG, Essahsah F, Fathallah LM, Offringa R, Drijfhout JW, Wafelman AR, Oostendorp J, Fleuren GJ, van der Burg SH, Melief CJM. Vaccination against HPV-16 Oncoproteins for Vulvar Intraepithelial Neoplasia. *N Engl J Med* [Internet]. 2009 Nov 5 [cited 2020 Jan 14];361(19):1838–1847. Available from: <http://www.nejm.org/doi/abs/10.1056/NEJMoa0810097>
 73. Walter S, Weinschenk T, Stenzl A, Zdrojowy R, Pluzanska A, Szczylik C, Staehler M, Brugger W, Dietrich PY, Mendrzyk R, Hilf N, Schoor O, Fritsche J, Mahr A, Maurer D, Vass V, Trautwein C, Lewandrowski P, Flohr C, Pohla H, Stanczak JJ, Bronte V, Mandruzzato S, Biedermann T, Pawelec G, Derhovanessian E, Yamagishi H, Miki T, Hongo F, Takaha N, Hirakawa K, Tanaka H, Stevanovic S, Frisch J, Mayer-Mokler A, Kirner A, Rammensee HG, Reinhardt C, Singh-Jasuja H. Multi-peptide immune response to cancer vaccine IMA901 after single-dose cyclophosphamide associates with longer patient survival. *Nat Med*. 2012 Aug;18(8):1254–1261. PMID: 22842478
 74. Melief CJM, Van Der Burg SH. Immunotherapy of established (pre)malignant disease by synthetic long peptide vaccines. *Nat Rev Cancer*. 2008;8(5):351–360.
 75. Kantoff PW, Schuetz TJ, Blumenstein BA, Glode LM, Billhartz DL, Wyand M, Manson K, Panicali DL, Laus R, Schlom J, Dahut WL, Arlen PM, Gulley JL, Godfrey WR. Overall survival analysis of a phase II randomized controlled trial of a Poxviral-based PSA-targeted immunotherapy in metastatic castration-resistant prostate cancer. *J Clin*

- Oncol [Internet]. 2010 Mar 1 [cited 2020 Jan 14];28(7):1099–105. Available from: <http://www.ncbi.nlm.nih.gov/pubmed/20100959> PMID: 20100959
76. Palucka K, Banchereau J. Cancer immunotherapy via dendritic cells. *Nature Reviews Cancer*. 2012. p. 265–277. PMID: 22437871
 77. Coulie PG, Van Den Eynde BJ, Van Der Bruggen P, Boon T. Tumour antigens recognized by T lymphocytes: At the core of cancer immunotherapy. *Nature Reviews Cancer*. 2014. p. 135–146.
 78. Chen YT, Scanlan MJ, Sahin U, Türeci Ö, Gure AO, Tsang S, Williamson B, Stockert E, Pfreundschuh M, Old LJ. A testicular antigen aberrantly expressed in human cancers detected by autologous antibody screening. *Proc Natl Acad Sci U S A. National Academy of Sciences*; 1997 Mar 4;94(5):1914–1918. PMID: 9050879
 79. Peng M, Mo Y, Wang Y, Wu P, Zhang Y, Xiong F, Guo C, Wu X, Li Y, Li X, Li G, Xiong W, Zeng Z. Neoantigen vaccine: An emerging tumor immunotherapy. *Molecular Cancer*. BioMed Central Ltd.; 2019.
 80. Schumacher TN, Hacohen N. Neoantigens encoded in the cancer genome. *Curr Opin Immunol*. Elsevier Ltd; 2016;41:98–103.
 81. Snyder A, Makarov V, Merghoub T, Yuan J, Zaretsky JM, Desrichard A, Walsh LA, Postow MA, Wong P, Ho TS, Hollmann TJ, Bruggeman C, Kannan K, Li Y, Elipenahli C, Liu C, Harbison CT, Wang L, Ribas A, Wolchok JD, Chan TA. Genetic Basis for Clinical Response to CTLA-4 Blockade in Melanoma. *N Engl J Med [Internet]*. 2014 Dec 4 [cited 2020 Jan 14];371(23):2189–2199. Available from: <http://www.nejm.org/doi/10.1056/NEJMoa1406498>
 82. Rizvi NA, Hellmann MD, Snyder A, Kvistborg P, Makarov V, Havel JJ, Lee W, Yuan J, Wong P, Ho TS, Miller ML, Rekhtman N, Moreira AL, Ibrahim F, Bruggeman C, Gasmir B, Zappasodi R, Maeda Y, Sander C, Garon EB, Merghoub T, Wolchok JD, Schumacher TN, Chan TA. Mutational landscape determines sensitivity to PD-1 blockade in non-small cell lung cancer. *Science (80-)*. American Association for the Advancement of Science; 2015 Apr 3;348(6230):124–128. PMID: 25765070
 83. Brown SD, Warren RL, Gibb EA, Martin SD, Spinelli JJ, Nelson BH, Holt RA. Neoantigens predicted by tumor genome meta-analysis correlate with increased patient survival. *Genome Res*. Cold Spring Harbor Laboratory Press; 2014;24(5):743–750. PMID: 24782321
 84. Giannakis M, Mu XJ, Shukla SA, Qian ZR, Cohen O, Nishihara R, Bahl S, Cao Y, Amin-Mansour A, Yamauchi M, Sukawa Y, Stewart C, Rosenberg M, Mima K, Inamura K, Noshu K, Nowak JA, Lawrence MS, Giovannucci EL, Chan AT, Ng K, Meyerhardt JA, Van Allen EM, Getz G, Gabriel SB, Lander ES, Wu CJ, Fuchs CS, Ogino S, Garraway LA. Genomic Correlates of Immune-Cell Infiltrates in Colorectal Carcinoma. *Cell Rep*. Elsevier B.V.; 2016 Apr 26;15(4):857–865.
 85. Van Allen EM, Miao D, Schilling B, Shukla SA, Blank C, Zimmer L, Sucker A, Hillen U,

Foppen MHG, Goldinger SM, Utikal J, Hassel JC, Weide B, Kaehler KC, Loquai C, Mohr P, Gutzmer R, Dummer R, Gabriel S, Wu CJ, Schadendorf D, Garraway LA. Genomic correlates of response to CTLA-4 blockade in metastatic melanoma. *Science* (80-). American Association for the Advancement of Science; 2015 Oct 9;350(6257):207–211.

86. Collisson EA, Campbell JD, Brooks AN, Berger AH, Lee W, Chmielecki J, Beer DG, Cope L, Creighton CJ, Danilova L, Ding L, Getz G, Hammerman PS, Hayes DN, Hernandez B, Herman JG, Heymach J V., Jurisica I, Kucherlapati R, Kwiatkowski D, Ladanyi M, Robertson G, Schultz N, Shen R, Sinha R, Sougnez C, Tsao MS, Travis WD, Weinstein JN, Wigle DA, Wilkerson MD, Chu A, Cherniack AD, Hadjipanayis A, Rosenberg M, Weisenberger DJ, Laird PW, Radenbaugh A, Ma S, Stuart JM, Byers LA, Baylin SB, Govindan R, Meyerson M, Gabriel SB, Cibulskis K, Kim J, Stewart C, Lichtenstein L, Lander ES, Lawrence MS, Getz E, Fulton R, Fulton LL, McLellan MD, Wilson RK, Ye K, Fronick CC, Maher CA, Miller CA, Wendl MC, Cabanski C, Mardis E, Wheeler D, Balasundaram M, Butterfield YSN, Carlsen R, Chuah E, Dhalla N, Guin R, Hirst C, Lee D, Li HI, Mayo M, Moore RA, Mungall AJ, Schein JE, Sipahimalani P, Tam A, Varhol R, Robertson AG, Wye N, Thiessen N, Holt RA, Jones SJM, Marra MA, Imielinski M, Onofrio RC, Hodis E, Zack T, Helman E, Pedamallu CS, Mesirov J, Saksena G, Schumacher SE, Carter SL, Garraway L, Beroukhi R, Lee S, Mahadeshwar HS, Pantazi A, Protopopov A, Ren X, Seth S, Song X, Tang J, Yang L, Zhang J, Chen PC, Parfenov M, Xu AW, Santoso N, Chin L, Park PJ, Hoadley KA, Auman JT, Meng S, Shi Y, Buda E, Waring S, Veluvolu U, Tan D, Mieczkowski PA, Jones CD, Simons J V., Soloway MG, Bodenheimer T, Jefferys SR, Roach J, Hoyle AP, Wu J, Balu S, Singh D, Prins JF, Marron JS, Parker JS, Perou CM, Liu J, Maglinte DT, Lai PH, Bootwalla MS, Van Den Berg DJ, Triche T, Cho J, DiCara D, Heiman D, Lin P, Mallard W, Voet D, Zhang H, Zou L, Noble MS, Gehlenborg N, Thorvaldsdottir H, Nazaire MD, Robinson J, Aksoy BA, Ciriello G, Taylor BS, Dresdner G, Gao J, Gross B, Seshan VE, Reva B, Sumer SO, Weinhold N, Sander C, Ng S, Zhu J, Benz CC, Yau C, Haussler D, Spellman PT, Kimes PK, Broom BM, Wang J, Lu Y, Ng PKS, Diao L, Liu W, Amos CI, Akbani R, Mills GB, Curley E, Paulauskis J, Lau K, Morris S, Shelton T, Mallery D, Gardner J, Penny R, Saller C, Tarvin K, Richards WG, Cerfolio R, Bryant A, Raymond DP, Pennell NA, Farver C, Czerwinski C, Huelsenbeck-Dill L, Iacocca M, Petrelli N, Rabeno B, Brown J, Bauer T, Dolzhanskiy CO, Potapova O, Rotin D, Voronina O, Nemirovich-Danchenko E, Fedosenko K V., Gal A, Behera M, Ramalingam SS, Sica G, Flieder D, Boyd J, Weaver JE, Kohl B, Thinh DHQ, Sandusky G, Juhl H, Duhig E, Illei P, Gabrielson E, Shin J, Lee B, Rogers K, Trusty D, Brock M V., Williamson C, Burks E, Rieger-Christ K, Holway A, Sullivan T, Asiedu MK, Kosari F, Rekhtman N, Zakowski M, Rusch VW, Zippile P, Suh J, Pass H, Goparaju C, Owusu-Sarpong Y, Bartlett JMS, Kodeeswaran S, Parfitt J, Sekhon H, Albert M, Eckman J, Myers JB, Morrison C, Gaudio C, Borgia JA, Bonomi P, Pool M, Liptay MJ, Moiseenko F, Zaytseva I, Dienemann H, Meister M, Schnabel PA, Muley TR, Peifer M, Gomez-Fernandez C, Herbert L, Egea S, Huang M, Thorne LB, Boice L, Salazar AH, Funkhouser WK, Rathmell WK, Dhir R, Yousem SA, Dacic S, Schneider F, Siegfried JM, Hajek R, Watson MA, McDonald S, Meyers B, Clarke B, Yang IA, Fong KM, Hunter L, Windsor M, Bowman R V., Peters S, Letovanec I, Khan KZ, Jensen MA, Snyder EE, Srinivasan D, Kahn AB, Baboud J, Pot DA, Shaw KRM, Sheth M, Davidsen T, Demchok JA, Yang L, Wang Z, Tarnuzzer R, Zenklusen JC, Ozenberger BA, Sofia HJ, Cheney R.

- Comprehensive molecular profiling of lung adenocarcinoma: The cancer genome atlas research network. *Nature*. Nature Publishing Group; 2014;511(7511):543–550.
87. van Rooij N, van Buuren MM, Philips D, Velds A, Toebes M, Heemskerk B, van Dijk LJA, Behjati S, Hilkmann H, el Atmioui D, Nieuwland M, Stratton MR, Kerkhoven RM, Keşmir C, Haanen JB, Kvistborg P, Schumacher TN. Tumor Exome Analysis Reveals Neoantigen-Specific T-Cell Reactivity in an Ipilimumab-Responsive Melanoma. *J Clin Oncol* [Internet]. 2013 Nov 10 [cited 2020 Jan 14];31(32):e439–e442. Available from: <http://ascopubs.org/doi/10.1200/JCO.2012.47.7521>
 88. Tran E, Ahmadzadeh M, Lu YC, Gros A, Turcotte S, Robbins PF, Gartner JJ, Zheng Z, Li YF, Ray S, Wunderlich JR, Somerville RP, Rosenberg SA. Immunogenicity of somatic mutations in human gastrointestinal cancers. *Science* (80-). American Association for the Advancement of Science; 2015 Dec 11;350(6266):1387–1390.
 89. Linnemann C, Van Buuren MM, Bies L, Verdegaal EME, Schotte R, Calis JJA, Behjati S, Velds A, Hilkmann H, Atmioui D El, Visser M, Stratton MR, Haanen JBAG, Spits H, Van Der Burg SH, Schumacher TNM. High-throughput epitope discovery reveals frequent recognition of neo-antigens by CD4⁺ T cells in human melanoma. *Nat Med*. Nature Publishing Group; 2015 Jan 1;21(1):81–85.
 90. Robbins PF, Lu YC, El-Gamil M, Li YF, Gross C, Gartner J, Lin JC, Teer JK, Clifton P, Tycksen E, Samuels Y, Rosenberg SA. Mining exomic sequencing data to identify mutated antigens recognized by adoptively transferred tumor-reactive T cells. *Nat Med*. 2013 Jun;19(6):747–752. PMID: 23644516
 91. Rajasagi M, Shukla SA, Fritsch EF, Keskin DB, DeLuca D, Carmona E, Zhang W, Sougnez C, Cibulskis K, Sidney J, Stevenson K, Ritz J, Neuberg D, Brusic V, Gabriel S, Lander ES, Getz G, Hacohen N, Wu CJ. Systematic identification of personal tumor-specific neoantigens in chronic lymphocytic leukemia. *Blood*. American Society of Hematology; 2014 Jul 17;124(3):453–462.
 92. Gubin MM, Zhang X, Schuster H, Caron E, Ward JP, Noguchi T, Ivanova Y, Hundal J, Arthur CD, Krebber WJ, Mulder GE, Toebes M, Vesely MD, Lam SSK, Korman AJ, Allison JP, Freeman GJ, Sharpe AH, Pearce EL, Schumacher TN, Aebbersold R, Rammensee HG, Melief CJM, Mardis ER, Gillanders WE, Artyomov MN, Schreiber RD. Checkpoint blockade cancer immunotherapy targets tumour-specific mutant antigens. *Nature*. Nature Publishing Group; 2014 Nov 27;515(7528):577–581. PMID: 25428507
 93. Tran E, Turcotte S, Gros A, Robbins PF, Lu YC, Dudley ME, Wunderlich JR, Somerville RP, Hogan K, Hinrichs CS, Parkhurst MR, Yang JC, Rosenberg SA. Cancer immunotherapy based on mutation-specific CD4⁺ T cells in a patient with epithelial cancer. *Science* (80-). American Association for the Advancement of Science; 2014;344(6184):641–645. PMID: 24812403
 94. Kreiter S, Vormehr M, Van De Roemer N, Diken M, Löwer M, Diekmann J, Boegel S, Schrörs B, Vascotto F, Castle JC, Tadmor AD, Schoenberger SP, Huber C, Türeci O, Sahin U. Mutant MHC class II epitopes drive therapeutic immune responses to cancer. *Nature*. Nature Publishing Group; 2015 Apr 30;520(7549):692–696. PMID: 25901682

95. Yadav M, Jhunjhunwala S, Phung QT, Lupardus P, Tanguay J, Bumbaca S, Franci C, Cheung TK, Fritsche J, Weinschenk T, Modrusan Z, Mellman I, Lill JR, Delamarre L. Predicting immunogenic tumour mutations by combining mass spectrometry and exome sequencing. *Nature*. Nature Publishing Group; 2014 Nov 27;515(7528):572–576.
96. Matsushita H, Vesely MD, Koboldt DC, Rickert CG, Uppaluri R, Magrini VJ, Arthur CD, White JM, Chen YS, Shea LK, Hundal J, Wendl MC, Demeter R, Wylie T, Allison JP, Smyth MJ, Old LJ, Mardis ER, Schreiber RD. Cancer exome analysis reveals a T-cell-dependent mechanism of cancer immunoediting. *Nature*. 2012 Feb 16;482(7385):400–404.
97. Dupage M, Mazumdar C, Schmidt LM, Cheung AF, Jacks T. Expression of tumour-specific antigens underlies cancer immunoediting. *Nature*. 2012 Feb 16;482(7385):405–409.
98. Castle JC, Kreiter S, Diekmann J, Löwer M, Van De Roemer N, De Graaf J, Selmi A, Diken M, Boegel S, Paret C, Koslowski M, Kuhn AN, Britten CM, Huber C, Türeci Ö, Sahin U. Exploiting the mutanome for tumor vaccination. *Cancer Res*. 2012 Mar 1;72(5):1081–1091.
99. Lawrence MS, Stojanov P, Polak P, Kryukov G V., Cibulskis K, Sivachenko A, Carter SL, Stewart C, Mermel CH, Roberts SA, Kiezun A, Hammerman PS, McKenna A, Drier Y, Zou L, Ramos AH, Pugh TJ, Stransky N, Helman E, Kim J, Sougnez C, Ambrogio L, Nickerson E, Shefler E, Cortés ML, Auclair D, Saksena G, Voet D, Noble M, Dicara D, Lin P, Lichtenstein L, Heiman DI, Fennell T, Imielinski M, Hernandez B, Hodis E, Baca S, Dulak AM, Lohr J, Landau DA, Wu CJ, Melendez-Zajgla J, Hidalgo-Miranda A, Koren A, McCarroll SA, Mora J, Lee RS, Crompton B, Onofrio R, Parkin M, Winckler W, Ardlie K, Gabriel SB, Roberts CWM, Biegel JA, Stegmaier K, Bass AJ, Garraway LA, Meyerson M, Golub TR, Gordenin DA, Sunyaev S, Lander ES, Getz G. Mutational heterogeneity in cancer and the search for new cancer-associated genes. *Nature*. 2013;499(7457):214–218. PMID: 23770567
100. Hoof I, Peters B, Sidney J, Pedersen LE, Sette A, Lund O, Buus S, Nielsen M. NetMHCpan, a method for MHC class I binding prediction beyond humans. *Immunogenetics*. 2009 Jan;61(1):1–13.
101. Lundegaard C, Lund O, Nielsen M. Prediction of epitopes using neural network based methods. *J Immunol Methods*. 2011 Nov 30;374(1–2):26–34.
102. Abelin JG, Keskin DB, Sarkizova S, Hartigan CR, Zhang W, Sidney J, Stevens J, Lane W, Zhang GL, Eisenhaure TM, Clauser KR, Hacohen N, Rooney MS, Carr SA, Wu CJ. Mass Spectrometry Profiling of HLA-Associated Peptidomes in Mono-allelic Cells Enables More Accurate Epitope Prediction. *Immunity*. Elsevier Inc.; 2017;46(2):315–326.
103. Carreno BM, Magrini V, Becker-Hapak M, Kaabinejadian S, Hundal J, Petti AA, Ly A, Lie WR, Hildebrand WH, Mardis ER, Linette GP. A dendritic cell vaccine increases the breadth and diversity of melanoma neoantigen-specific T cells. *Science (80-)*. American Association for the Advancement of Science; 2015 May 15;348(6236):803–808.

104. Keskin DB, Anandappa AJ, Sun J, Tirosh I, Mathewson ND, Li S, Oliveira G, Giobbie-Hurder A, Felt K, Gjini E, Shukla SA, Hu Z, Li L, Le PM, Allesøe RL, Richman AR, Kowalczyk MS, Abdelrahman S, Geduldig JE, Charbonneau S, Pelton K, Iorgulescu JB, Elagina L, Zhang W, Olive O, McCluskey C, Olsen LR, Stevens J, Lane WJ, Salazar AM, Daley H, Wen PY, Chiocca EA, Harden M, Lennon NJ, Gabriel S, Getz G, Lander ES, Regev A, Ritz J, Neuberg D, Rodig SJ, Ligon KL, Suvà ML, Wucherpfeffig KW, Hacohen N, Fritsch EF, Livak KJ, Ott PA, Wu CJ, Reardon DA. Neoantigen vaccine generates intratumoral T cell responses in phase Ib glioblastoma trial. *Nature*. Nature Publishing Group; 2019. p. 234–239. PMID: 30568305
105. Hilf N, Kuttruff-Coqui S, Frenzel K, Bukur V, Stevanović S, Gouttefangeas C, Platten M, Tabatabai G, Dutoit V, van der Burg SH, thor Straten P, Martínez-Ricarte F, Ponsati B, Okada H, Lassen U, Admon A, Ottensmeier CH, Ulges A, Kreiter S, von Deimling A, Skardelly M, Migliorini D, Kroep JR, Idorn M, Rodon J, Piró J, Poulsen HS, Shraibman B, McCann K, Mendrzyk R, Löwer M, Stieglbauer M, Britten CM, Capper D, Welters MJP, Sahuquillo J, Kiesel K, Derhovanessian E, Rusch E, Bunse L, Song C, Heesch S, Wagner C, Kemmer-Brück A, Ludwig J, Castle JC, Schoor O, Tadmor AD, Green E, Fritsche J, Meyer M, Pawlowski N, Dorner S, Hoffgaard F, Rössler B, Maurer D, Weinschenk T, Reinhardt C, Huber C, Rammensee HG, Singh-Jasuja H, Sahin U, Dietrich PY, Wick W. Actively personalized vaccination trial for newly diagnosed glioblastoma. *Nature*. Nature Publishing Group; 2019. p. 240–245. PMID: 30733620
106. Johanns TM, Miller CA, Liu CJ, Perrin RJ, Bender D, Kobayashi DK, Campian JL, Chicoine MR, Dacey RG, Huang J, Fritsch EF, Gillanders WE, Artyomov MN, Mardis ER, Schreiber RD, Dunn GP. Detection of neoantigen-specific T cells following a personalized vaccine in a patient with glioblastoma. *Oncoimmunology*. Taylor and Francis Inc.; 2019 Apr 3;8(4).
107. Stern LJ, Brown JH, Jardetzky TS, Gorga JC, Urban RG, Strominger JL, Wiley DC. Crystal structure of the human class II MHC protein HLA-DR1 complexed with an influenza virus peptide. *Nature*. 1994;368(6468):215–221.
108. Jones EY, Fugger L, Strominger JL, Siebold C. MHC class II proteins and disease: A structural perspective. *Nature Reviews Immunology*. 2006. p. 271–282.
109. Park HY, Tan PS, Kavishna R, Ker A, Lu J, Chan CEZ, Hanson BJ, MacAry PA, Caminschi I, Shortman K, Alonso S, Lahoud MH. Enhancing vaccine antibody responses by targeting Clec9A on dendritic cells. *npj Vaccines* [Internet]. Springer US; 2017;2(1). Available from: <http://dx.doi.org/10.1038/s41541-017-0033-5>
110. Mildner A, Jung S. Development and function of dendritic cell subsets. *Immunity*. Cell Press; 2014. p. 642–656.
111. Gerner MY, Casey KA, Kastenmuller W, Germain RN. Dendritic cell and antigen dispersal landscapes regulate T cell immunity. *J Exp Med*. Rockefeller University Press; 2017;214(10):3105–3122.
112. Woroniecka K, Chongsathidkiet P, Rhodin K, Kemeny H, Dechant C, Harrison Farber S, Elsamadicy AA, Cui X, Koyama S, Jackson C, Hansen LJ, Johanns TM, Sanchez-Perez L,

- Chandramohan V, Yu YRA, Bigner DD, Giles A, Healy P, Dranoff G, Weinhold KJ, Dunn GP, Fecci PE. T-cell exhaustion signatures vary with tumor type and are severe in glioblastoma. *Clin Cancer Res. American Association for Cancer Research Inc.*; 2018 Sep 1;24(17):4175–4186.
113. Verma V, Shrimali RK, Ahmad S, Dai W, Wang H, Lu S, Nandre R, Gaur P, Lopez J, Sade-Feldman M, Yizhak K, Bjorgaard SL, Flaherty KT, Wargo JA, Boland GM, Sullivan RJ, Getz G, Hammond SA, Tan M, Qi J, Wong P, Merghoub T, Wolchok J, Hachohen N, Janik JE, Mkrtychyan M, Gupta S, Khleif SN. PD-1 blockade in subprimed CD8 cells induces dysfunctional PD-1+CD38hi cells and anti-PD-1 resistance. *Nat Immunol. Nature Publishing Group*; 2019 Sep 1;20(9):1231–1243.
 114. Fisher S, Barry A, Abreu J, Minie B, Nolan J, Delorey TM, Young G, Fennell TJ, Allen A, Ambrogio L, Berlin AM, Blumenstiel B, Cibulskis K, Friedrich D, Johnson R, Juhn F, Reilly B, Shammas R, Stalker J, Sykes SM, Thompson J, Walsh J, Zimmer A, Zwirko Z, Gabriel S, Nicol R, Nusbaum C. A scalable, fully automated process for construction of sequence-ready human exome targeted capture libraries. *Genome Biol [Internet]*. 2011 [cited 2020 Jan 31];12(1):R1. Available from: <http://genomebiology.biomedcentral.com/articles/10.1186/gb-2011-12-1-r1>
 115. Chapman MA, Lawrence MS, Keats JJ, Cibulskis K, Sougnez C, Schinzel AC, Harview CL, Brunet JP, Ahmann GJ, Adli M, Anderson KC, Ardlie KG, Auclair D, Baker A, Bergsagel PL, Bernstein BE, Drier Y, Fonseca R, Gabriel SB, Hofmeister CC, Jagannath S, Jakubowiak AJ, Krishnan A, Levy J, Liefeld T, Lonial S, Mahan S, Mfuko B, Monti S, Perkins LM, Onofrio R, Pugh TJ, Rajkumar SV, Ramos AH, Siegel DS, Sivachenko A, Stewart AK, Trudel S, Vij R, Voet D, Winckler W, Zimmerman T, Carpten J, Trent J, Hahn WC, Garraway LA, Meyerson M, Lander ES, Getz G, Golub TR. Initial genome sequencing and analysis of multiple myeloma. *Nature*. 2011 Mar 24;471(7339):467–472. PMID: 21430775
 116. Berger MF, Lawrence MS, Demichelis F, Drier Y, Cibulskis K, Sivachenko AY, Sboner A, Esgueva R, Pflueger D, Sougnez C, Onofrio R, Carter SL, Park K, Habegger L, Ambrogio L, Fennell T, Parkin M, Saksena G, Voet D, Ramos AH, Pugh TJ, Wilkinson J, Fisher S, Winckler W, Mahan S, Ardlie K, Baldwin J, Simons JW, Kitabayashi N, MacDonald TY, Kantoff PW, Chin L, Gabriel SB, Gerstein MB, Golub TR, Meyerson M, Tewari A, Lander ES, Getz G, Rubin MA, Garraway LA. The genomic complexity of primary human prostate cancer. *Nature*. 2011 Feb 10;470(7333):214–220.
 117. Cibulskis K, McKenna A, Fennell T, Banks E, DePristo M, Getz G. ContEst: estimating cross-contamination of human samples in next-generation sequencing data. *Bioinformatics [Internet]*. 2011 Sep 15 [cited 2020 Jan 31];27(18):2601–2602. Available from: <https://academic.oup.com/bioinformatics/article-lookup/doi/10.1093/bioinformatics/btr446>
 118. Robinson JT, Thorvaldsdóttir H, Winckler W, Guttman M, Lander ES, Getz G, Mesirov JP. Integrative genomics viewer. *Nature Biotechnology*. 2011. p. 24–26. PMID: 21221095
 119. McKenna A, Hanna M, Banks E, Sivachenko A, Cibulskis K, Kernytsky A, Garimella K,

- Altshuler D, Gabriel S, Daly M, DePristo MA. The Genome Analysis Toolkit: A MapReduce framework for analyzing next-generation DNA sequencing data. *Genome Res.* 2010 Sep;20(9):1297–1303.
120. Carter SL, Cibulskis K, Helman E, McKenna A, Shen H, Zack T, Laird PW, Onofrio RC, Winckler W, Weir BA, Beroukheim R, Pellman D, Levine DA, Lander ES, Meyerson M, Getz G. Absolute quantification of somatic DNA alterations in human cancer. *Nat Biotechnol.* Nature Publishing Group; 2012;30(5):413–421.
 121. Dobin A, Davis CA, Schlesinger F, Drenkow J, Zaleski C, Jha S, Batut P, Chaisson M, Gingeras TR. STAR: Ultrafast universal RNA-seq aligner. *Bioinformatics.* 2013 Jan;29(1):15–21. PMID: 23104886
 122. Li B, Dewey CN. RSEM: accurate transcript quantification from RNA-Seq data with or without a reference genome. *BMC Bioinformatics* [Internet]. 2011 Dec 4 [cited 2020 Jan 31];12(1):323. Available from: <https://bmcbioinformatics.biomedcentral.com/articles/10.1186/1471-2105-12-323>
 123. Deluca DS, Levin JZ, Sivachenko A, Fennell T, Nazaire MD, Williams C, Reich M, Winckler W, Getz G. RNA-SeQC: RNA-seq metrics for quality control and process optimization. *Bioinformatics.* 2012;28(11):1530–1532.
 124. Sarkizova S, Klaeger S, Le PM, Li LW, Oliveira G, Keshishian H, Hartigan CR, Zhang W, Braun DA, Ligon KL, Bachireddy P, Zervantonakis IK, Rosenbluth JM, Ouspenskaia T, Law T, Justesen S, Stevens J, Lane WJ, Eisenhaure T, Lan Zhang G, Clauser KR, Hacohen N, Carr SA, Wu CJ, Keskin DB. A large peptidome dataset improves HLA class I epitope prediction across most of the human population. *Nat Biotechnol* [Internet]. 2019 Dec 16 [cited 2020 Jan 14]; Available from: <http://www.ncbi.nlm.nih.gov/pubmed/31844290> PMID: 31844290
 125. Sarkizova S, Klaeger S, Le PM, Li LW, Oliveira G, Keshishian H, Hartigan CR, Zhang W, Braun DA, Ligon KL, Bachireddy P, Zervantonakis IK, Rosenbluth JM, Ouspenskaia T, Law T, Justesen S, Stevens J, Lane WJ, Eisenhaure T, Lan Zhang G, Clauser KR, Hacohen N, Carr SA, Wu CJ, Keskin DB. A large peptidome dataset improves HLA class I epitope prediction across most of the human population. *Nat Biotechnol.* Nature Research; 2019; PMID: 31844290
 126. Roemer MGM, Advani RH, Redd RA, Pinkus GS, Natkunam Y, Ligon AH, Connelly CF, Pak CJ, Carey CD, Daadi SE, Chapuy B, De Jong D, Hoppe RT, Neuberg DS, Shipp MA, Rodig SJ. Classical Hodgkin lymphoma with reduced β 2M/MHC class I expression is associated with inferior outcome independent of 9p24.1 status. *Cancer Immunol Res.* American Association for Cancer Research Inc.; 2016 Nov 1;4(11):910–916.
 127. Cai A, Keskin DB, DeLuca DS, Alonso A, Zhang W, Zhang GL, Hammond NN, Nardi V, Stone RM, Neuberg D, Sidney J, Brusci V, Wu CJ. Mutated BCR-ABL generates immunogenic T-cell epitopes in CML patients. *Clin Cancer Res.* 2012 Oct 15;18(20):5761–5772.
 128. Truex NL, Holden RL, Wang B-Y, Chen P-G, Hanna S, Hu Z, Shetty K, Olive O,

- Neuberg D, Hacohen N, Keskin DB, Ott PA, Wu CJ, Pentelute BL. Automated Flow Synthesis of Tumor Neoantigen Peptides for Personalized Immunotherapy. *Sci Rep* [Internet]. 2020 [cited 2020 Jan 31];10(1):723. Available from: <http://www.nature.com/articles/s41598-019-56943-5>
129. Borducchi EN, Liu J, Nkolola JP, Cadena AM, Yu WH, Fischinger S, Broge T, Abbink P, Mercado NB, Chandrashekar A, Jetton D, Peter L, McMahan K, Moseley ET, Bekerman E, Hesselgesser J, Li W, Lewis MG, Alter G, Geleziunas R, Barouch DH. Antibody and TLR7 agonist delay viral rebound in SHIV-infected monkeys. *Nature*. Nature Publishing Group; 2018 Nov 15;563(7731):360–364.
 130. Day CL, Seth NP, Lucas M, Appel H, Gauthier L, Lauer GM, Robbins GK, Szczepiorkowski ZM, Casson DR, Chung RT, Bell S, Harcourt G, Walker BD, Klenerman P, Wucherpfennig KW. Ex vivo analysis of human memory CD4 T cells specific for hepatitis C virus using MHC class II tetramers. *J Clin Invest*. American Society for Clinical Investigation; 2003 Sep 15;112(6):831–842. PMID: 12975468
 131. Jang M-H, Seth NP, Wucherpfennig KW. Ex Vivo Analysis of Thymic CD4 T Cells in Nonobese Diabetic Mice with Tetramers Generated from I-A g7 /Class II-Associated Invariant Chain Peptide Precursors . *J Immunol*. The American Association of Immunologists; 2003 Oct 15;171(8):4175–4186.
 132. Picelli S, Faridani OR, Björklund ÅK, Winberg G, Sagasser S, Sandberg R. Full-length RNA-seq from single cells using Smart-seq2. *Nat Protoc*. 2014 Jan;9(1):171–181. PMID: 24385147
 133. Dodt M, Roehr JT, Ahmed R, Dieterich C. FLEXBAR-flexible barcode and adapter processing for next-generation sequencing platforms. *Biology (Basel)*. MDPI AG; 2012 Dec 14;1(3):895–905.
 134. Stuart T, Butler A, Hoffman P, Hafemeister C, Papalexi E, Mauck WM, Hao Y, Stoeckius M, Smibert P, Satija R. Comprehensive Integration of Single-Cell Data. *Cell*. Cell Press; 2019 Jun 13;177(7):1888-1902.e21. PMID: 31178118
 135. Li S, Sun J, Allesøe R, Datta K, Bao Y, Oliveira G, Forman J, Jin R, Olsen LR, Keskin DB, Shukla SA, Wu CJ, Livak KJ. RNase H–dependent PCR-enabled T-cell receptor sequencing for highly specific and efficient targeted sequencing of T-cell receptor mRNA for single-cell and repertoire analysis. *Nat Protoc*. Nature Publishing Group; 2019 Aug 1;14(8):2571–2594.
 136. Zhang L, Liu R, Luan YY, Yao YM. Tumor necrosis factor- α induced protein 8: Pathophysiology, clinical significance, and regulatory mechanism. *International Journal of Biological Sciences*. Ivyspring International Publisher; 2018. p. 398–405.
 137. Wong WKM, Jiang G, Sørensen AE, Chew YV, Lee-Maynard C, Liuwantara D, Williams L, O’Connell PJ, Dalggaard LT, Ma RC, Hawthorne WJ, Joglekar M V., Hardikar AA. The long noncoding RNA MALAT1 predicts human islet isolation quality. *JCI Insight*. American Society for Clinical Investigation; 2019 Aug 22;4(16).

138. Hamid O, Robert C, Daud A, Hodi FS, Hwu WJ, Kefford R, Wolchok JD, Hersey P, Joseph R, Weber JS, Dronca R, Mitchell TC, Patnaik A, Zarour HM, Joshua AM, Zhao Q, Jensen E, Ahsan S, Ibrahim N, Ribas A. Five-year survival outcomes for patients with advanced melanoma treated with pembrolizumab in KEYNOTE-001. *Ann Oncol*. Oxford University Press; 2019;30(4):582–588.
139. Robert C, Ribas A, Schachter J, Arance A, Grob JJ, Mortier L, Daud A, Carlino MS, McNeil CM, Lotem M, Larkin JMG, Lorigan P, Neyns B, Blank CU, Petrella TM, Hamid O, Su SC, Krepler C, Ibrahim N, Long G V. Pembrolizumab versus ipilimumab in advanced melanoma (KEYNOTE-006): post-hoc 5-year results from an open-label, multicentre, randomised, controlled, phase 3 study. *Lancet Oncol*. Lancet Publishing Group; 2019 Sep 1;20(9):1239–1251.
140. Robert C, Grob JJ, Stroyakovskiy D, Karaszewska B, Hauschild A, Levchenko E, Chiarion Sileni V, Schachter J, Garbe C, Bondarenko I, Gogas H, Mandalá M, Haanen JBAG, Lebbé C, MacKiewicz A, Rutkowski P, Nathan PD, Ribas A, Davies MA, Flaherty KT, Burgess P, Tan M, Gasal E, Voi M, Schadendorf D, Long G V. Five-year outcomes with dabrafenib plus trametinib in metastatic melanoma. *N Engl J Med*. Massachusetts Medical Society; 2019 Aug 15;381(7):626–636.
141. Eggermont AMM, Blank CU, Mandalá M, Long G V., Atkinson V, Dalle S, Haydon A, Lichinitser M, Khattak A, Carlino MS, Sandhu S, Larkin J, Puig S, Ascierto PA, Rutkowski P, Schadendorf D, Koornstra R, Hernandez-Aya L, Maio M, van den Eertwegh AJM, Grob J-J, Gutzmer R, Jamal R, Lorigan P, Ibrahim N, Marreaud S, van Akkooi ACJ, Suciú S, Robert C. Adjuvant Pembrolizumab versus Placebo in Resected Stage III Melanoma. *N Engl J Med* [Internet]. 2018 May 10 [cited 2020 Feb 2];378(19):1789–1801. Available from: <http://www.nejm.org/doi/10.1056/NEJMoa1802357>
142. Weber J, Mandalá M, Del Vecchio M, Gogas HJ, Arance AM, Cowey CL, Dalle S, Schenker M, Chiarion-Sileni V, Marquez-Rodas I, Grob J-J, Butler MO, Middleton MR, Maio M, Atkinson V, Queirolo P, Gonzalez R, Kudchadkar RR, Smylie M, Meyer N, Mortier L, Atkins MB, Long G V., Bhatia S, Lebbé C, Rutkowski P, Yokota K, Yamazaki N, Kim TM, de Pril V, Sabater J, Qureshi A, Larkin J, Ascierto PA. Adjuvant Nivolumab versus Ipilimumab in Resected Stage III or IV Melanoma. *N Engl J Med* [Internet]. 2017 Nov 9 [cited 2020 Feb 2];377(19):1824–1835. Available from: <http://www.nejm.org/doi/10.1056/NEJMoa1709030>
143. Long G V., Hauschild A, Santinami M, Atkinson V, Mandalá M, Chiarion-Sileni V, Larkin J, Nyakas M, Dutriaux C, Haydon A, Robert C, Mortier L, Schachter J, Schadendorf D, Lesimple T, Plummer R, Ji R, Zhang P, Mookerjee B, Legos J, Kefford R, Dummer R, Kirkwood JM. Adjuvant Dabrafenib plus Trametinib in Stage III *BRAF* - Mutated Melanoma. *N Engl J Med* [Internet]. 2017 Nov 9 [cited 2020 Feb 2];377(19):1813–1823. Available from: <http://www.nejm.org/doi/10.1056/NEJMoa1708539>
144. Owen RE, Sinclair E, Emu B, Heitman JW, Hirschhorn DF, Epling CL, Tan QX, Custer B, Harris JM, Jacobson MA, McCune JM, Martin JN, Hecht FM, Deeks SG, Norris PJ. Loss of T cell responses following long-term cryopreservation. *J Immunol Methods*. NIH

Public Access; 2007 Sep 30;326(1-2):93-115.

145. Peptide Storage and Handling Guidelines [Internet]. [cited 2020 Feb 9]. Available from: https://www.genscript.com/peptide_storage_and_handling.html
146. Zhang J, Fujimoto J, Zhang J, Wedge DC, Song X, Zhang J, Seth S, Chow CW, Cao Y, Gumbs C, Gold KA, Kalhor N, Little L, Mahadeshwar H, Moran C, Protopopov A, Sun H, Tang J, Wu X, Ye Y, William WN, Lee JJ, Heymach J V., Hong WK, Swisher S, Wistuba II, Futreal PA. Intratumor heterogeneity in localized lung adenocarcinomas delineated by multiregion sequencing. *Science* (80-). American Association for the Advancement of Science; 2014 Oct 10;346(6206):256-259.
147. Zugazagoitia J, Guedes C, Ponce S, Ferrer I, Molina-Pinelo S, Paz-Ares L. Current Challenges in Cancer Treatment. *Clinical Therapeutics*. Excerpta Medica Inc.; 2016. p. 1551-1566.
148. Lee Ventola C. Cancer immunotherapy, part 3: Challenges and future trends. *P T. Medi Media USA Inc*; 2017 Aug 1;42(8):514-521. PMID: 28781505
149. Goldrath AW, Bevan MJ. Selecting and maintaining a diverse T-cell repertoire. *Nature*. 1999. p. 255-262.
150. Waickman AT, Victor K, Li T, Hatch K, Rutvisuttinunt W, Medin C, Gabriel B, Jarman RG, Friberg H, Currier JR. Dissecting the heterogeneity of DENV vaccine-elicited cellular immunity using single-cell RNA sequencing and metabolic profiling. *Nat Commun*. Nature Publishing Group; 2019 Dec 1;10(1).
151. Neu KE, Guthmiller JJ, Huang M, La J, Vieira MC, Kim K, Zheng NY, Cortese M, Tepora ME, Hamel NJ, Rojas KT, Henry C, Shaw D, Dulberger CL, Pulendran B, Cobey S, Khan AA, Wilson PC. Spec-seq unveils transcriptional subpopulations of antibody-secreting cells following influenza vaccination. *J Clin Invest*. American Society for Clinical Investigation; 2019 Jan 2;129(1).
152. Fehlings M, Jhunjhunwala S, Kowanetz M, O’Gorman WE, Hegde PS, Sumatoh H, Lee BH, Nardin A, Becht E, Flynn S, Ballinger M, Newell EW, Yadav M. Late-differentiated effector neoantigen-specific CD8⁺ T cells are enriched in peripheral blood of non-small cell lung carcinoma patients responding to atezolizumab treatment. *J Immunother Cancer* [Internet]. BioMed Central Ltd.; 2019 Dec 12 [cited 2020 Feb 9];7(1):249. Available from: <https://jitc.biomedcentral.com/articles/10.1186/s40425-019-0695-9>
153. Carrington M, Nelson GW, Martin MP, Kissner T, Vlahov D, Goedert JJ, Kaslow R, Buchbinder S, Hoots K, O’Brien SJ. HLA and HIV-1: Heterozygote advantage and B*35-Cw*04 disadvantage. *Science* (80-). 1999 Mar 12;283(5408):1748-1752. PMID: 10073943
154. Rudd BD, Venturi V, Davenport MP, Nikolich-Zugich J. Evolution of the Antigen-Specific CD8 + TCR Repertoire across the Life Span: Evidence for Clonal Homogenization of the Old TCR Repertoire . *J Immunol*. The American Association of Immunologists; 2011 Feb 15;186(4):2056-2064.

155. Meyer-Olson D, Shoukry NH, Brady KW, Kim H, Olson DP, Hartman K, Shintani AK, Walker CM, Kalams SA. Limited T cell receptor diversity of HCV-specific T cell responses is associated with CTL escape. *J Exp Med*. 2004 Aug 2;200(3):307–319.
156. Savage PA, Boniface JJ, Davis MM. A kinetic basis for T cell receptor repertoire selection during an immune response. *Immunity*. Cell Press; 1999;10(4):485–492.
157. Zehn D, Lee SY, Bevan MJ. Complete but curtailed T-cell response to very low-affinity antigen. *Nature*. 2009 Mar 12;458(7235):211–214.
158. Memarnejadian A, Meilleur CE, Shaler CR, Khazaie K, Bennink JR, Schell TD, Mansour Haeryfar SM. PD-1 blockade promotes epitope spreading in anticancer CD8 + T cell responses by preventing fratricidal death of subdominant clones to relieve immunodomination HHS Public Access. *J Immunol*. 2017;199(9):3348–3359.
159. Hodge JW, Sharp HJ, Gameiro SR. Abscopal regression of antigen disparate tumors by antigen cascade after systemic tumor vaccination in combination with local tumor radiation. *Cancer Biother Radiopharm*. Mary Ann Liebert, Inc.; 2012 Feb 1;27(1):12–22.
160. Disis ML, Wallace DR, Gooley TA, Dang Y, Slota M, Lu H, Coveler AL, Childs JS, Higgins DM, Fintak PA, dela Rosa C, Tietje K, Link J, Waisman J, Salazar LG. Concurrent trastuzumab and HER2/neu-specific vaccination in patients with metastatic breast cancer. *J Clin Oncol* [Internet]. American Society of Clinical Oncology; 2009 Oct 1 [cited 2020 Feb 7];27(28):4685–92. Available from: <http://www.ncbi.nlm.nih.gov/pubmed/19720923> PMID: 19720923
161. Chapuis AG, Roberts IM, Thompson JA, Margolin KA, Bhatia S, Lee SM, Sloan HL, Lai IP, Farrar EA, Wagener F, Shibuya KC, Cao J, Wolchok JD, Greenberg PD, Yee C. T-Cell Therapy Using Interleukin-21-Primed Cytotoxic T-Cell Lymphocytes Combined With Cytotoxic T-Cell Lymphocyte Antigen-4 Blockade Results in Long-Term Cell Persistence and Durable Tumor Regression. *J Clin Oncol* [Internet]. American Society of Clinical Oncology; 2016 Nov 1 [cited 2020 Feb 7];34(31):3787–3795. Available from: <http://www.ncbi.nlm.nih.gov/pubmed/27269940> PMID: 27269940
162. Corbière V, Chapiro J, Stroobant V, Ma W, Lurquin C, Lethé B, Van Baren N, Van Den Eynde BJ, Boon T, Coulie PG. Antigen spreading contributes to MAGE vaccination-induced regression of melanoma metastases. *Cancer Res*. American Association for Cancer Research; 2011 Feb 15;71(4):1253–1262.
163. Ott PA, Govindan R, Naing A, Friedlander TW, Margolin K, Lin JJ, Bhardwaj N, Hellmann MD, Awad MM, Wanamaker A, Cleary LD, Rooney MS, Scherer J, Bushway ME, Moles M, Khondker Z, Gaynor RB, Srinivasan L, Chi A, Greshock J, Hu-Lieskovan S. Disease-Related Biomarkers are Associated with Extended Progression-Free Survival After Treatment with NEO-PV-01 in Combination with Anti-PD-1 in Patients with Metastatic Cancers Introduction NEO-PV-01 + Nivolumab Leads to Longer PFS and OS Versus Historical Benchmarks.
164. Kitaura K, Shini T, Matsutani T, Suzuki R. A new high-throughput sequencing method for determining diversity and similarity of T cell receptor (TCR) α and β repertoires and

- identifying potential new invariant TCR α chains. *BMC Immunol.* BioMed Central Ltd.; 2016 Oct 11;17(1).
165. Robins HS, Campregher P V., Srivastava SK, Wacher A, Turtle CJ, Kahsai O, Riddell SR, Warren EH, Carlson CS. Comprehensive assessment of T-cell receptor β -chain diversity in $\alpha\beta$ T cells. *Blood.* 2009 Nov 5;114(19):4099–4107.
 166. Hu Z, Anandappa AJ, Sun J, Kim J, Leet DE, Bozym DJ, Chen C, Williams L, Shukla SA, Zhang W, Tabbaa D, Steelman S, Olive O, Livak KJ, Kishi H, Muraguchi A, Guleria I, Stevens J, Lane WJ, Burkhardt UE, Fritsch EF, Neuberg D, Ott PA, Keskin DB, Hacohen N, Wu CJ. A cloning and expression system to probe T-cell receptor specificity and assess functional avidity to neoantigens. *Blood.* NLM (Medline); 2018 Nov 1;132(18):1911–1921.
 167. Lundegaard C, Lamberth K, Harndahl M, Buus S, Lund O, Nielsen M. NetMHC-3.0: accurate web accessible predictions of human, mouse and monkey MHC class I affinities for peptides of length 8-11. *Nucleic Acids Res [Internet].* 2008 [cited 2020 Jan 28];36:509–512. Available from: <http://www.cbs.dtu.dk/>

Figures

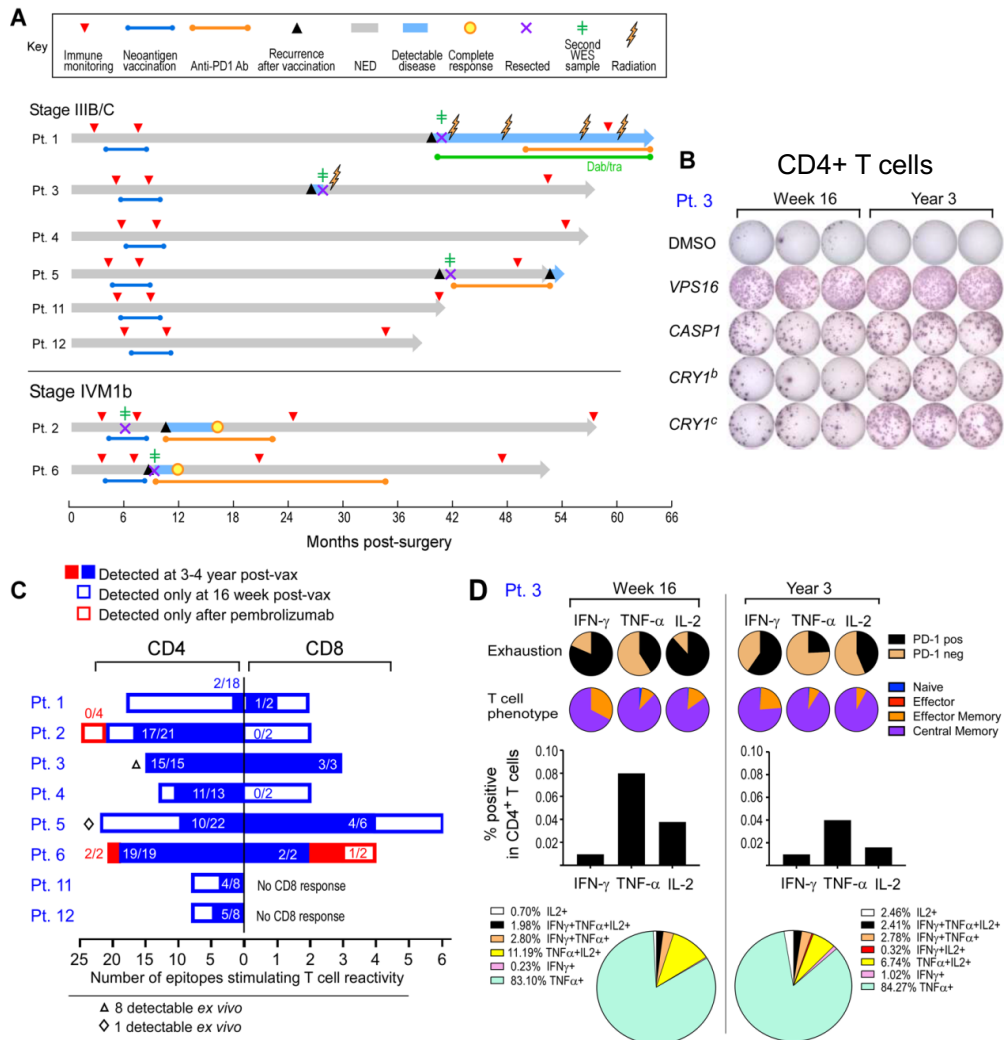


Figure 1. Vaccine-induced neoantigen specific T cells persist over several years. **A.** Clinical course of 8 patients (Pts) who received personalized neoantigen vaccines starting at the time of melanoma resection until data cutoff (24-59 months from study initiation). **B.** Representative IFN- γ ELISPOT response of Pt. 3 neoantigen-specific CD4⁺ T cell lines specific for 4 ASP peptides at 16 weeks and 3 years post-vaccination, respectively. **C.** Frequencies of neoantigen-specific T cell responses at 2 to 4 years post-vaccination as a percentage of neoantigen-specific T cells observed at 16 weeks post-vaccination (previously reported¹) and after anti-PD-1 therapy (Pts. 2 and 6). Proportion of neoepitopes stimulating T cell reactivity that have persisted to 2-4 years (shaded blue and red) out of the responses detected at 16 weeks (blue outline), and after anti-PD-1 therapy in Pts. 2 and 6 (red outline). **D.** Percentages of Pt. 3 CD4⁺ T cells secreting cytokines in response to pools of ASP peptides that had previously generated *ex vivo* CD4⁺ responses as measured by intracellular cytokine staining after *ex vivo* stimulation with ASP pools, 16 weeks and 3-4 years after vaccination. Negative controls (unstimulated CD4⁺ T cells) have been subtracted. Pie charts depict T cell phenotypes, PD-1 expression, and cytokine polyfunctionality among the cytokine-producing CD4⁺ T cells.

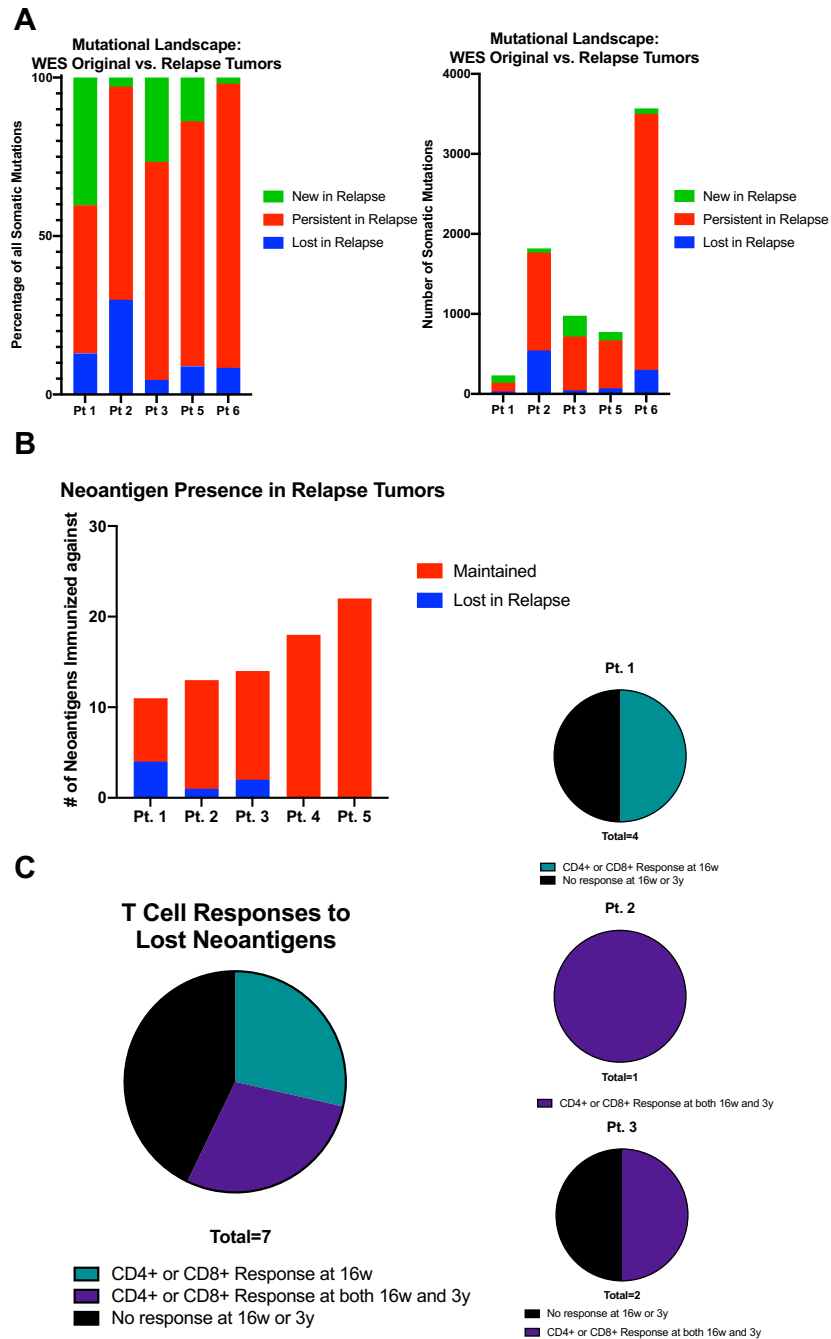


Figure 2. Mutational landscape of relapsed tumors compared to originally resected tumors. **A.** Quantification of somatic mutations in the relapsed tumors of Pts. 1, 2, 3, 5 and 6 in comparison to their original tumors. **B.** Presence of vaccine-targeted neoantigens in relapsed tumors. **C.** CD4⁺ and CD8⁺ T cell reactivity of lost neoantigens 16 weeks (blue) and 3-4 years after vaccination (pie charts, teal: T cell responses detected at 16 weeks; purple: T cell responses detected at both 16 weeks and 3-4 years; red: no T cell response detected at either timepoint). See **Supplementary Table 3** for somatic mutations identified in relapsed tumors. Original tumor somatic mutations were reported previously.¹

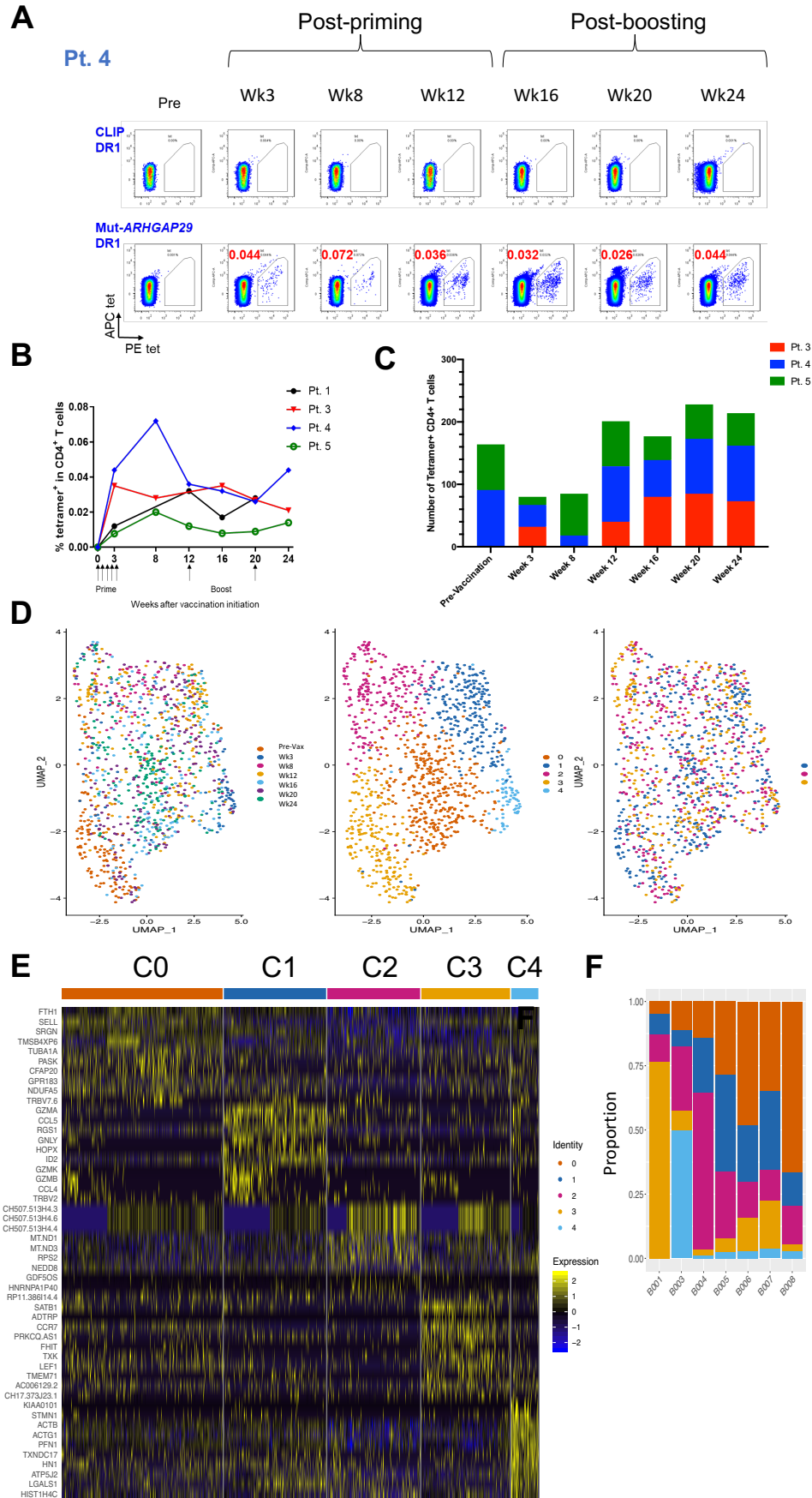
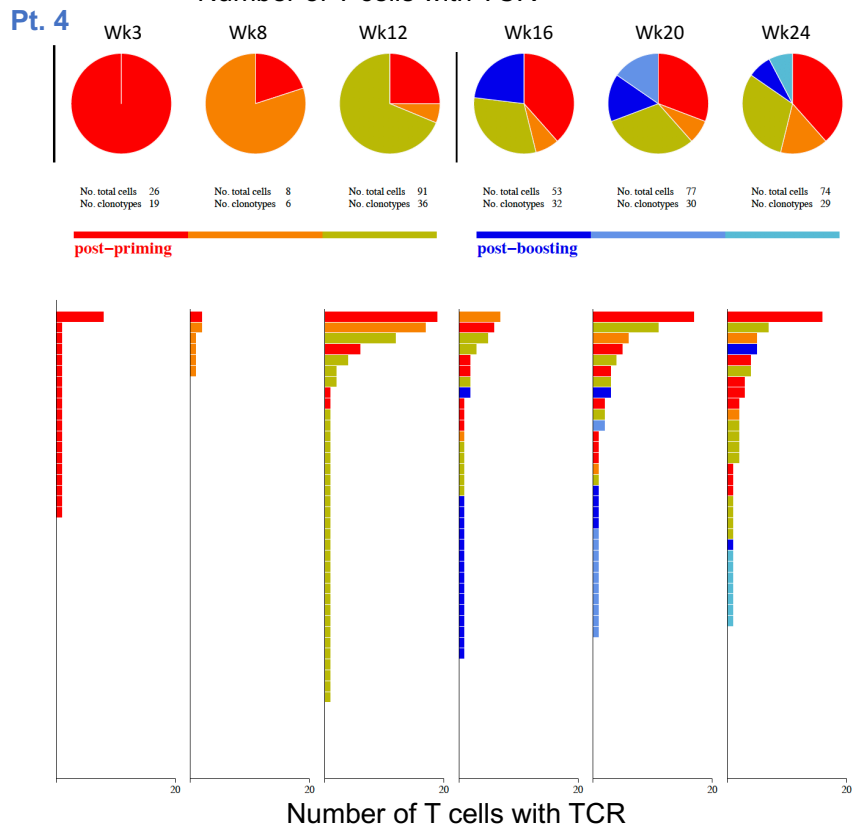
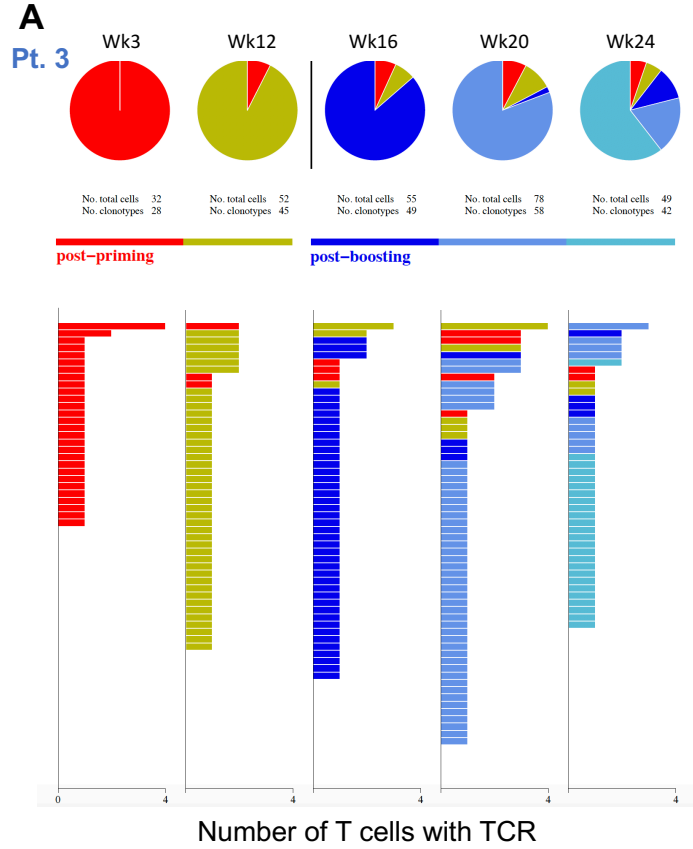
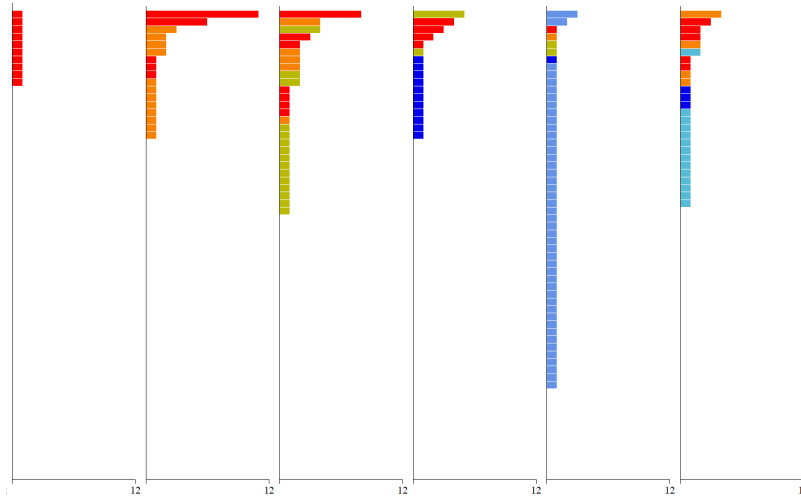
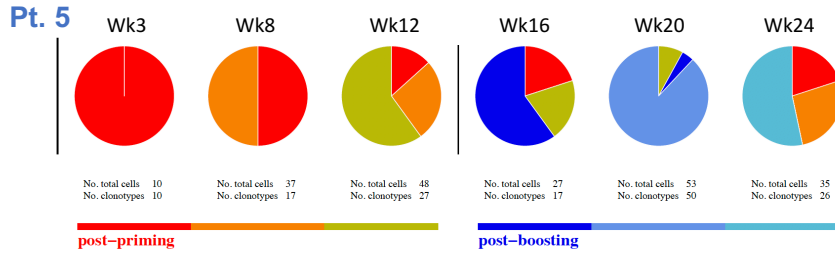


Figure 3. Transcriptional profile of neoantigen-specific T cells in relation to vaccination.

A. Representative plots of *ex vivo* MHC class II tetramer staining of Pt. 4 (mut-*ARHGAP29*) CD4⁺ T cells at a series of timepoints (pre-vaccination, weeks 3-24) following vaccination. Flow plots were pre-gated on CD4⁺ T cells. **B.** Kinetics of *ex vivo* tetramer-specific CD4⁺ T cell frequencies (mut-*RUSC2*, -*ADAMT27*, -*ARHGAP29* and -*ZNF281* tetramers for Pts. 1, 3, 4 and 5, respectively) following vaccination. **C.** Quantification of tetramer-specific or non-tetramer specific (Pre-Vaccination) CD4⁺ T cells isolated at each timepoint. **D.** Clustering of tetramer-specific CD4⁺ T cells for Pts. 3, 4 and 5, depicted by timepoint, cluster, and patient, respectively. **E.** Heatmap of top 10 differentially expressed genes per cluster. **F.** Timepoint membership by cluster. See **Supplementary Table 9** for differentially expressed genes.





B

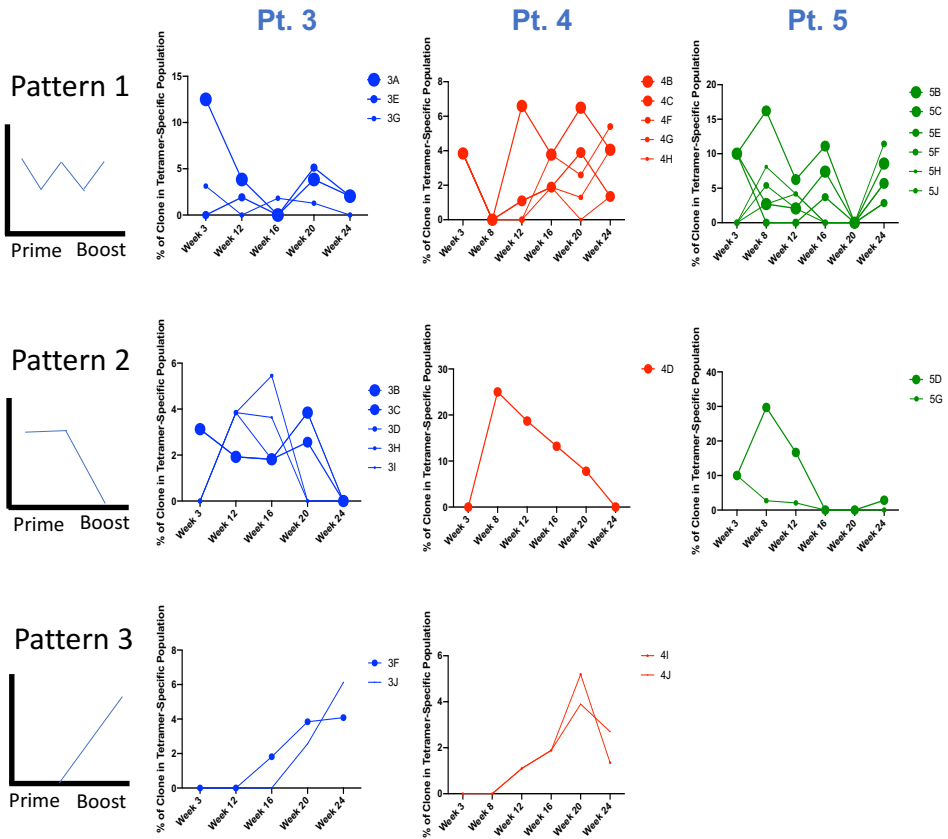


Figure 4. Kinetics of TCR repertoire of neoantigen-specific T cells in relation to vaccination. **A.** Paired TCR α and β sequences of mut-*ADAMT27* CD4⁺ T cells, mut-*ARHGAP29*-specific CD4⁺ T cells, and mut-*ZNF281*-specific CD4⁺ T cells for Pts. 3, 4 and 5, respectively, from pre-vaccination and different time points post-vaccination. Colors indicate the first appearance of the TCR clone for that time point. Pie charts indicate the proportions of TCR clones originating from each time point. **B.** Patterns of clonal expansion and contraction among the dominant CD4⁺ T cell TCR clonotypes for each patient. The size of the bubble indicates the relative dominance of the clonotype. See **Supplementary Table 11** for TCR clonotypes and **Methods** for TCR dominance criteria.

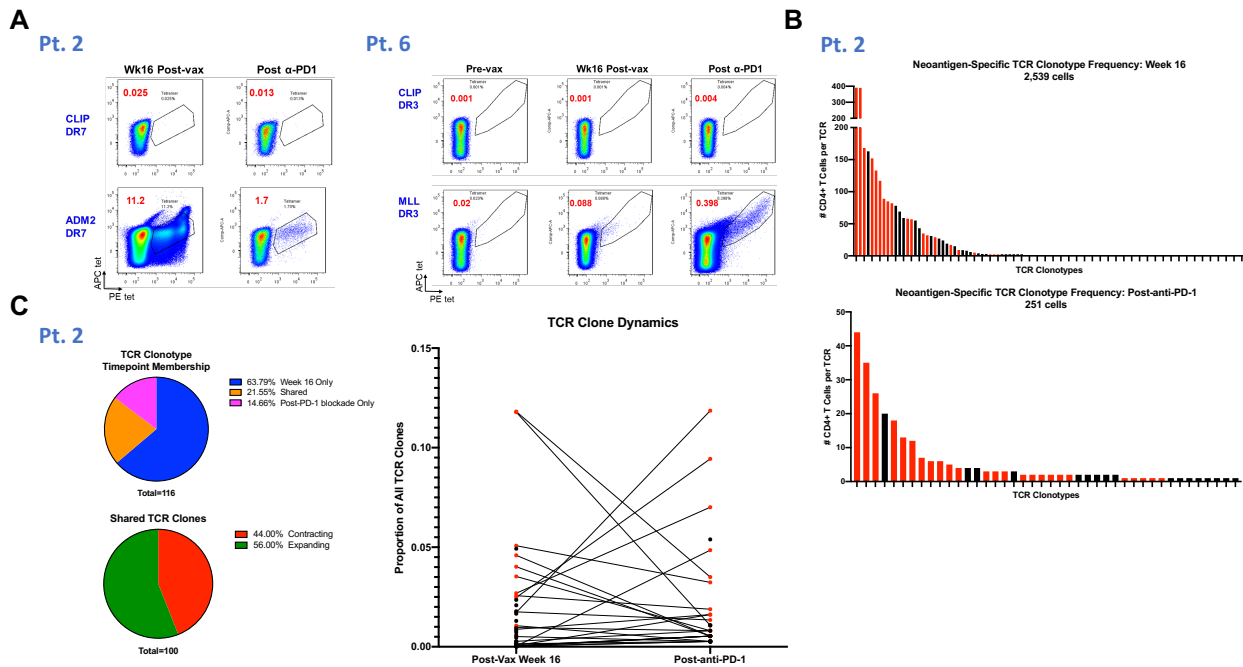


Figure 5. Neoantigen-specific T cells dynamics following vaccination and checkpoint blockade. **A.** Plots of MHC class II tetramer staining of Pt. 2 (mut-*ADM2*) and Pt. 6 (mut-*MLL*) CD4⁺ T cells from peripheral blood following *in vitro* stimulation isolated at 16 weeks after vaccination and following anti-PD-1 therapy (pembrolizumab). Flow plots were pre-gated on CD4⁺ T cells. **B.** Single-cell TCR sequencing analysis of Pt. 2 neoantigen-specific CD4⁺ T cells shows enrichment of particular clonotypes. Red bars indicate clonotypes that appeared at both week 16 and following pembrolizumab. **C.** Kinetics of Pt. 2 neoantigen-specific CD4⁺ TCR clonotypes between week 16 and post-pembrolizumab. Pie charts depict i) proportions of neoantigen-specific TCRs present at only one timepoint and preserved in both timepoints, and ii) proportions of the preserved TCR clones that contracted or expanded after pembrolizumab. See **Supplementary Table 12** for TCR clonotypes.

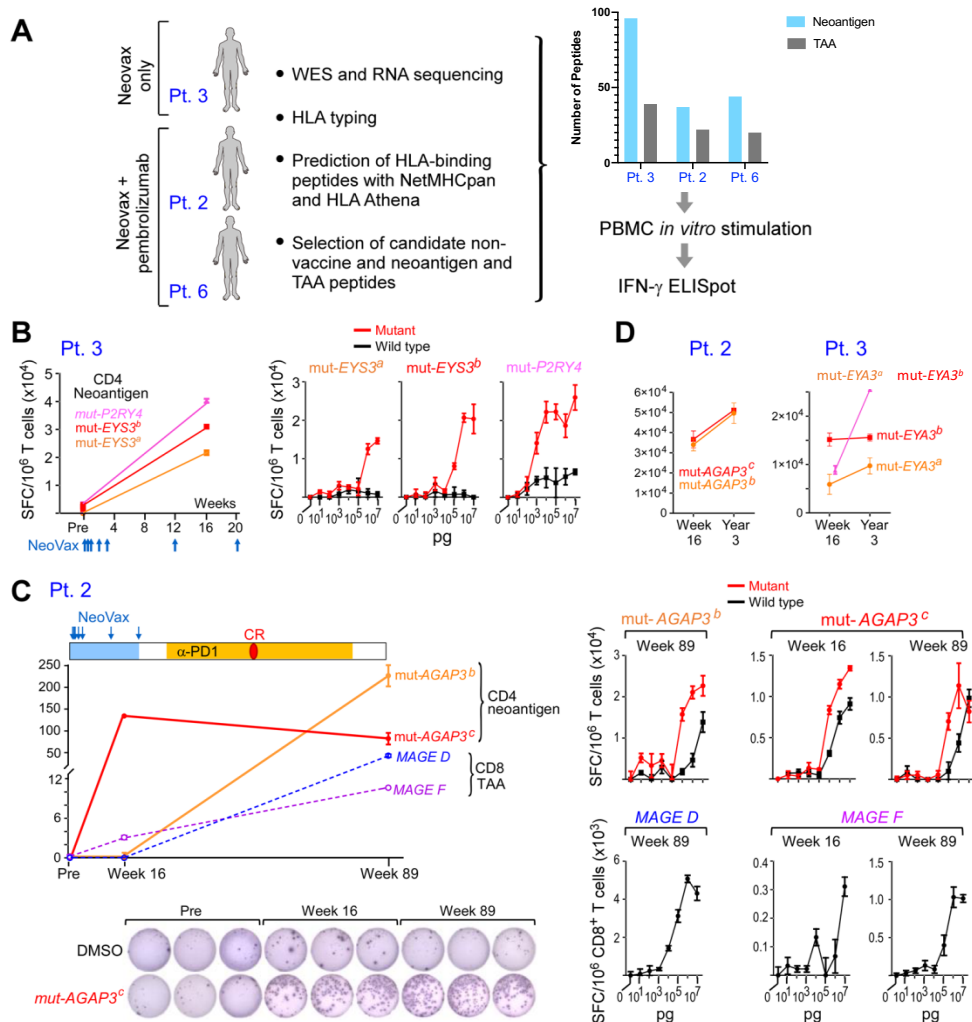
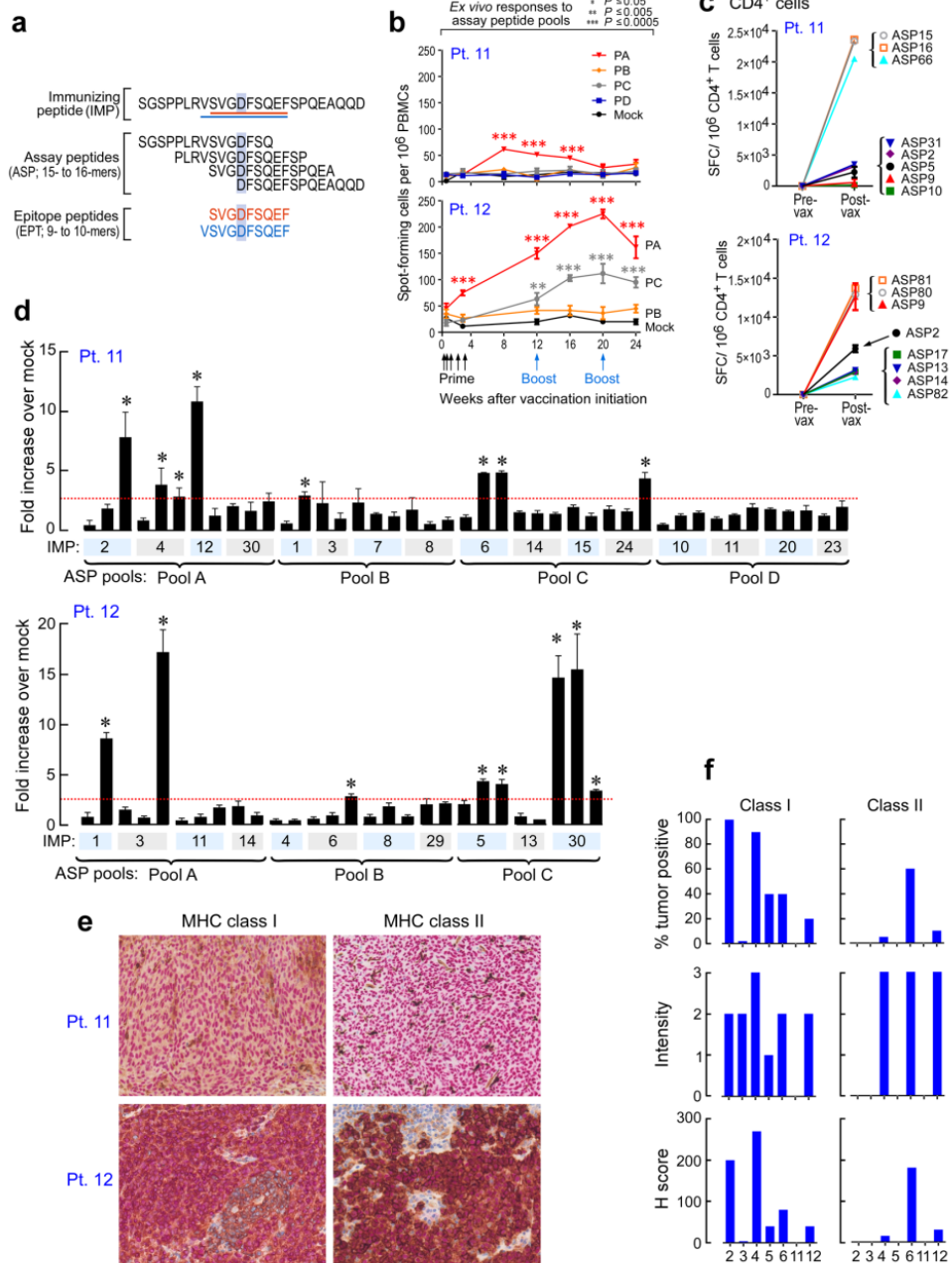


Figure 6. Vaccine-induced T cell responses spread to non-vaccine neoantigen and TAA epitopes. **A.** Somatic mutations and tumor-associated antigens were identified by WES of melanoma and germline DNA and their expression was confirmed by tumor RNA-seq. Non-vaccine neoantigen and TAA epitope spreading peptides were selected on the basis of HLA binding predictions (**Methods**). PBMC were then stimulated *in vitro* with epitope spreading peptides and reactivity was confirmed through IFN- γ ELISPOTs. **B.** Pt. 3 IFN- γ secretion of CD4⁺ T cell lines stimulated with 3 non-vaccine neoantigen ASP measured by ELISPOT in triplicates at pre-vaccination and week 16. Inset: IFN- γ secretion of neoantigen-specific CD4⁺ T cell lines tested across a range of concentrations of mutated and wildtype peptides. **C.** Pt. 2 IFN- γ secretion of T cell lines stimulated with 2 non-vaccine neoantigen ASP and 2 TAA EPT as measured by ELISPOT in triplicates at week 16 and week 89 (after anti-PD-1 therapy). Inset: Representative IFN- γ ELISPOT response of mut-AGAP3^c-specific CD4⁺ T cells; IFN- γ secretion of neoantigen-specific CD4⁺ T cell lines tested across a range of concentrations of mutated and wildtype peptides; TAA-specific CD8⁺ T cell lines against TAA peptides (lower panels), respectively. **D.** IFN- γ ELISPOT responses of CD4⁺ T cell lines specific for non-vaccine neoantigens persist up to 3 years post-vaccination in Pts. 2 and 3. ELISPOT experiments were performed in duplicate or triplicate wells/condition (error bars, s.e.m).

Extended Data Figures



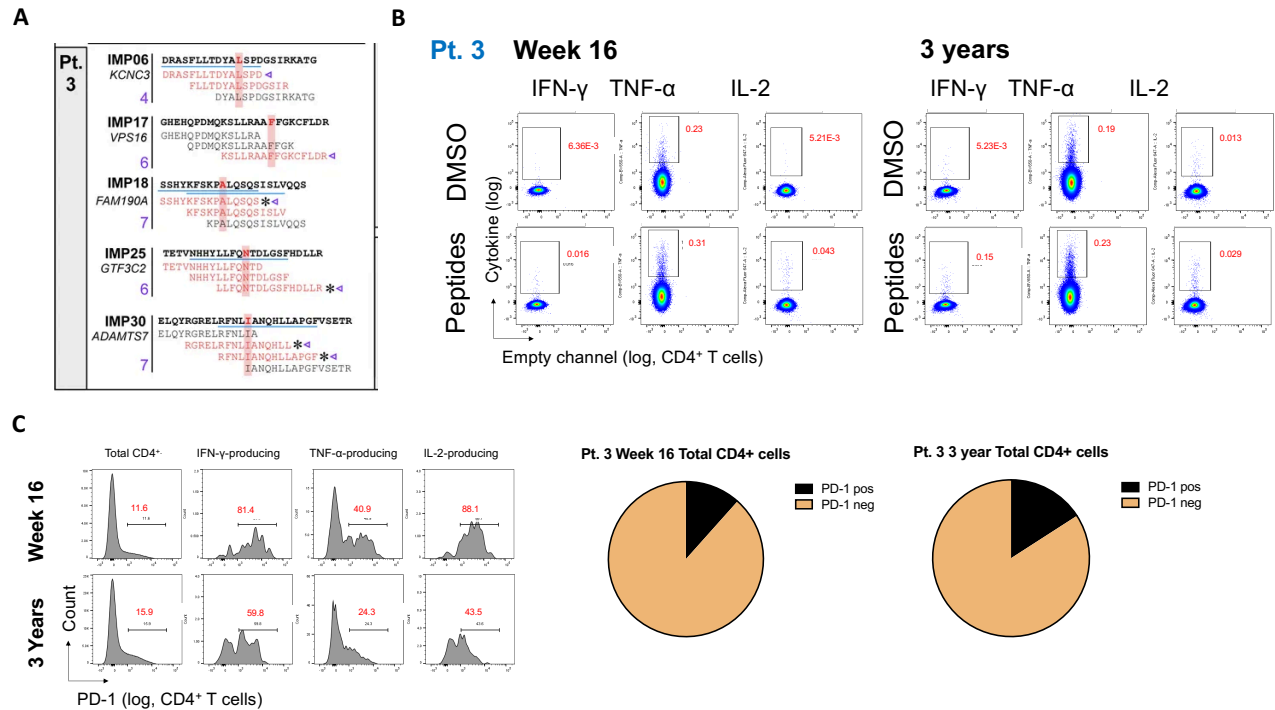
Extended Data Figure 1. Vaccination induces strong multi-functional CD4⁺ T-cell responses in two additional patients with high-risk melanoma. **A.** Schema of immunizing (IMP), assay (ASP), and epitope (EPT) peptides. Mutated amino acid is shaded. **B.** Ex vivo IFN- γ ELISPOT results for Pts. 11 and 12 after PBMCs were tested against peptide pools PA-PD in triplicate wells at each time point (error bars, s.e.m.; see Methods for statistical analysis). **C.** IFN- γ ELISPOT results after one round of *in vitro* stimulation of PBMCs from pre- and post- vaccination with the peptide pools. Only the positive peptides are shown here. **D.** Deconvolution of T-cell reactivity against individual ASP by *ex vivo* IFN- γ ELISPOT using the week 16 post-vaccination PBMCs, tested in duplicate or triplicate wells per peptide (error bars, s.e.m.). *Responses were scored

positive if >55 spot-forming cells (SFC) were detected and were at least 1.5 s.d. over the DMSO control. **E.** Dual chromogenic immunohistochemical staining of Pts. 11 and 12 excised FFPE tumors (see **Methods** for details) for HLA class I and HLA class II. Red: melanoma transcription factor SOX10; brown: HLA class I or class II. **F.** Summary of immunohistochemical results of seven patients with available FFPE tissue. Semi-quantitative scoring was performed for the intensity of positive staining of melanoma cell membranes for class I or II (0, negative; 1, weak; 2, moderate; 3, strong) and for the percentage of positive staining malignant cells (0–100%). A cumulative *H* score was obtained by multiplying intensity score by the percentage of malignant cells with positive staining.

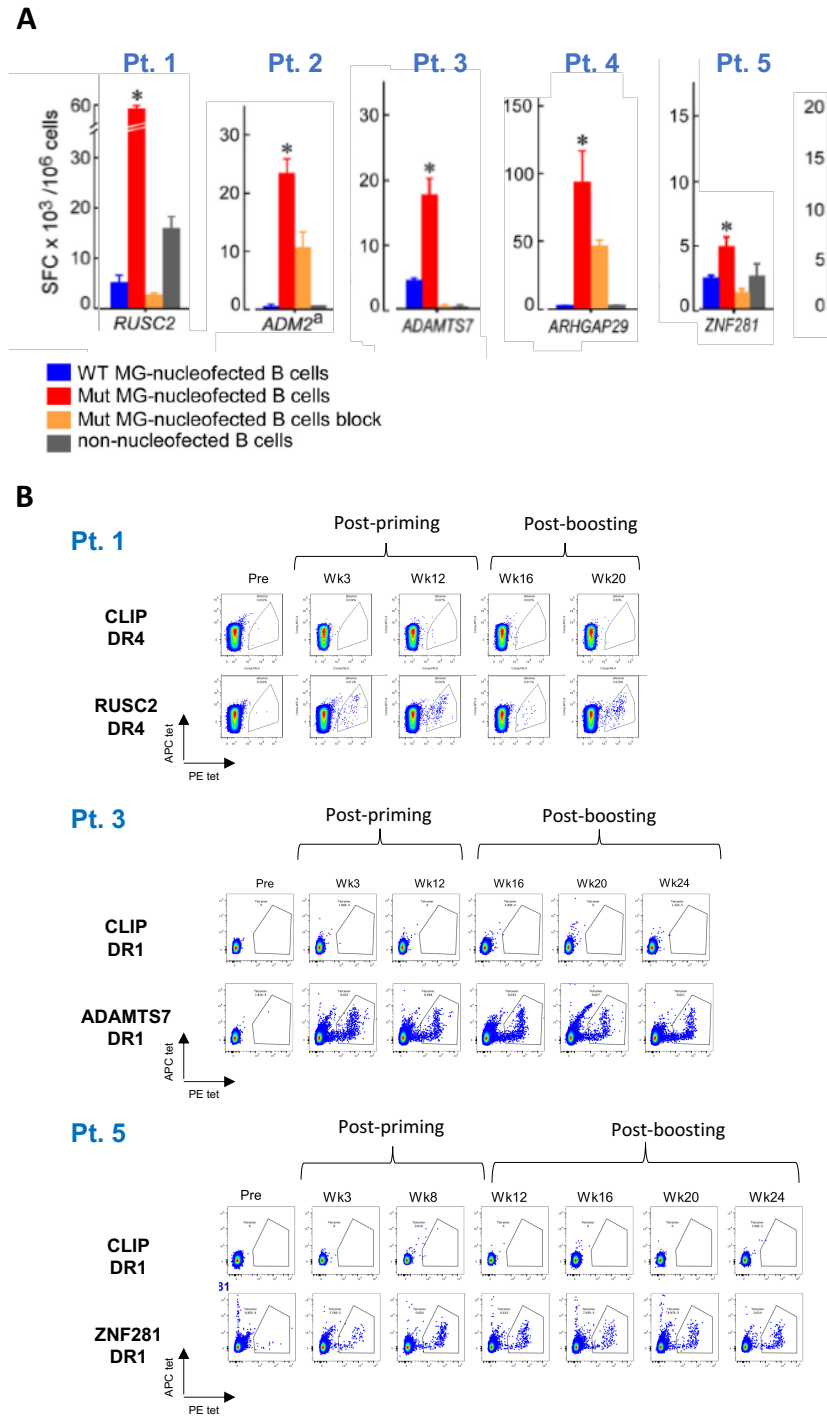
CD4⁺ T cell responses after *in vitro* stimulation

Pt. 11	Pt. 12	Key:
IMP01 <i>DDX19B</i> EVLQRDPNSPLYSVKSLKSFG EVLQRDPNSPLYSVKLS <u>DPNSPLYSVKSLKSFG</u>	IMP01 <i>CRELD2</i> TPGPALRGLPGFVAAFVNIHL TPGPALRGLPGFVAAF <u>LRGLPGFVAAFVNIHL</u>	Key: Blue font: positive epitopes after <i>in vitro</i> stimulation Blue underline: class I predicted epitopes with IC ₅₀ <300nM. Red highlight: Mutated amino acid. If no highlight, the neoantigen is a neoORF.
IMP02 <i>MGAT1</i> VEDDLEVAPDFFQYFRATYPLLKAD VEDDLEVAPDFFQYF LEVAPDFFQYFRATYP <u>DFQYFRATYPLLKAD</u>	IMP03 <i>SETBP1</i> KLSKMIENESPLVGLETGGNAEKV KLSKMIENESPLVGL MIENESPLVGLETGG <u>ESPLVGLETGGNAEKV</u>	
IMP04 <i>ABCC1</i> LKVDENQKAYYSIVANRWLAVRLE LKVDENQKAYYSIV ENQKAYYSIVANRWL <u>YSSIVANRWLAVRLE</u>	IMP05 <i>BAZZB</i> RTTDAHTRTEATFFPPLGIPPLFA RTTDAHTRTEATFFP AHTRTEATFFPPLGLI <u>EATFFPPLGIPPLFA</u>	
IMP06 <i>DMXL2</i> VYLAHPRAVTGFLWRKTSKYMPRGS VYLAHPRAVTGFLWR HPRAVTGFLWRKTSKY <u>TGFLWRKTSKYMPRGS</u>	IMP06 <i>GALC</i> EAKKRNPNTLIGLPWSFLGWLGK EAKKRNPNTLIGLP RNPNTLIGLPWSFL <u>ITLIGLPWSFLGWLGK</u>	
IMP12 <i>KIAA1958</i> TKIPAVKLNKLLNFYVTV TKIPAVKLNKLLNF AVKLNKLLNFYVTV	IMP30 <i>B3GNT1</i> NQWGGTALVVPVFEIRRARRMPMN NQWGGTALVVPVFEI GTALVVPVFEIRRAR <u>VVPVFEIRRARRMPMN</u>	
IMP24 <i>SLIT3</i> LSNNKIKEVREGVFDGAASVQELML LSNNKIKEVREGVFD KIKEVREGVFDGAASV <u>REGVFDGAASVQELML</u>		

Extended Data Figure 2. Mapping of CD4⁺ and CD8⁺ T-cell responses to individual ASP and EPT to the IMP for Pts. 11 and 12. ASP covering the IMP are shown for the IMP that induced T-cell responses in Pts. 11 and 12. T cells from week 16 PBMCs were tested. Red bold and shading: mutated amino acids, absent in IMP arising from neoORFs. Blue underline: for class I epitopes, predicted epitopes (IC₅₀ < 300 nM) based on NetMHCpan (Supplementary Table 6). Blue font: peptides that generated a T-cell response after one round of pre-stimulation with peptides.



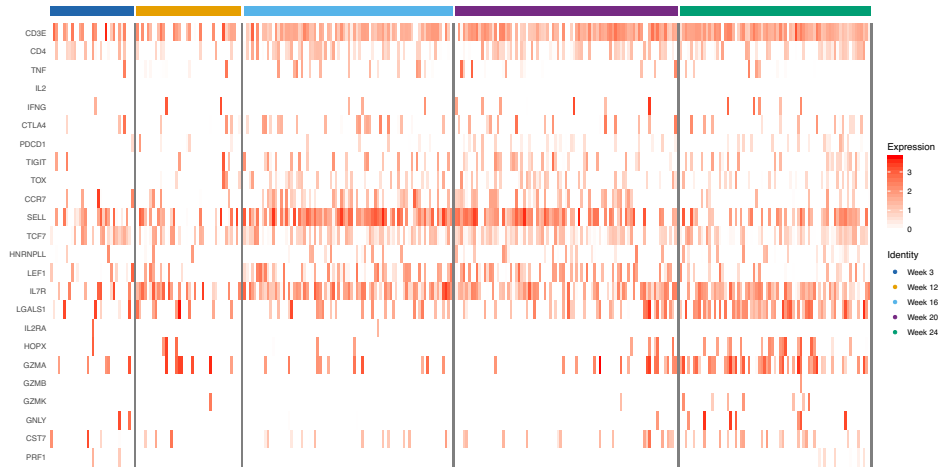
Extended Data Figure 3. Polyfunctional neoantigen-specific CD4⁺ T-cell responses are induced by vaccination in Pts. 11 and 12. **A.** ASP covering the IMP are shown for the IMP that induced *ex vivo* T-cell responses in Pt. 3 at week 16. T cells from week 16 PBMCs were tested. Red bold and shading: mutated amino acids. Blue underline: for class II epitopes, predicted epitopes <10th percentile based on the Immune Epitope Database and Analysis Resource (IEDB)-recommended consensus approach combining NN-align, SMM-align, and CombLib if allele predictions are available, otherwise NetMHCIIpan^{1,167}. Red font, peptides that generated an *ex vivo* CD4⁺ T-cell response; Triangle, ASP-specific T cells that also recognized a corresponding mutated minigene; *T-cell responses against minigenes that were blocked by pan anti-HLA-DR blocking antibodies. This data was previously reported¹. **B.** Frequencies of Pt. 3 CD4⁺ T cells secreting cytokines in response to the peptides in A as measured by ICS after stimulation of PBMCs *ex vivo* with peptides in A. T cells were detected by flow cytometry at week 16 after vaccination and at 3 years for Pt. 3. Red values, frequencies of ASP-pool-reactive cytokine-producing cells as a proportion of all CD4⁺ T cells. **C.** Frequency of PD-1 expression among Pt. 3 total CD4⁺ T cells and cytokine-producing cells. Red values, frequencies of PD-1+ cytokine-producing cells. All fluorescence-activated cell sorting (FACS) plots were pre-gated on CD4⁺ T cells.



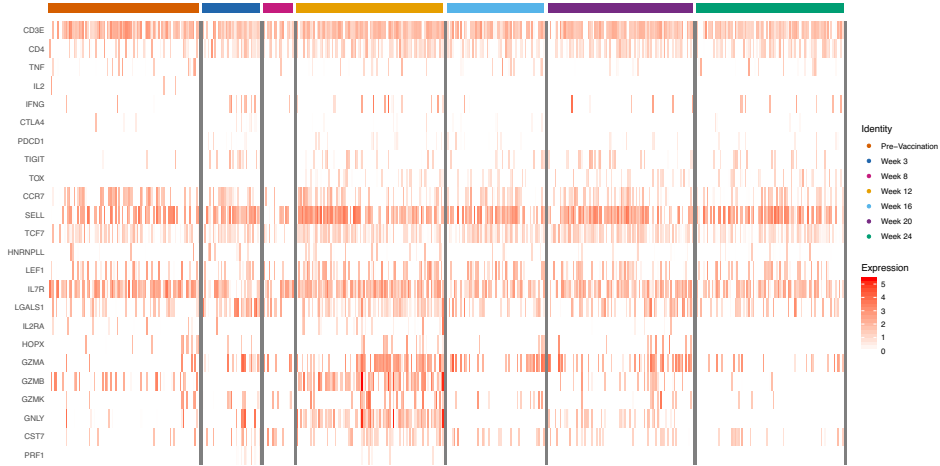
Extended Data Figure 4. Neoantigen-specific CD4⁺ T cells are isolated at serial timepoints after vaccination using tetramer staining. **A.** IFN- γ secretion by neoantigen-specific T-cell lines against B cells nucleofected with minigenes (MG) encoding wildtype or mutant neoantigens chosen for tetramers, with and without anti-HLA DR antibodies (block), data are mean \pm s.d. (figure from our previous publication¹). **B.** *Ex vivo* HLA class II tetramer staining of Pts. 1, 3, and 5 CD4⁺ T cells at a series of timepoints (pre-vaccination, weeks 3-24) following vaccination. Flow plots were pre-gated on CD4⁺ T cells.

A

Pt 3

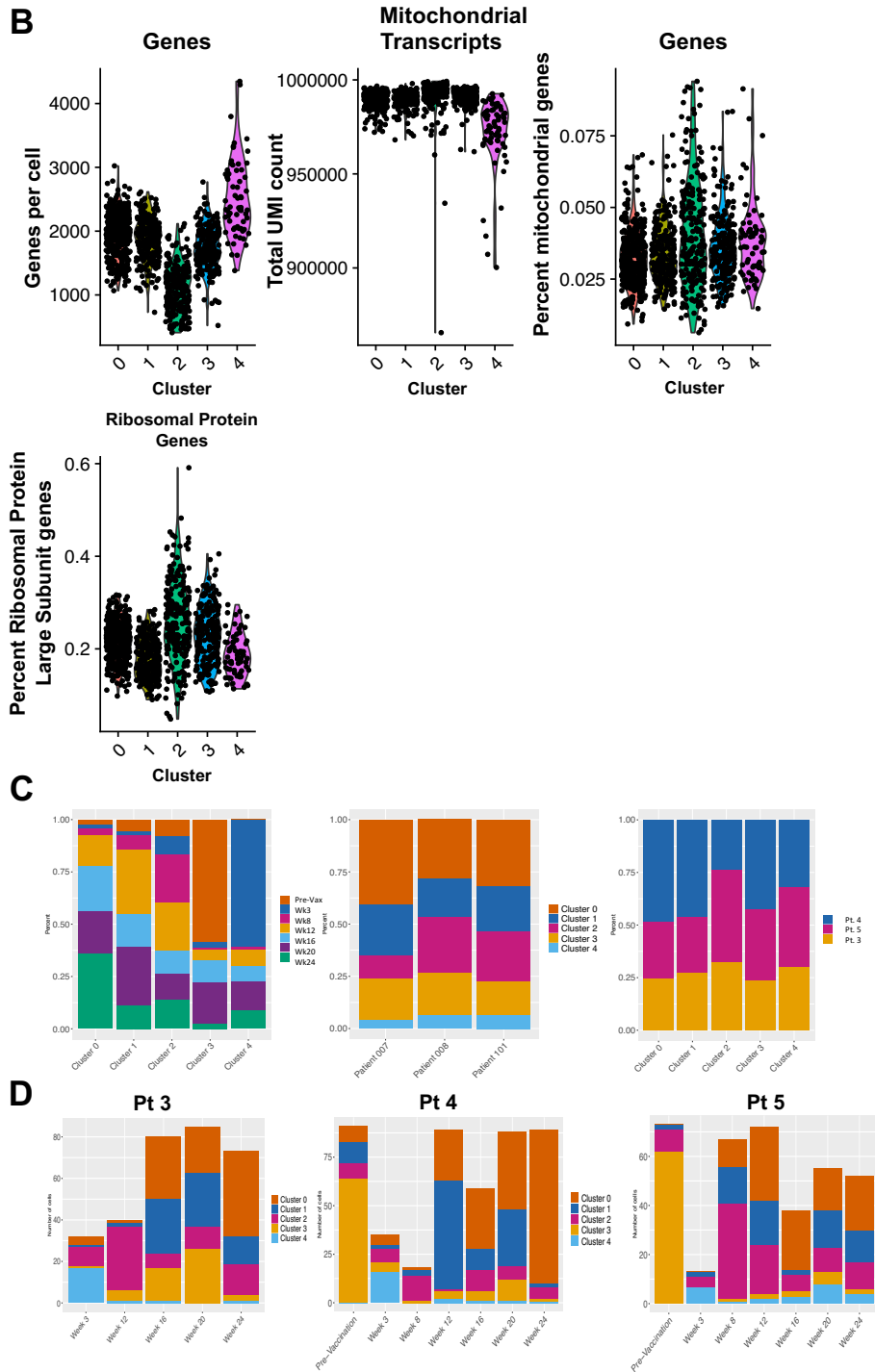


Pt 4

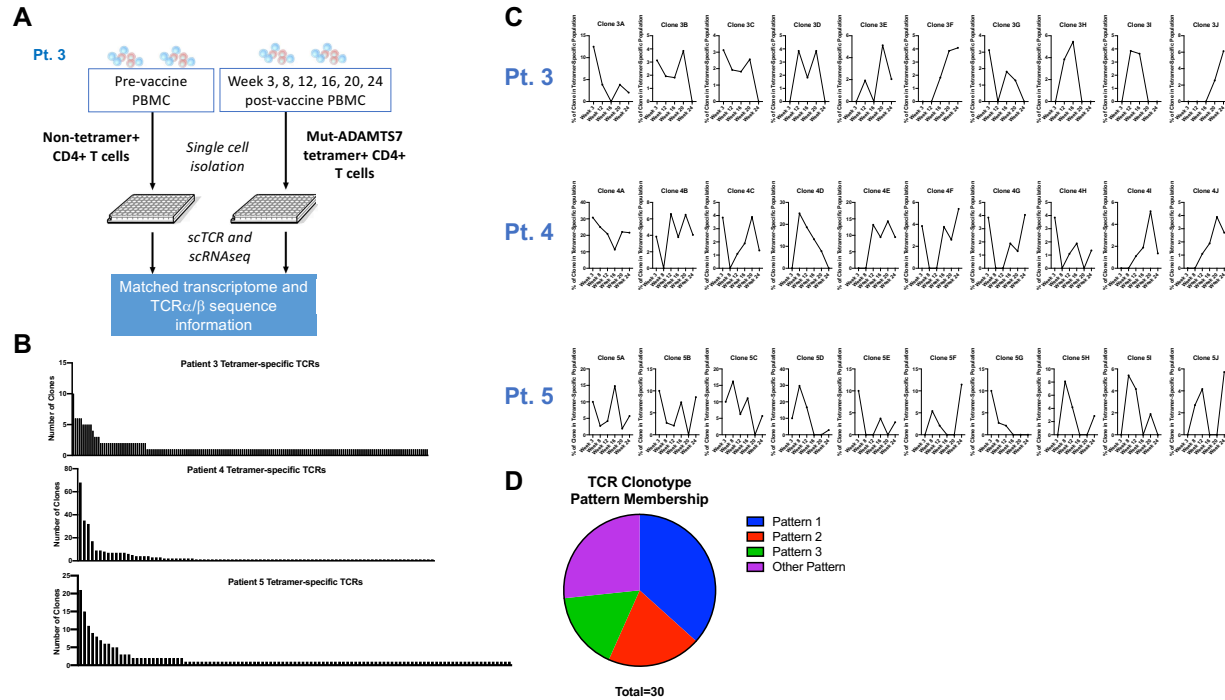


Pt 5





Extended Data Figure 5. Neoantigen-specific CD4⁺ T cells exhibit transcriptional changes through vaccination. **A.** Single-cell transcriptome analysis of CD4⁺ neoantigen-specific (weeks 3-24) and non-neoantigen specific T cells (Pre-Vaccination) from Pts. 3 ($n = 383$), 4 ($n = 469$), and 5 ($n = 370$) showing selected immunologic genes. **B.** Quality control metrics for all clusters. **C.** i) Timepoint membership by cluster, ii) cluster membership by patient, and iii) patient membership by cluster. **D.** Numbers of neoantigen-specific CD4⁺ T cells in each cluster by timepoint for Pts. 3-5.



Extended Data Figure 6. Neoantigen-specific CD4⁺ T cells harbor diverse TCR clonotypes.

A. Schema of representative single-cell TCR and single-cell RNA sequencing analysis of non-specific (non-tetramer-positive) CD4⁺ T cells and neoantigen-reactive CD4⁺ T cells isolated from pre-vaccination PBMCs and post-vaccination PBMCs, respectively, of Pt. 3. **B.** All TCR clonotypes observed in neoantigen-reactive T cell lines generated from PBMCs of Pts. 3, 4, and 5 based on single-cell-targeted TCRαβ sequencing. **C.** Top 10 dominant neoantigen-specific TCR clonotypes for each patient, selected as described in **Fig. 4** and **Methods**. **D.** Overall Pattern membership (see **Fig. 4**) of 30 dominant clones across Pts. 3, 4, and 5.

CD4+ T cell responses after *in vitro* stimulation

Pt. 2	AGAP3	SAVSAASIPAMHINQATNGGGS SAVSAASIPAMHINQ <u>AASIPAMHINQATNG</u> <u>IPAMHINQATNGGGS</u>	Pt. 3	EYA3	ISTSS T IANL L AAAVASIS N QDYPT Y T <u>ISTSSTIANLLAAAV</u> IANLAAAVASIS N Q
				P2RY4	TSISVHRYLGICH S L R ALRWGR P RL TSISVHRYLGICH S L <u>HRYLGICHSLRALRW</u> ICH S L R ALRWGR P RL

CD8+ T cell responses after *in vitro* stimulation

Pt. 2	MAGEF1	<u>TVAELVQFL</u>
	MAGED2	<u>DVYPEIER</u>

Extended Data Figure 8. Mapping of CD4⁺ and CD8⁺ epitope spreading T-cell responses to individual ASP and EPT to the non-vaccine IMP and TAAs for Pts. 2 and 3. ASP and EPT covering the non-vaccine IMP are shown for the IMP that induced T-cell responses. Red bold and shading: mutated amino acids, absent in neoORFs. EPT covering the TAA are shown for the TAA that induced T-cell responses. Blue underline: for class I epitopes, predicted epitopes ($IC_{50} < 300$ nM) based on NetMHCpan. Blue font: peptides that generated a T-cell response after one round of pre-stimulation with peptides. (Supplementary Table 7).

Supplementary Table Legends

Supplementary Table 1. Clinical and sample information for Pts. 1-6 and 11-12.

Supplementary Table 2. QC metrics of (a) whole-exome sequencing for Patients 1-6 and 11-12, (b) whole-exome sequencing for relapsed tumors, (c) RNA sequencing for Patients 1-6, and (d) RNA sequencing for Patients 11-12. (excel)

Supplementary Table 3. (a) Somatic mutations (SNPs) identified from Pts. 11-12 original tumors and Pts. 1-3, 5-6 relapsed tumors and (b) Somatic mutations (indels) identified from Pts. 11-12 original tumors and Pts. 1-3, 5-6 relapsed tumors. (excel)

Supplementary Table 4. Summary of the number of identified somatic mutations, predicted HLA binders and synthesized immunizing peptides. (excel)

Supplementary Table 5. (a) HLA allotypes and (b) Treatment-related adverse events in vaccinated patients.

Supplementary Table 6. Expression and class I prediction related to immunizing peptides. (excel)

Supplementary Table 7. Expression and class I prediction related to epitope spreading peptides. (excel)

Supplementary Table 8. Antibody panels used for intracellular cytokine staining assays.

Supplementary Table 9. Differential analysis of single cell gene expression of clustered CD4⁺ T cells pre-vaccination and tetramer-positive CD4⁺ T cells post-vaccination for Patients 3, 4, and 5. (excel)

Supplementary Table 10. Targeted TCR sequencing primers. (excel)

Supplementary Table 11. Single-cell TCR sequences from Pts. 3-5 tetramer-positive CD4⁺ T cells at timepoints throughout vaccination. (excel)

Supplementary Table 12. Single-cell CDR3 α/β sequences from Pt. 2 tetramer-positive CD4⁺ T cells at (a) week 16 post-vaccination and (b) following pembrolizumab. (excel)

Supplementary Table 13. Class II tetramer information for Pts. 1-6.

****Excel data files for supplementary tables are available upon request**

Supplementary Tables

Supplementary Table 1. Clinical and sample information for Pts. 1-6 and 11-12.

Patient ID	Age	Gender	Primary site	Site of resected disease	Stage	Previous Treatment	Recurrence after NeoVax Y/N (Wks)	Site of tumor recurrence
1	26	M	Back	Axillary LN	IIIC (T3bN3M0)	IFN α	Y (37)	Brain
2	68	F	Back	Lung (RML)	IVM1b (T4aN0M1b)	None	Y (6)	Lung (RLL)
3	51	F	Left Calf	Skin - in transit (L posterior calf)	IIIC (T3bN2cM0)	None	Y (21)	Skin – in transit (L posterior calf)
4	56	M	Back	Axillary LN	IIIC (T4bN2bM0)	None	N	N/A
5	58	F	Left Arm	Skin (L upper arm)	IIIC(T2aN2cM0)	None	Y (36, 48)	Lung (RUL)
6	61	M	Chest	Lung (LUL)	IVM1b (T2aN0M1b)	IFN α	Y (4)	Skin (L back)
7	28	F	Unknown	Cervical LN	IIIB (TxN1bM0)	None	N/A	
8	63	M	Back	Skin - Satellite Nodule	IIIB (T3aN2cM0)	None	N/A	
9	71	M	Shoulder	Axillary LN	IIIB (T2aN1bM0)	IFN α	N/A	
10	34	M	Right Foot	Femoral LN	IIIC (T4aN3M0)	None	N/A	
11	65	F	Right Foot	Skin	IIIC(TxN2cM0)	IFN α	N	N/A
12	63	F	Right Forearm	Axillary LN	IIIC(T2aN1bM0)	None	N	N/A

M: male; F: female; LN: lymph node; N/A: not applicable; IFN α : Interferon alpha. *: Weeks from vaccination initiation to recurrence on vaccine. Red: New data since original report.

Supplementary Table 2. QC metrics of (a) whole-exome sequencing for Patients 1-6 and 11-12, (b) whole-exome sequencing for relapsed tumors, (c) RNA sequencing for Patients 1-6, and (d) RNA sequencing for Patients 11-12 (excel)

Supplementary Table 3. (a) Somatic mutations (SNPs) identified from Pts. 11-12 original tumors and Pts. 1-3, 5-6 relapsed tumors and (b) Somatic mutations (indels) identified from Pts. 11-12 original tumors and Pts. 1-3, 5-6 relapsed tumors. (excel)

Supplementary Table 4. Summary of the number of identified somatic mutations, predicted HLA binders and synthesized immunizing peptides (excel).

Supplementary Table 5. (a) HLA allotypes and (b) Treatment-related adverse events of vaccinated patients.

(a) HLA allotypes of enrolled patients

Patient ID	HLA-A	HLA-A	HLA-B	HLA-B
1	2:01	24:02:00	44:02:00	15:01
2	1:01	1:01	38:01:00	56:01:00
3	2:01	3:01	47:01:00	27:05:00
4	2:01	25:01:00	18:01	27:02:00
5	66:01:00	23:01	41:02:00	35:01:00
6	66:01:00	1:03	8:01	8:01
7	1:01	3:01	8:01	35:01:00
8	68:01:00	24:02:00	35:03:00	13:02
9	1:01	1:01	37:01:00	8:01
10	24:02:00	24:02:00	52:01:00	27:05:00
11	1:01	2:01	7:02	57:01:00
12	2:01	2:02	13:02	40:02:00

Red: New data since original report.

(b) Treatment-related adverse events of vaccinated patients.

Event*	Grade 1	Grade 2-5
	Number of patients (%)	
Injection site reaction	8 (100)	0
Fatigue	5 (63)	0
Flu-like symptoms	4 (50)	0
Arthralgia	3 (38)	0
Rash	3 (38)	0
Fever	3 (38)	0
Pruritus	2 (25)	0
Bruising	2 (25)	0
Headache	2 (25)	0
*Treatment related events that occurred in > 1 patient.		

Supplementary Table 6. Expression and class I prediction related to immunizing peptides. (excel)

Supplementary Table 7. Expression and class I prediction related to epitope spreading peptides. (excel)

Supplementary Table 8. Antibody panels used for intracellular cytokine staining assays.

Laser	Channel	Marker	Clone	Company
488nm LASER 100 mW	BB700	CD279	EH12.1	BD Pharmingen
561 LASER 100 mW	ECD	CD69	TP1.55.3	BECKMAN COULTER
405 LASER 100 mW	BV480	Aqua L/D		ThermoFisher
	BV570	CD8	RPA-T8	BIOLEGEND
	BV650	TNF α	Mab11	BD Pharmingen
	BV711	CD4	L200	BD Pharmingen
	BV786	CD27	O323	BIOLEGEND
355 LASER 60 mW	BUV395	IFN γ	B27	BD Pharmingen
	BUV737	IL-2	MQ1-17H12	BD Pharmingen
637 LASER 140 mW	APC-R700	CD3	UCHT1	BD Pharmingen
	APC-H7	CD45RA	5H9	BD Pharmingen

Supplementary Table 9. Differential analysis of single cell gene expression of clustered CD4⁺ T cells pre-vaccination and tetramer-positive CD4⁺ T cells post-vaccination for Patients 3, 4, and 5. (excel)

Supplementary Table 10. Targeted TCR sequencing primers. (excel)

Supplementary Table 11. Single-cell TCR sequences from Pts. 3-5 tetramer-positive CD4⁺ T cells at timepoints throughout vaccination. (excel)

Supplementary Table 12. Single-cell CDR3 α/β sequences from Pt. 2 tetramer-positive CD4⁺ T cells at (a) week 16 post-vaccination and (b) following pembrolizumab. (excel)

Supplementary Table 13. Class II tetramer information for Pts. 1-6.

Pt	Gene	Peptide sequence for tetramer	HLA allele	Predicted class II epitope sequence	Predicted percentile rank*
1	<i>RUSC2</i>	SVGDFSQEFSPIQEAQQD (K-dansyl)-amide	HLA- DRB1*04:01	SVGDFSQEFSPIQEA	2.16
			HLA- DRB1*04:01	DFSQEFSPIQEAQQD	5.77
2	<i>ADM2</i>	RTQLLWTPAAPTAMAE(K-dansyl)-amide	HLA- DRB1*07:01	RTQLLWTPAAP PTAMA	2.91
			HLA- DRB1*07:01	TQLLWTPAAP TAMAE	4.28
3	<i>ADAMTS7</i>	RGRELRFNLIANQHLLAP GF(K-dansyl)-amide	HLA- DRB1*01:01	RGRELRFNLIAN NQHL	2.28
			HLA- DRB1*01:01	RFNLIANQHLL APGF	4.57
4	<i>ARHGAP29</i>	PGKIHLFEAEFTQVAKKE (K-dansyl)-amide	HLA- DRB1*01:01	LPGKIHLFEAE FTQV	24.59
			HLA- DRB1*01:01	IHLFEAEFTQV AKKE	28.84
5	<i>ZNF281</i>	SQRTSWEFLQSLVSIKQE K(K-dansyl)-amide	HLA- DRB1*01:01	SQRTSWEFLQS LVSI	8.87
			HLA- DRB1*01:01	SWEFLQSLVSI KQEK	9.63
6	<i>MLL</i>	SRLQTRKNKKLALSSTPS N(K-dansyl)-amide	HLA- DRB1*03:01	KNKKLALSSTP SNIA	5.64
			HLA- DRB1*03:01	TRKNKKLALS STPSN	7.97
*Consensus method in IEDB					